

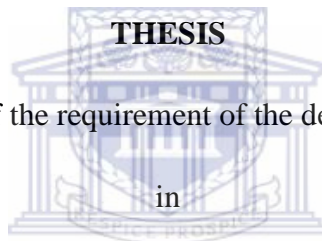


**UNIVERSITY of the
WESTERN CAPE**

**THE LITHOGEOCHEMICAL CHARACTERIZATION OF THE
HONDEKLOOF NICKEL MINERALIZATION, KLIPRAND AREA,
GARIES TERRANE, NAMAQUALAND, SOUTH AFRICA**

by

REDDY NGILI BOKANA



presented in fulfilment of the requirement of the degree of Master of Science

in

ECONOMIC GEOLOGY
WESTERN CAPE

in the

FACULTY OF NATURAL SCIENCE

of the

UNIVERSITY OF THE WESTERN CAPE, SOUTH AFRICA

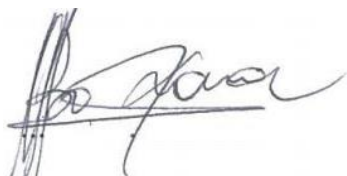
Supervisor: Dr. Russell Hope Bailie

Co-supervisor: Prof. Jan van Bever Donker

April 2015

1. DECLARATION

I hereby declare that this thesis submitted for the degree of Masters to the Faculty of Natural Sciences at the University of the Western Cape, apart from the guidance and supervision of Dr. R.H. Bailie and Prof. J. van Bever Donker, is my own work and has not been previously submitted either entirely or partly to any other university or institution of higher education for obtaining a qualification.

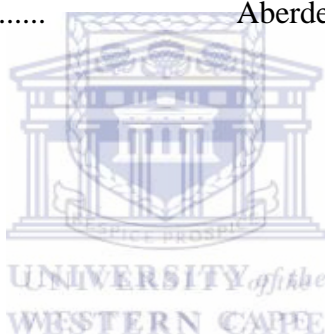


Reddy Ngili Bokana

2015/10/28.....

Aberdeen, Scotland, United Kingdom....

Date



Place

2. ABSTRACT

A magmatic Ni-Cu (\pm Co-Zn) sulphide deposit, named the Hondekloof prospect, is present in the Kliprand area at the border between the Northern Cape and Western Cape Provinces of South Africa. The deposit occurs in the central part of the polyphase deformed and highly metamorphosed Garies Terrane, in the Namaqua Sector, along the south-western margin of the Mesoproterozoic Namaqua-Natal Metamorphic Province. Given the sub-economic concentrations yielded from evaluation of three of its known massive-sulphide lenses evaluated, the Hondekloof prospect has received relatively little consideration in terms of ongoing scientific research. Consequently, many aspects related to the genesis, classification and tectonic evolution of the deposit, to date, remain relatively unclear and unknown. The present contribution has therefore been geared to addressing some of those issues in view of the new data obtained on the country rocks and host rocks to the mineralization.

Six exploration boreholes were logged, sampled and examined at the deposit site in Kliprand. A total of seven host rocks, namely meta-gabbro, biotite gneiss, feldspathic-biotite-garnet gneiss, pink gneiss, meta-syenite as well as enderbite along with a garnetiferous quartzofeldspathic rock occur in association with the sulphide mineralization. The origin, protoliths and tectonic settings of the host lithological units were determined and discussed in terms of modern plate tectonic principles. The meta-gabbro (the actual ore host), which had a magmatic protolith and forms part of the pre- to syn-tectonic Oorkraal Suite, displays the chemical characteristics of a depleted mantle origin (source of MORB-like melt), generated within a continental tectonic rift environment. Country rocks with sedimentary protoliths have chemical characteristics indicating a psammitic, felsic to intermediate provenance deposited within a regional subduction-related tectonic setting. A number of geochemical indices, of which the combination of element-ratios (such as $\text{Fe}_2\text{O}_3/\text{Al}_2\text{O}_3$ vs. $\text{TiO}_2/\text{Al}_2\text{O}_3$, as well as Cr vs. Ni, amongst others) created as exploration vectors towards mineralisation, have shown potential for pointing towards the direction of the mineralization. Based on classification schemes of magmatic Ni sulphide deposits, it has been suggested that the Hondekloof prospect could be classified as a low MgO, conduit-type, disseminated magmatic nickel sulphide deposit.

3. ABBREVIATIONS:

NNMP: Namaqua-Natal Metamorphic Province

OCC: Okiep Copper Company

Qtz: quartz

Bio: Biotite

Hbl: Hornblende

Plag: Plagioclase

Grt: Garnet

Opx: Orthopyroxene

Cpx: Clinopyroxene

And: Andalusite

Kfs: K-feldspar

Sill: Sillimanite

Epid: epidote

H₂O: Water



4. ACKNOWLEDGEMENTS

Many, many thanks and a huge debt of gratitude to my wonderful, efficient and resourceful supervisors Dr. Russell Bailie and Prof. Jan van Bever Donker for their support, patience, and enthusiasm shown during the time we spent working on this project. Special thanks go to both NRF and Inkaba yeAfrica programmes for their multiple financial supports (scholarship, analytical costs, conference costs, etc.). All the academic staff of the Department of Earth Sciences of the University of the Western Cape (UWC) (the H.O.D, Prof. Charles Okujeni, Dr. Abdi-Mohamoud Siad, Dr. Mimonitu Opuwari, Dr. Silvia Lanes, Prof. Sokari Braide, Mrs. Yafah Williams, Mrs. Wasielah Davids) are thanked for their contribution to my academic growth. The Division of postgraduate study of UWC, most especially, Prof. Lorna Holtman (the director), and Mr. Brenton are thanked for their everlasting tremendous support.

I am also deeply indebted to all the technical staff of the Department of Earth Sciences (at UWC - Mr. Peter Meyer, Mr. Lucas van Vuuren, Ms. Janine Becorney) for providing technical support in anything technical-related to this project. Special thanks and a huge debt of gratitude goes to Mr. Johnny Dreyer, his wife, Liezl, and his kids for their hospitality and the good-times during the time I spent in the jungle of Kliprand. The friendly and helpful folks at PRISE, Marc Ngama, Tshipeng (James) Mwenze, Eric Saffou, Stephané Tsakou, Hakundwi (Mike) Mandende, Sedzani Nethenzheni and Fritz Agbor, to mention a few, are thanked for the fun, laughter and all the good times we spent together in the labs working on our different projects and/or in the transport or hotel rooms while attending different conferences. My immense gratitude is due to all the conference organizers both locally (in South Africa) and internationally for their positive feedback and the opportunity given to me to present the project in some of the biggest international platforms.

I am also deeply grateful and indebted to my family and close friends, my late father (Bokana Ngili Felix), my mother (Henriette Milambo), my brother (Serge Bokana, his wife Anna), my sister (Solange Milambo and her husband Eddy Mpeleka), my uncle (Jean Paul Tambwe and his wife, Ms Veronica Yabadi), my step father (Mr. Pierre Yala), my Pastor (Pastor Elie Ngilasi and his wife), my grandfather and friend (Abraham Nzambe and all Nzambe' family) to mention a few, for all kind of supports (moral, prayer, financial, advice etc.) that each of them has contributed towards my personal growth. Last but not least I thank Dr. Johan Hattingh, the Lehoumo Resources manager for giving us access to all resources related to the Hondekloof Nickel Project (cores, confidential reports etc.) which made this study possible.

5. TABLE OF CONTENTS

1. DECLARATION.....	i
2. ABSTRACT	ii
3. ABBREVIATIONS:.....	iii
4. ACKNOWLEDGEMENTS.....	iv
5. TABLE OF CONTENTS	v
1. CHAPTER I.....	1
INTRODUCTION.....	1
1.1 Introduction	1
1.2 Aims and objectives.....	3
1.3 Review of Magmatic sulphide deposits.....	4
1.4 Exploration and mapping History of the Hondekloof orebody	7
2. CHAPTER II	10
GEOLOGICAL SETTING	10
2.1 Regional Geological Setting.....	10
2.2 Local Geological Setting	14
3. CHAPTER III.....	21
METHODOLOGY	21
3.1 Introduction	21
3.2 Data collection.....	21
3.3 Petrography.....	21
3.4 Geochemistry.....	21
4. CHAPTER IV.....	23
LITHOLOGICAL DESCRIPTION	23
4.1 Introduction	23
4.2 Meta-gabbro norite	24
4.3 Garnetiferous quartzofeldspathic rock.....	29
4.4 Biotite gneiss	31
4.5 Feldspathic biotite garnet gneiss.....	33
4.6 Pink gneiss	35
4.7 Meta-syenite	37
4.8 Enderbite.....	38

4.9 Summary.....	40
4.10 Estimation of the metamorphic grade.....	41
5. CHAPTER V	44
GEOCHEMISTRY.....	44
5.1 Introduction	44
5.2 General classification	44
5.3 Determination of protoliths	54
5.4 Geostatistical analysis.....	74
6. CHAPTER VI.....	79
DISCUSSION, CONCLUSIONS AND RECOMMENDATIONS FOR FUTURE RESEARCH.....	79
6.1 Discussion.....	79
6.2 Conclusion.....	96
6.3 Recommendation and future work	97
7. REFERENCES	98
8. APPENDICES	113
Appendix 1. Extended abstract published and presented on the 27th edition of international applied geochemistry symposium in Tucson, Arizona, United States of America, 2015.	114
Appendix 2 Field description of the examined boreholes.....	119
Field Geology of the examined boreholes.....	120

List of figures

Figure 1-1: Location of the Hondekloof deposit. Adapted from Lehumo Resources Technical report (2008)	3
Figure 2-1: Simplified geological map of southern Africa.....	11
Figure 2-2: Terrane map of the Namaqua Sector.....	13
Figure 2-3: A simplified geological map of the southwestern and western portion of the Namaqua Sector.....	19
Figure 4-1: The three lenses of the Hondekloof prospect on the simplified geological map of the Kliprand area.....	23
Figure 4-2: Strip logs showing the vertical distribution of the different lithologies examined in the different boreholes.	40
Figure 4-3: A generalised pressure and temperature petrogenesis phase diagram used to estimate the degree of metamorphism from the meta-gabbro-norite of the Hondekloof deposit	41

Figure 5-1: Bivariate plots using MgO in wt% as the abscissa plotted against all the major oxides.....45

Figure 5-2: Bivariate plots with MgO in wt.% as the abscissa plotted against some selected trace elements.....47

Figure 5-3: Discrimination diagram to determine sedimentary and igneous precursors55

Figure 5-4: Comparative classification diagrams for protoliths and provenance composition (after Winchester and Floyd 1977), (a) Nb/Y vs. Zr/TiO₂ and (b) Zr/TiO₂ vs. SiO₂. Alk-Bas: Alkaline basalt, SB-AB: Sub-alkaline basalt.56

Figure 5-5: (a) Total alkali vs. silica diagram for separating the alkaline and sub-alkaline basalts, (b) Na₂O vs. K₂O diagram for subdividing the alkaline magmas (after Middlemost 1975), (c) Zr vs. P₂O₅ diagram (after Winchester and Floyd, 1976) for separating the alkaline and tholeiitic basalts, (d) AFM diagram (after Irvine and Barager, 1971)58

Figure 5-6: (a) La/Ba vs. La/Nb diagram displaying asthenospheric and lithospheric mantle sources, and (b) Zr/Y vs. Ti/Y showing the MORB and OIB characteristics of the mantle melt for the meta-gabbronorite59

Figure 5-7: (a)- (e) Discrimination diagrams showing different tectonic settings based on natural logarithm transformation of major-element ratio (Verma et al., 2006).60

Figure 5-8: Mafic samples of the meta-gabbronorite in five new multidimensional diagrams based on log-ratios of major and trace elements (TiO₂, MgO, P₂O₅, Nb, Y and Zr) for discrimination of island arc (IAB), continental rift (CRB), ocean island (OIB), and mid-ocean ridge (MORB) tectonic settings (Verma et al. 2013).....62

Figure 5-9: Mafic samples of the meta-gabbronorite in five new multidimensional diagrams based on log-ratios of immobile trace elements (Yb, La, Ce, Sm, Nb, Th, Y and Zr) for discrimination of island arc (IAB), continental rift (CRB), ocean island (OIB), and mid-ocean ridge (MORB) tectonic settings (Verma et al. 2013).....63

Figure 5-10: Multi-element spider diagrams normalized to primitive mantle (after McDonough and Sun, 1995) and REE plots normalized to the chondritic values of Nakamura (1974) for various meta-magmatic rocks of the western Namaqua Sector.65

Figure 5-11: a. SiO₂ vs. Al₂O₃+K₂O+Na₂O paleoclimatic discriminant diagram, b CaO+Na₂O+K₂O-Al₂O₃-Fe₂O₃+MgO ternary plot for discriminating element exchange in the siliciclastic sediments during weathering.69

Figure 5-12: (a.) Discriminant diagram for determining the composition of the provenance to the metasedimentary rocks. (b) Th/Sc vs. Sc plot illustrating the relative contributions from mafic and felsic provenance to the rocks (after McLennan et al., 1990; 1993). (c). K₂O-MgO-Na₂O plot indicating the arkosic composition of the protoliths to the investigated rocks (after Reid, 1997).....71

Figure 5-13: Spider plot normalized to the primitive mantle values of McDonough and Sun (1995), with the REEs normalised to the chondrite values of Nakamura (1974).73

Figure 5-14: a) La-Th-Sc and b) Th-Sc-Zr/10 discriminant diagrams for the metasedimentary rocks (after Bhatia and Crook, 1986). A: Oceanic island arc, B: continental island arc, C: active continental margin, D: passive margin.73

Figure 5-15: Dendrogram showing rock association groups based on the Ward method.....75

Figure 5-16: Indices to distinguish between the actual host-rock and the other associated host-rocks. Group 1 represents the meta-gabbronorite and group 2 all the other rock-types. TiO₂ vs

Al₂O₃ and Al₂O₃ vs. TiO₂+CaO+MgO provide the best differentiation between the two groups. 77

Figure 6-1: Two schematic models for the metamorphic regime of the western Namaqua Sector. 84

Figure 6-2: Simplified analogues explaining the tectonic evolution of the Kliprand area, taking into consideration both local scale (a) and regional scale (b) deformation. 88

Figure 6-3: Chemostratigraphic indices for discrimination of the actual host, the meta-gabbro, from the other rocks..... 91

Figure 6-4: Graphical representation of the element indicators to mineralization within the actual host. 92

Figure 8-1. Simplified geological map of southern Africa, from Cornell et al. (2006)..... 115

Figure 8-2. Geochemical indices as vectors for pointing towards the direction of the mineralization. 117

List of plates

Plate 4-1: Core photographs of the meta-gabbro. 25

Plate 4-2: a and b: Thin section photomicrographs of a meta-norite at the Hondekloof deposit.. 26

Plate 4-3: Core photograph of the two varieties of the garnetiferous quartzofeldspathic rock. 29

Plate 4-4: Thin section photomicrographs of a garnetiferous quartzo-feldspathic rock from the Hondekloof deposit. 30

Plate 4-5: Core photographs showing the varieties of the biotite gneiss. 31

Plate 4-6: Thin section photomicrographs of a biotite gneiss from the Hondekloof deposit.. 32

Plate 4-7: Core photographs showing different variations of the feldspathic biotite garnet gneiss..... 33

Plate 4-8: Thin section photomicrographs of the feldspathic biotite garnet gneiss from the Hondekloof deposit..... 34

Plate 4-9: The two varieties of pink gneiss. 35

Plate 4-10: Thin section photomicrographs of a pink gneiss from the Hondekloof deposit. The red arrows indicate the plane of foliation marked by mineral recrystallization into smaller grains (in photo a), and that marked by mineral elongation and alignment (in photo c). Ser-plg: sericitized plagioclase, Qtz: quartz, Bio: biotite, Mic: microcline. Crd: cordierite, Orth: orthoclase. Photos a and c are taken in crossed polars and b and d in plane polarized light. ... 36

Plate 4-11: Core photographs showing the meta-syenite of the Hondekloof deposit. a. variety 1; b. variety 2. 37

Plate 4-12: Thin section photomicrographs of the meta-syenite of the Hondekloof deposit..
 Orth: orthoclase, Qtz: quartz, Bio-Hbl: hornblende → biotite, Chl-Hbl: hornblende → chlorite.
38

Plate 4-13: Core photographs displaying the enderbite of the Hondekloof deposit.39

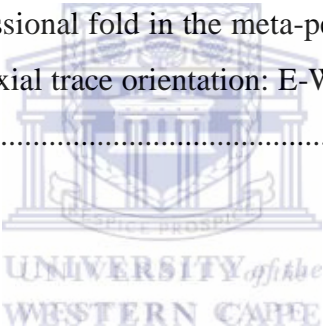
Plate 4-14: Thin section photomicrographs of the enderbite from the Hondekloof deposit.
 Notice the even distribution of the feldspars (plagioclase and alkali feldspar). Opx:
 orthopyroxene, Orth: orthoclase, Plg: plagioclase, Slph: sulphide. Photo a is shown in crossed
 polars and b in plane polarised light.39

Plate 8-1: Field evience of “east-west and north-south-south Syn-kinematic joints on the augen
 gneiss of the Little namaland Siute within the western lense of the Hondekloof deposit. 120

Plate 8-2: a: Sharp intrusion of the meta-gabbronorite into the meta-pelitic gneiss of the
 Kamiesberg Group. b: A feldspathic vein crosscutting the weathered meta-gabbronorite. . 120

Plate 8-3: Evidence of the garnetiferous quartzofeldspathic veins cutting through the pink
 gneiss. Photo taken in the eastern extension of the orebody..... 121

Plate 8-4: a: North south compressional fold in the meta-pelitic gneiss. Interlimb angle: 115-
 120°; limb thickness: 10-15 cm; axial trace orientation: E-W. Evidence of N-S compressional
 folding event. 121



UNIVERSITY of the
WESTERN CAPE

List of tables

Table 2-1: Rocks of the Garies terrane in the Kliprand area 16

Table 4-1: List of boreholes examined and their location within the orebody24

Table 4-2: Summarized petrographic descriptions of the host lithologies to the Hondekloof
 deposit.....27

Table 5-1: Major element composition of the host rocks to the Hondekloof deposit.....48

Table 5-2: Trace element composition of the host rocks to the Hondekloof deposit50

Table 5-3: Discriminant ratios for determining the chemical characteristics of sedimentary
 rocks.....68

Table 5-4: Element discrimnation function for determining the actual ore-host rock (the meta-
 gabbronorite) (group 1) and the associated host rocks (group 2) 76

Table 5-5: correlation table showing element relationships in the dataset 78

Table 5-6: Element predictors and their predictibility percentage as pathfinders for Ni, Co and
 Zn in the meta-gabbronorite and in all the host-rocks 79

Table 6-1: Proposed protoliths82

Table 6-2: Determination of a mineralized and a less mineralized meta-gabbronorite sample93

Table 6-3: criteria for classifying a magmatic Ni sulphide deposit95



1. CHAPTER I

INTRODUCTION

1.1 Introduction

South Africa is known as one of the world's most prolific mining countries on earth in terms of mineral resources. In itself it hosts several of the world's largest mineral deposits, such as the platinum group elements (PGE) deposits in the Bushveld Complex, gold deposits in the Witwatersrand Basin, diamond deposits at Kimberley, the world's richest chromium deposits (LG6 in the Bushveld Complex), and the world's richest manganese deposits (in the Transvaal Supergroup, Griqualand West Basin), all of which, to some extent, control the economy of the entire country. While much attention has been given to such areas in the search of additional resources for future exploitation (and for economic growth), relatively little attention has been given to other areas in terms of exploration. Such areas include the Namaqua-Natal Metamorphic Province, the Cape Fold Belt (in the Saldania Belt) and others.

Despite having been given relatively little consideration in terms of exploration, the Namaqua-Natal Metamorphic Province (NNMP), particularly the Namaqua Sector, has proven to be one of the remarkable mineralized sectors in the country, hosting one of the world's giant volcanic hosted massive sulphide (VHMS) deposits, namely the Copperton (Prieska Copper Mine) deposit (Cornell et al., 1986; Cornell et al., 1990a, 1990b, Cornell et al., 1992; Bailie et al., 2010; Bailie and Gutzmer, 2011). Several other VHMS deposits have also been documented in the Namaqua Sector, near to the Copperton (Prieska Copper Mine) deposit, namely Annex, Areachap, Kantienpan, Kielder and Smouspan prospects (Ghavami-Riabi et al., 2008; Bailie et al., 2010; Bailie and Gutzmer, 2011). In addition other equivalent deposits such as sulphide ores in the Springbok area of Namaqualand, also known as the Okiep Copper District, have also been a major source of copper for South Africa (McIver et al., 1983; Lombaard et al., 1986; Schoch and Conradie, 1990; Cawthorn and Meyer, 1993; Clifford et al., 1995; Clifford and Barton, 2012; Van Zwieten et al., 1996; 2004; Robb et al., 1999; Duchesne et al., 2007, Maier et al., 2013). One of the world's largest sedimentary exhalative (SEDEX) resources, in the form of the Broken Hill and Black Mountain Pb-Zn-Ag deposits, is also hosted in the supracrustal succession of the

Bushmanland Group (in the central region of the Namaqua Sector, Northern Cape Province) near the town of Aggeneys (Ryan et al., 1986; Moore et al., 1990; Bailie et al., 2007a, b).

Unlike the northern part of the Namaqua Sector where, at least, a number of studies have been carried out given the presence of economic occurrences of Cu-Zn-rich deposits in the Upington area and copper deposits in the Springbok area, the southern part of the Namaqua Sector, in comparison (to the northern part), remains very much underexplored. Not much has been done either in terms of mineral exploration or field investigation for tectonic studies in the past two decades. As a result, the geological and economic prospectivity of some of its areas (terrains) have, therefore, remained poorly constrained.

The Hondekloof deposit represents a family of small, orthomagmatic massive sulphide Ni-Cu-(Co-Zn) deposits that occur in the southern central portion of western Namaqualand (specifically the central part of the Garies terrane). The deposit is located on the farm Nuwefontein, approximately 4 km west of the village of Kliprand (Fig 1.1; Bekker, 1980; Taylor, 1990; Andreoli et al., 1991a, 1991b; Hamman et al., 1996), and is ca. 120 km southeast of the Okiep Copper district (Taylor 1990; Andreoli and Moore 1991; Hamman et al., 1996; Andreoli et al., 2006). The prospect is restricted to a 200-m-wide, 3.5-km-long zone and occurs in three massive sulphide lenses, having a structural configuration forming small boudinage (Lehumo Technical Report, 2008).

Resources calculated for the two largest deposits (lenses) amount to 2 Mt of ore with a grade of 0.88% Ni, 0.2% Cu, 410 ppm Co and <1 ppm platinum-group elements plus gold (Hamman et al., 1996; Macey et al., 2011). Andreoli et al. (1987, 1991a) argued that the suite of mafic rocks, which act as the main ore bearers at the Hondekloof Ni ± Co and Steenkampskraal monazite deposits, have the characteristics and associations typical of the late-tectonic Koperberg Suite (a nearby cupriferous mafic suite from which the Okiep terrane had inherited its nickname of the Okiep Copper District). This is in contrast to Hamman et al. (1996), who suggested that the meta-noritoids at the Hondekloof deposit are related to the pre- to syn-tectonic mafic rocks of the Oorkraal Suite.

Shallow drilling for resource and reserve estimation was done in the early 1980s (Maier et al., 2013), and was renewed again more recently in early 2006. Since then, however, very little to no work has been done on the Hondekloof deposit in terms of exploration and exploitation. Until

today, the deposit remains largely unclassified and uncharacterized (Hamman et al., 1996). Its age has also not been determined, making its tectonic evolution enigmatic. As such, many aspects of the deposit remain poorly understood.

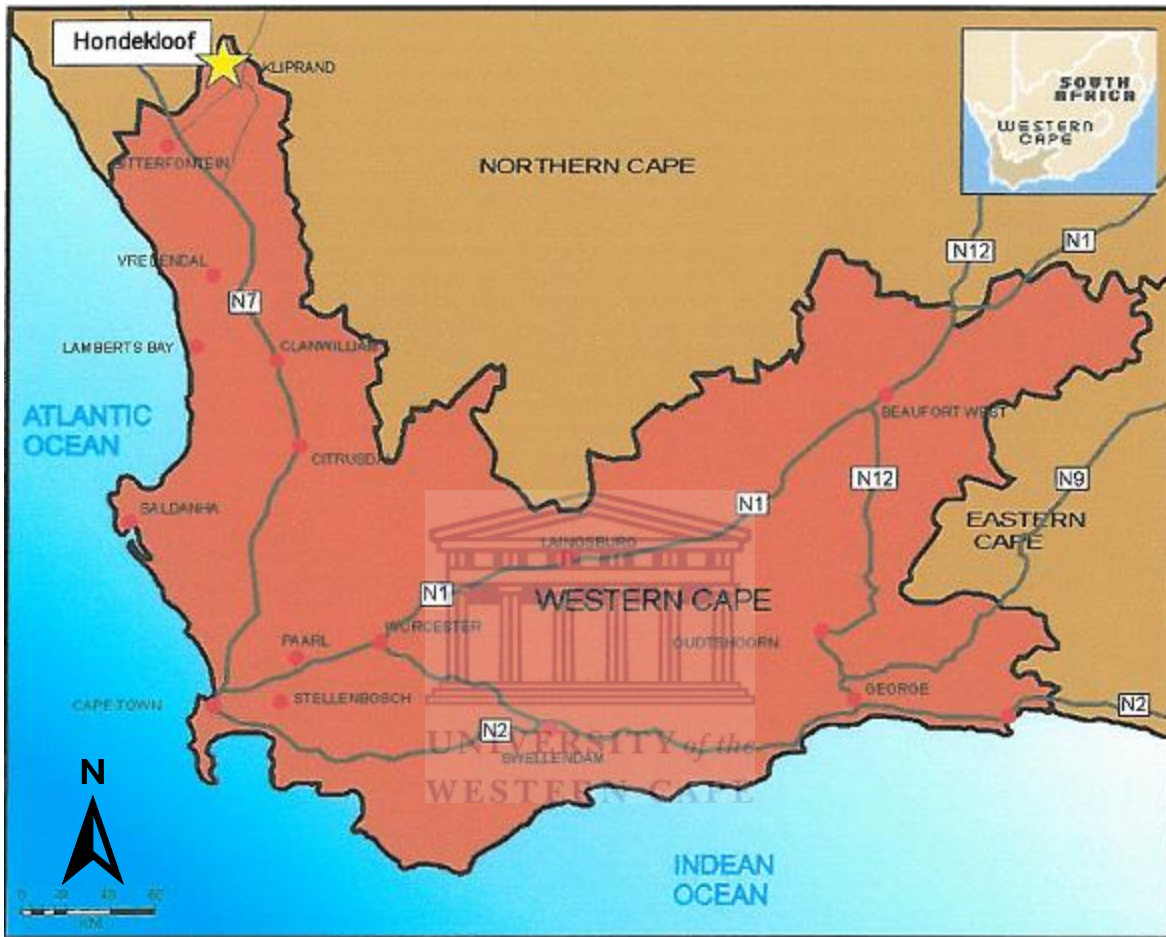


Figure 1-1: Location of the Hondekloof deposit. Adapted from Lehmo Resources Technical report (2008)

1.2 Aims and objectives

Several other prospects of varying size and nature have also been noted in the Garies terrane (Maier et al., 2013), making the Kliprand area an interesting and suitable area for future and further exploration activities. Therefore, for a contribution, this study is aimed at placing constraints on the Hondekloof deposit in terms of classification and characterization. It aims to:

- ❖ Characterize the deposit by determining the nature of its sulphide mineralization, as well as the types and characteristics of its host rocks,
- ❖ Examine the host rocks and constrain their origin (source area and provenance), protoliths and tectonic setting,
- ❖ Understand the genesis of the deposit and be able to create a geological framework which can explain the formation and influence of tectonism thereafter on the mineralization.

In addition the project also aims at addressing some issues related to vectoring towards the mineralization. Taking into consideration that the Hondekloof deposit and, in fact, the whole of southern Namaqualand (around the Kliprand area) is not well studied, this project is therefore of great interest, and will serve as a contribution to further, and broaden our understanding of the geology and economic prospectivity of the area.

1.3 Review of Magmatic sulphide deposits

As the name suggests, magmatic sulphide deposits are formed by the emplacement of magmatic bodies (Buchanan and Nolan, 1979; Holwell and McDonald, 2010). They develop when a fractionating body of magma intruded into the crust has reached sulphide saturation, that is, the point whereby magma can no longer hold sulphur in solution, and, an immiscible sulphide liquid exsolves from the silicate melt, to form its own separated phase (Holwell and McDonald, 2010). However, there are two processes, namely magma fractionation and sulphide liquid segregation that govern the formation of all magmatic sulphide deposits. Both processes are fundamentally controlled by the rate of temperature drop or rate of cooling of the melt. In addition to that, the process of silicate-sulphide immiscibility and sulphide globule melt interaction also plays a central role in determining, controlling and dictating the way in which metals are partitioned between sulphide and silicate melt during the time of segregation (Burnham, 1967). The latter mechanism (silicate-sulphide immiscibility) is a well-recognised example (Haughton et al., 1974; Buchanan and Nolan, 1979; Wendlandt, 1982; Mavrogenes and O'Neill, 1999; Naldrett, 2004) commonly used to describe the way in which a large and economic magmatic sulphide deposit can be generated from a fractionating body of magma. Furthermore, sulphide-metal associations can also be explained in terms of metal (or element) affinity to particular phases (for example lithophile elements to silicate, chalcophile elements to sulphide/sulphur, siderophile elements to iron, and atmophile elements to gas), as extensively described by Goldschmidt rules.

The extent to which metals partition between sulphide and silicate melts (i.e. the magnitudes of the relevant sulphide-silicate partition coefficients), will determine the ability of an immiscible sulphide fraction to concentrate both base and precious metals during the formation of a magmatic sulphide deposit ((Burnham, 1979). Following the separation of a sulphide liquid from a silicate magma within the temperature range of approximately 1200 to 1000°C, for example, that being the point at which the magma reaches sulphide saturation, chalcophile elements such as Cu, Ni, the PGEs, gold, silver and some semi-metals, such as Bi and Te, will effectively be collected by any sulphide liquid (globule) rather than remaining in the silicate melt. Certain metals, such as Cu, Ni and Co, often partition strongly into the sulphide phase in substantial proportions compared to the others. The partitioning of these elements is strongly pronounced because they (those metals) have a very high distribution coefficient between sulphide and silicate melts (Holwell and McDonald, 2010).

During the initial stages in the development of such magmatic sulphide deposits, apart from having a buoyant body of magma to be emplaced at some level of the crust, one of the most fundamental factors is that, at first, that magma has to attain sulphide saturation. The mechanisms by which this is achieved are numerous and may be difficult to determine. Candela and Holland (1984), and Candela (1991) proposed a number of scenarios which can theoretically explain how a body of magma may reach sulphide saturation, namely, sulphide saturation can be achieved: (1) as solidification proceeds and magma temperature falls, (2) by virtue of increasing fO_2 in the magma, or (3) by continuously decreasing the amount of ferrous iron in the magma (such as might occur during the extraction of an Fe-rich phase). Other factors, such as the addition of externally derived sulphur, or an ingress of new magma, can also promote saturation and the formation of an immiscible sulphide phase. Holwell and McDonald (2010) expanded on these concepts and argued that assimilation of country rock-hosted sulphur must also be considered as an essential factor in producing sulphide saturation in high-degree (high temperature) mantle melts, such as komatiites. According to Burnham (1967) sulphide saturation and the generation of economic sulphide mineralisation can be achieved through other types of contamination as well. Silica contamination, due to the assimilation of felsic country rocks, can decrease the solubility of sulphur in a mafic magma (Li and Naldrett, 1993), and can also trigger sulphide saturation. In addition, an increase in magma oxygen fugacity (fO_2), for example in response to the assimilation of oxygen-bearing

country rocks, can lower the iron (II) oxide content and thus the sulphur-carrying capacity of the magma, and also trigger sulphide saturation (Buchanan and Can, 1979).

Segregated sulphide melts have enormous potential to host concentrations of metals with both chalcophile and siderophile tendencies, such as base (Cu, Ni, Co) and precious (Au, Pt) metal ores. However, after a number of discoveries of magmatic sulphide deposits in a variety of tectonic settings, it has become a known fact, with concrete examples, that most, if not all, of the large and important ore deposits associated with the development of an immiscible sulphide fraction usually have the tendency to be hosted in magmas with mafic and ultramafic compositions (Holwell and McDonald, 2010). Typical examples include the varieties of magmatic sulphide deposits found in layered mafic intrusions, e.g. Voisey's Bay, Noril'sk. As a variety of contamination-related processes are capable of inducing sulphide saturation and promoting magma-sulphide liquid segregation, sulphide mineralisation commonly occurs at the base and margins of intrusions, where contamination is most prevalent (Holwell and McDonald, 2010). *"The Platreef of the Bushveld Complex; the Basal Series of the Stillwater Complex; the Penikat-Portimo Complex, Finland; the Muskox intrusion, Canada; the Fedorov-Pansky intrusion, Russia; and conduit systems such as Noril'sk, Russia and the Uitkomst Complex, South Africa, are all typical examples of magmatic sulphide deposits that occur at the base and margin of an intrusive body"* (Ripley et al., 2003; Holwell and McDonald, 2010).

1.3.1 Current understanding of the development of magmatic sulphide deposits

Before anything else, a fractionating body of magma, which is sulphide-rich, has to be emplaced at some level of the crust, and must also be controlled by the rate of cooling, which is determined by the temperature of the intrusive body, the temperature of the intruded country rocks, and the rate of crystallisation, so that sulphide saturation can be reached, and thus trigger the process called magmatic segregation or sulphide liquid exsolution so that a magmatic sulphide deposit can be generated.

Following the separation of a sulphide liquid from a silicate magma at temperatures of around 1200°C (typical of mafic magmas), the first phase to crystallise from the sulphide droplet is called monosulphide solid solution (mss), at around 1000°C (Holwell and McDonald, 2010; Maier et al., 2013). Ni is generally compatible with mss and will partition into it at this stage. This leaves a Cu-

rich residual liquid behind, which subsequently crystallises to a phase called intermediate solid solution (iss) at around 900°C (Holwell and McDonald, 2010). Consequently, at this stage there is a Ni-rich mss portion and a Cu-rich iss portion segregated but partly coexisting in the melt. As the temperature cools to below 650°C, the mss recrystallises to pyrrhotite (FeS) and pentlandite ((Fe, Ni)₉S₈) and the iss recrystallises to chalcopyrite (CuFeS₂) (Holwell and McDonald, 2010). The precise temperature of these recrystallisations is dependent on how rich the mss is in sulphur. The end product results in a typical sulphide assemblage of pyrrhotite-pentlandite-chalcopyrite commonly found in association with natural magmatic sulphide mineralization. The mss type usually results in Ni-rich and PGE-poor magmatic sulphide deposits, whereas the iss type, by contrast, frequently gives rise to Cu-PGE-rich types of magmatic sulphide deposits (Holwell and McDonald, 2007). Deep mantle-derived magma containing mafic and ultramafic bodies will, if fractionated (during the first phase of sulphide saturation), in the earlier stages, give rise to mss or Ni-rich types of sulphide deposits (forming at deeper crustal levels). With continuous fractionation, as the magma approaches an advanced phase of sulphide saturation, an iss or Cu-PGE type deposit will be generated (Hutchinson and McDonald, 2008). This also explains the abundance of pyrrhotite and pentlandite ores for the mss type of deposits while changing to chalcopyrite for the iss type of magmatic sulphide deposits.

1.4 Exploration and mapping History of the Hondekloof orebody

As early as 1970, Gold Fields of South Africa Ltd. (GFSA) was reported to have been the first company to have initiated an exploration program to investigate a broad aerial-electromagnetic anomaly over the Kliprand dome. Their drilling program was focused on the central part of the dome but unfortunately failed to locate any geological feature of economic interest. Nine years later (in 1979), Okiep Copper Company Ltd. (OCC) launched a regional stream sediment sampling program in southern Namaqualand involving both sediment and soil sampling. This stream sediment sampling, after completion, led to the discovery of the Hondekloof nickeliferous gossan outcrops in the Kliprand area. This discovery was immediately followed up by a diversity of exploration activities, such as surface mapping, exploration geochemistry, geophysics (magnetics, induced polarization and electromagnetic polarization) and surface drilling, all of which came to an end around 1983.

Further activities, mainly in the form of field assessments, were thereafter undertaken by different teams of consulting companies in the following years. For example, Cooke (1989) reassessed the Hondekloof prospect by re-evaluating the existing data already used by the Okiep Copper Company Ltd. Anomalously high Cu, Ni and Co values were reported in the soil samples of the Hondekloof gossan outcrops and were found to be laterally extending beyond the sampling grid for at least 700 m. Both Cu and Co showed a dispersion of some 900 m down-slope, northwards, towards the nearby old riverbed located to the north of the Hondekloof gossan outcrops. Ni, in turn, showed a limited dispersion anomaly, and only formed a halo of about 400 m down-slope. With the erratic distribution of Pb, Zn and Mn, Co was considered as an important pathfinder to the Hondekloof nickeliferous orebody (Cooke, 1989). A brief inspection of the area was again undertaken by Rand Mines Ltd. in 1990, and followed by Gold Fields Ltd. which also had a re-look of the area in 1996.

The area was regionally mapped by Albat (1984) as part of a research mapping project under the sponsorship of the Precambrian Research Unit of the University of Cape Town. A detailed map, which straddles the discontinuous main gossan exposures on Hondekloof (1500 m × 600 m compiled to a scale of 1:2 000) was produced by the Okiep Copper Company Ltd. (in 1980). According to the technical report of Lehumo Resources Ltd. (2008), reconnaissance mapping of the Hondekloof gossan outcrops and surroundings was done by Taylor (1990) as part of an Honours project at the University of the Witwatersrand. Andreoli et al. (1991a; 1991b) broadly advanced the study of Taylor (1990) and briefly discussed the field relationships and petrogenetic aspects of some of the host lithological units based on field sketches. Hamman et al. (1996) re-investigated the area as part of an MSc study at some later stage, and also brought slight improvements to the detailed map produced by the Okiep Copper Company Ltd.

As mentioned earlier, an early drilling program was undertaken by Gold Fields of South Africa Ltd. in 1970. The program was again reactivated by Okiep Copper Company Ltd. during 1980 and 1982, and was done in two drilling phases in those respective years. A total of 29 diamond drill holes were drilled on 10 approximately parallel sections, totalling 2 619.6 m. Most boreholes were inclined towards the south with angles varying from -40 to -80°, with only two boreholes drilled vertically. Of the 29 boreholes drilled, 14 intersected sulphide mineralisation of significance. The drilling program was again rejuvenated in early 2005 by Lehumo Resources Ltd. under the name

Hondekloof Nickel project (Pty.) Ltd. A two-phase drilling program were initiated, with the first drilling phase starting in March 2006 and completed by mid-November of the same year. A total of 133 diamond drill holes were drilled on 33 approximately parallel sections spaced 50 m apart (with 20 m strikes on the drill lines, totalling 9 909.55m). The drill angles varied between -45 and -75° with 13 holes drilled vertically. Of the 133 boreholes drilled, roughly half of the holes intersected sulphide mineralization of significance. The second phase of drilling started in mid-November 2006 and was completed three months later (in February 2007). A total of 14 boreholes were drilled east of the first phase area and 22 west of the first phase area. This second drilling phase covered a distance of 7 km, and the boreholes were drilled in 36 locations spaced 200 m apart along strike.

Since the recovery of the borehole data several studies have been undertaken using different methods, mainly for assessing the economic viability of the deposit. Certain aspects such as pre-feasibility and feasibility studies, operational strategy, an economic model, geotechnical assessments as well as flotation test-work and logistics have already been completed and finalised by the Lehumo Resource Company Ltd. (since 2008). Although the production has currently been put on hold because the deposit is currently economically not viable (based on current economic standards), further studies are needed, particularly those that can provide clues as to further constraining the characteristics of the deposits and aiding understanding of the economic prospectivity of the area. The studies involving classification and vectoring are all yet to be done on this deposit. This work has therefore contributed in filling some of those gaps.

2. CHAPTER II

GEOLOGICAL SETTING

2.1 Regional Geological Setting

This study is based in the West Coast region of South Africa in the vicinity of the settlement called Kliprand (Albat, 1984) on the Nuwefontein Farm. The area is generally referred to as Namaqualand, and forms part of the Garies terrane (De Beer et al., 2010; Macey et al., 2011). The Garies terrane, together with the Okiep terrane, have been interpreted as the representative fragments or crustal blocks of Mesoproterozoic age, having rocks which formed or were deformed during the Namaquan orogenic event, at ~1200 to 1000 Ma (De Beer et al., 2010). Every rock which formed, or deformed, or the pre-existing rocks which have been tectonized during this particular tectonic event, in southern Africa, have been broadly interpreted to form part of a single metamorphic belt termed the Namaqua-Natal Mobile belt (Cornell et al., 2006; Eglinton, 2006; Colliston and Schoch, 2006; Moen and Toogood, 2007). Different names for this particular tectonic area and its subdivisions have frequently been given based on various interpretations offered by different authors. Stowe (1986), Raith et al. (2003), Cornell et al. (2006) and Ghavami-Riabi et al. (2008) referred to it as the Namaqua-Natal Metamorphic Province, whilst Matthews (1981), Taylor (1990), Eglinton (2006) and Colliston and Schoch (2006) preferred to use the name the Namaqua-Natal Mobile belt instead. However, this study follows the nomenclature of Namaqua-Natal Metamorphic Province as defined by Stowe (1986).

2.1.1 Geological evolution of the Namaqua-Natal Metamorphic Province

The Namaqua-Natal Metamorphic Province (NNMP), in southern Africa, is one of a number of medium to high-grade metamorphic belts of Mesoproterozoic age in sub-Saharan Africa (Thomas et al., 2000; Eglinton and Armstrong, 2003). Hoffman (1991) considered the Namaqua-Natal Metamorphic Province (NNMP) as being one of the dispersed remnants that formed part of the Mesoproterozoic orogenic systems in Africa, and has also marked the formation and break-up of the ~1.0-0.7 Ga supercontinent Rodinia (Groenewald et al., 1991; Jacobs et al., 1995; Dalziel et al., 2000). Its age spans between 1250 Ma and 950 Ma (Dalziel et al., 2000), and it formed a part of the Kalahari Craton of southern Africa (Jacobs et al., 1995; Grantham et al., 2001; Frimmel, 2004). It extends from southern Namibia south-eastwards through the Northern Cape Province of

South Africa, towards Kwazulu-Natal (on the eastern seaboard where it is truncated by the Indian Ocean), and generally covers nearly 35 to 40% of the landmass in the local geological framework of South Africa (Eglington, 2006; Fig. 2.1). Relatively old rocks, of Archean age, of the Kaapvaal craton, bound the province to its north and northeast (in a tectonic style represented by thrusting, trans-current faulting and magnetic anomalies- Fig. 2.1; Cornell et al., 2006), whilst the younger rocks of the Pan-African orogeny (represented by the Gariep and Saldania belts) truncate the province to the southwest and south (Fig. 2.1).

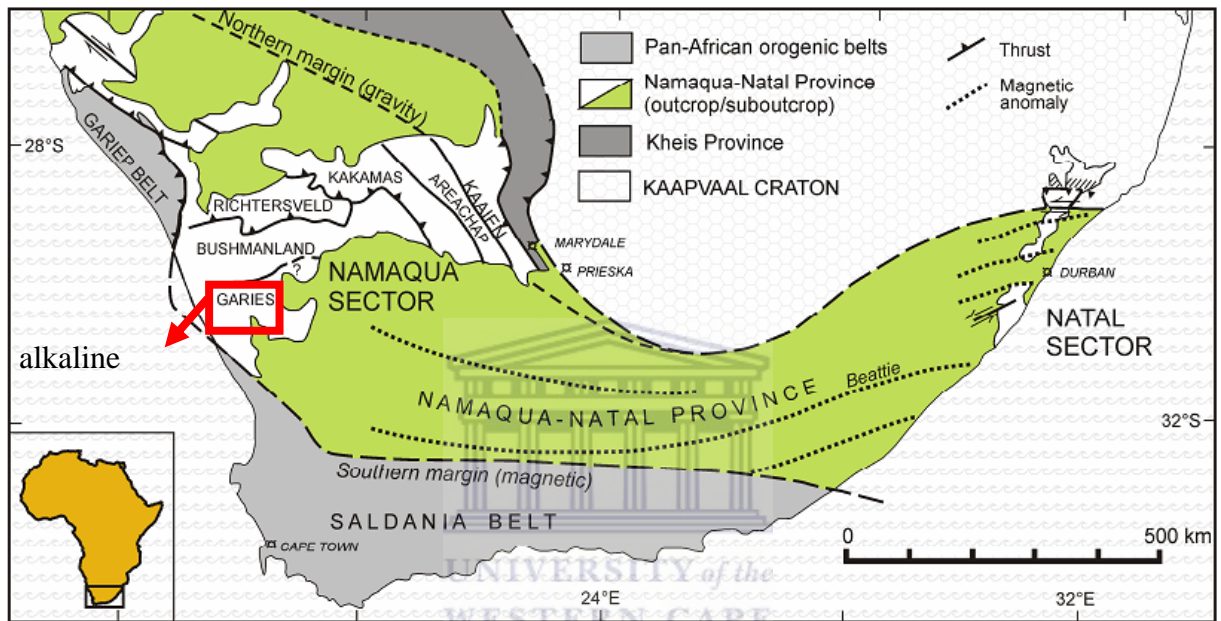


Figure 2-1: Simplified geological map of southern Africa, from Cornell et al. (2006)

Rocks of similar age and common characteristics have also been documented elsewhere (besides South Africa), for example, in Namibia (Becker et al., 2006), and in Botswana (Singletary et al., 2003), as well as in Mozambique (Grantham et al., 2003), Zambia (Hanson et al., 1988) as well as in Argentina (Thomas et al., 2000) and Antarctica (Groenewald et al., 1991). But in relation to the geographical subdivision of South Africa, where this study is based, the NNMP is only well represented in two of the country's nine provinces. It outcrops extensively (1) in the Northern Cape Province, covering a region of approximately 100 000 km² in areal extent, as well as (2) in KwaZulu-Natal where the area covered extends to about 20 000 km² (Stowe, 1983; Hartnady et al., 1985; Thomas et al., 1994).

In general the NNMP is subdivided into two broad and coeval sectors namely the Namaqua Sector (or Namaqualand) in the west and the Natal Sector in the east (Nicolaysen and Burger, 1965; Stacey and Kramers, 1975; Pettersson et al., 2007; Fig. 2.1). A regional gravity and magnetic survey studies carried out by De Beer and Meyer (1984), together with crustal xenolith evidence from kimberlite diatremes in Lesotho and a few deep boreholes drilled by Soekor (Eglinton and Armstrong, 2003, and references therein), show that the two sectors are part of a single and continuous (1400-km-long and 400-km wide) arcuate orogenic belt, with each sector having rocks which formed, or deformed, during the main episodes of the Namaqua-Natal orogenic event, at ~1200 to 1000 Ma.

Occupying the eastern portion of the NNMP is the Natal Sector (McCourt et al., 2006; Fig. 2.1), stretching for 1500 km long (Gose et al., 2004) and rimming the south-eastern margin of the Archean Kaapvaal craton (Grantham et al., 2000a; Jacobs et al., 1993; Jacobs and Thomas, 2001; McCourt et al., 2006). Thomas (1989) subdivided the Natal Sector, from north to south, into three tectonically distinct terranes (namely the Tugela, Mzumbe and Margate terranes). Jacobs et al. (1993) elaborated on this subdivision of Thomas (1989), and pointed out that the boundaries between the terranes are everywhere tectonic (Matthews, 1981; De Beer and Meyer, 1984; Jacobs et al., 1993; Thomas et al., 2000; McCourt et al., 2006).

Located in the western portion of the NNMP is the Namaqua Sector, which covers an area of approximately 22 000 km² (McClung, 2008). The Namaqua Sector is crosscut by several large transcurrent faults which, according to Joubert (1980, 1986) and Stowe (1989), allow the Namaqua Sector to be subdivided into: (1) the Kheis, (2) the Gordonia, (3) the Bushmanland and (4) the Richtersveld Subprovinces (Hartnady et al., 1985; Pettersson et al., 2009; Fig. 2.2).

The Kheis sub-province occupies the portion which serves as the border between the Archean Kaapvaal Craton and the Namaqua Sector (Fig. 2.2). It comprises highly metamorphosed sequences which, according to van Niekerk (2006), have been tectonised to amphibolite facies conditions. These rocks have ages ranging between 1600 to 1900 Ma (van Niekerk, 2006), and are reported to have been deformed between 1100 to 1300 Ma, during the Namaquan Orogeny (SACS, 1980; Moen, 1999).

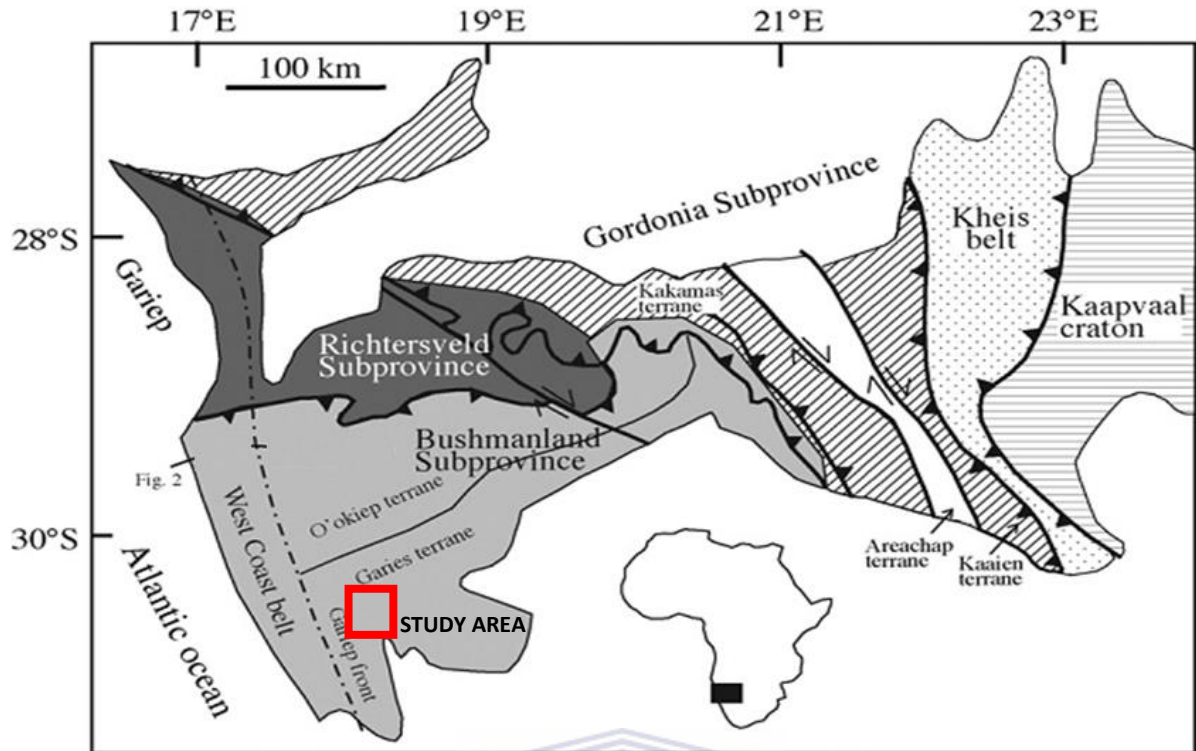


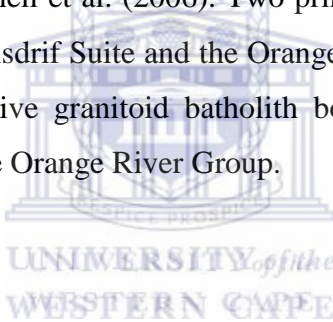
Figure 2-2: Terrane map of the Namaqua Sector (from Hartnady et al. (1985) and Thomas et al. (1994)). The overall study area region is shown by a red square.

To the west of the Kheis Subprovince is the Gordonia Subprovince of the Namaqua Sector (Fig. 2.2). Its contact with the Kheis Subprovince to the east is marked by a number of eastwards-directed subduction configuration zones (Cornell et al., 1990a; Pettersson et al., 2007; Cornell and Pettersson, 2007; Bailie et al., 2010). Bailie et al. (2011) advocated that the above configuration zones mark the subduction history of the Namaqua Sector subducting underneath the Kaapvaal Craton. According to Van Bever Donker (1980), the Gordonia Subprovince can be further subdivided into the Areachap terrane and the Kakamas terrane. Both terranes are comprised of highly metamorphosed metasedimentary rocks which are metamorphosed to upper amphibolite to granulite facies conditions (Bailie et al., 2011). The Areachap terrane has rocks dating from 1.29–1.24 Ga in age (Cornell et al., 1992; Cornell and Pettersson, 2007), whilst those of the Kakamas terrane have ages limited between 2.0 Ga to 1.10 Ga (Thomas et al., 1994).

To the west of the Gordonia Subprovince is the Bushmanland Subprovince, which occupies most of the central, southern and southwestern portion of the Namaqua Sector (Fig. 2.2). Cornell et al. (2006), and Pettersson et al. (2008) considered the Bushmanland Subprovince to be the largest

subprovince in the Namaqua Sector (i.e. an areal coverage of some 60 000 km²). This subprovince is, however, also considered to be the most poorly exposed, and the least understood domain of all the domains of the Namaqua Sector's geology (Schmitz and Bowring, 2004). Following the simplified subdivision of Raith et al. (2003) and Andreoli et al. (2006), the Bushmanland Subprovince can be subdivided from north to south into: (1) the Aggeneys, (2) Okiep, (3) Garies and (4) Steenkampskraal terranes. Each of these terranes is different in terms of its local geology (Raith et al., 2003). They are, however, marked by the presence of metasedimentary sequences which are intruded by a series of small mafic suites (Clifford et al., 1981; Andreoli et al., 2006).

Adjacent to the Bushmanland Subprovince, to the north and west, is the Richtersveld Subprovince (Fig. 2.2). According to Reid (1979) and Reid et al. (1987), the Richtersveld Subprovince is one of the few areas in the Namaqua Sector which preserves some of the oldest rocks in the history of the Namaqua-Natal Metamorphic Province. A comprehensive subdivision of the Richtersveld Subprovince was provided by Cornell et al. (2006). Two principal components, called domains, were determined, namely the Vioolsdrif Suite and the Orange River Group. The Vioolsdrif Suite is characterized by having extensive granitoid batholith bodies which intruded the volcano-sedimentary sequences found in the Orange River Group.



2.2 Local Geological Setting

2.2.1 The Kliprand Area

Geologically the Kliprand area is situated in the southern portion of the Namaqua Sector, along the mountainous escarpment that separates the inland Bushmanland plateau from the sandy area of the west coast plain (Baars, 1990). The area preserves rocks that outcrop partly in the lowermost sequences of the Karoo Supergroup, and partly in the Namaqua-Natal Metamorphic Province (Macey et al., 2011). The western and south-eastern parts of the area are predominantly underlain by intensely deformed and high-grade ortho- and para-gneisses that form part of the Garies terrane of the Namaqua Sector (Albat, 1983). Within this zone, intrusions of voluminous post-tectonic granite and granitoid batholiths occur in various sizes (Moore, 1983; Moore and Verwoerd, 1985; 1989; Macey et al., 2011). Diverse varieties of metamorphosed mafic rocks and magmatic rocks, having ages from Mesoproterozoic to Recent, have also been mapped by Macey et al. (2011).

The eastern part of the area is underlain by the Permian-to-Carboniferous sequences of both the Dwyka and Ecca Groups of the Karoo Supergroup (Macey et al., 2011). These rocks are relatively unmetamorphosed and are the only exposed basal units that form part of the Karoo Supergroup in the area (Macey et al., 2011).

The Namaqua Sector comprises a number of tectonostratigraphic terranes separated by major tectonic structures distinguished on the basis of their lithostratigraphy, tectonic histories and metamorphic grades (Hartnady et al., 1985; Thomas et al., 1994; Andreoli et al. 2006). Of these terranes, only the Garies terrane outcrops cover a large lateral extent in the Kliprand area (Albat, 1989).

A comprehensive geological study of the Kliprand area was undertaken by Albat (1983, 1984, 1989) and Macey et al. (2011). According to these authors, six to seven main stratigraphic units are identified in the Kliprand area. Two criteria, (1) based on the type of lithologies preserved, and (2) based on their ages relative to the age of the main Namaqua deformation (at ca. 1.15 Ga.), D₂ (Joubert, 1971; Van Aswegen, 1974) are used to separate these units.

In relation to this D₂ deformation event, pre-, syn- to post-tectonic units are generally identified based on: (1) the way in which the orientation of their fabrics (foliation + lineation) correspond with the orientation of E-W trending foliations developed during the main phase of the Namaquan event (Macey et al., 2011).

The Mesoproterozoic intrusive rocks are dominated by granitoids which are subdivided into two major suites, the pre- to syn-tectonic Little Namaqualand Suite and the late- to post-tectonic Spektakel Suite (SACS, 1980; Joubert, 1986). The pre-tectonic mafic granulites are referred to as the Oorkraal Suite, whereas the group of post-tectonic intermediate to mafic intrusive rocks are collectively referred to as the Koperberg Suite (SACS, 1980; Clifford et al., 1995).

Gneisses with clear supracrustal precursors are included in the Kamiesberg Group, following the suggestion of Moore (1989). The five lithodemic units recognised here are pelites, semi-pelites, quartzitic rocks, calc-silicates and marbles, and heterogeneous migmatitic grey biotite-quartz-feldspar gneisses. It remains unclear whether the pink quartzofeldspathic gneisses have either intrusive igneous or sedimentary precursors. As such it has therefore not been included in either

the Little Namaqualand Suite or the Kamiesberg Group, and has thus been grouped separately, on its own, as the Lekkerdrink Gneiss (Moore, 1989).

While the origins and ages of certain units, such as the Lekkerdrink Gneiss, are very enigmatic and remain controversial, those of others, such as the Ibequas granite, are believed to have been the products of dehydration melting (that took place during the peak metamorphism associated with the Namaquan event). Table 2.1 provides a comprehensive summary of the lithological units (in their relative geochronological order) documented in the Kliprand area.

2.2.2 Metamorphism

The supracrustal rocks of the Bushmanland Subprovince in the Kliprand area have undergone granulite-facies metamorphism (Albat, 1984). This granulite-facies zone is defined by the following pelitic assemblage: quartz-K-feldspar-cordierite-plagioclase-garnet-sillimanite-opaques \pm biotite, which most likely formed by the following prograde dehydration melting reaction (Waters, 1986a):



This dehydration reaction marks the transition from upper-amphibolite to granulite facies conditions (Waters and Whales, 1984; Waters, 1986b). Further evidence for this transition was determined by the presence of local partial melts in the rocks (for example the development of abundant coarse-grained quartz-feldspar \pm garnet segregations, giving the rock a migmatitic appearance).

Most rocks in the area fall within this upper granulite-facies subzone and have peak metamorphic conditions of $\sim 750\text{--}870^\circ\text{C}$ and 4.5–6 kbars (Albat, 1979, 1984; Waters, 1986b, 1989; Baars, 1990; Norwicki et al., 1995). The advance to granulite-facies conditions was marked by the dehydration of hydrous assemblages, the formation of two-pyroxene mafic granulites and the onset of partial melting (Waters, 1989; Baars, 1990).

Table 2-1: Rocks of the Garies terrane in the Kliprand area (Adapted after Joubert & Waters, 1980; Zelt, 1980; Albat, 1984; Macey et al., 2011)

Regional coverage	Groups and Suites	Rock Types	Remarks
The Garies terrane in the Bushmanland Region of the Namaqua-Natal Province	Spektakel Suite	Ibequas Granite	Characteristically megacrystic and locally charnockitic. Predominantly comprise sheet-like bodies of weakly foliated, medium grained equigranular K-feldspar leucogranite with very low biotite contents. Share common resemblance with the Little Namaqualand Suite, but differ from the latter by being less deformed, hence post-tectonic. Occur as voluminous and largely megacrystic late to post-tectonic granites and charnockite, intruded into the earlier formed grey gneisses and the Little Namaqualand Suite orthogneisses.
		Osdam Granite	
		Klein-Lieslap	
		Charnockite	
		Kootjiesfontein Granite	
		Kliphoek Granite	
Kamiesberg Group	Kamiesberg Group	Garies Granite	Pre-tectonic supracrustal rocks of the Bushmanland Subprovince that occur with east-west trending regional tectonic fabrics. This group derived its name from the Kamiesberg Mountain, a region within which several belts of supracrustal rocks occur.
		Lepel se Kop Granite	
		Brandkraal Granite	
		Uilklip Granite	
		Banke Granodiorite	
		Burton's Put Granite	
Oorkraal Suite	Oorkraal Suite	Platklip Granite	Deformed and metamorphosed mafic rocks of the Namaqua Sector. Occur as melanocratic black, fine to medium grained rocks, and have moderate to strong granoblastic texture and locally a compositionally banded texture. Are pre-tectonic in age.
		Brakfontein Granite	
		Meta-Pelitic Gneiss	
Little Namaqualand Suite	Little Namaqualand Suite	Meta-Psammitic Gneiss	Predominantly composed of grey, pre-tectonic supracrustal orthogneisses of the Bushmanland Subprovince. Characterised by their granitic composition (orthogneisses), and their pre- to syn-tectonic age, indicated by strong penetrative augen and streaky gneiss fabrics. Further characterised by being compositionally heterogeneous, and occur in a variety of textures.
		Calc-silicate and Marble	
		Metaquartzite	
		Grey Gneiss Complex	
		Landplaas Gneiss	
		Karagas Gneiss	
Lekkerdrink Gneiss	Lekkerdrink Gneiss	Darterpoort Gneiss	Characterized by a pink colour, occurring as a group of texturally variable quartzofeldspathic gneisses. It is unclear as to whether it was originated from an intrusive or sedimentary protolith. Hence unclassified.
		Grootberg Gneiss	
		Mesklip Gneiss	

2.2.3 Structure

The structural sequence for the Bushmanland Subprovince was originally established by Joubert (1971). Albat (1984) and Macey et al. (2011) re-advanced the study of Joubert (1971) around the Kliprand area. Following the interpretation of these authors, at least three main phases of high-grade ductile deformation have been identified in southwestern Namaqualand (Joubert, 1971, 1986; Baars, 1990; Jackson, 1998; Grantham, 2000a, 2000b), and most particularly in the Kliprand area (Albat, 1984; Macey et al., 2011). D₁ is described as an early deformation phase, followed by D₂ (the main Namaquan event), and two late folding events (D₃ and D₄).

The metasedimentary and metavolcanic rocks display a gneissic banding which is folded by, and therefore predates, the main regional D₂ fold generation. This banding is interpreted either as the original primary layering (bedding), or as a tectonically produced surface (S₁) (Albat, 1984). Evidence of D₁ episode is observed as rootless isoclinal intrafolial folds preserved within the gneissic layering of the supracrustal rocks (Macey et al. 2011).

The second deformation phase (D₂) is considered as the principal phase of the Namaquan orogeny (Joubert, 1971). In comparison to D₁, the D₂ deformation is characterised by large-scale, large-amplitude and short-wavelength isoclinal folding which produced a regional, generally E–W-trending, penetrative S₂ foliation (gneissic banding) and an L₂ stretching lineation or mineral elongation (Joubert, 1971, 1986). Albat (1984) interpreted this D₂ deformation as being an isoclinal structural event. The gneissic fabric is observed in all the pre-tectonic rock types, but is best developed in the pre-tectonic gneisses of the Little Namaqualand Suite (Albat, 1984). Strongly recrystallized elongate K-feldspar augen porphyroblasts and the preferred orientation of platy minerals, especially biotite (streaky and stripy textures), define the S₂ fabric in these rocks.

The D₃ deformation event is characterised by kilometre-scale E–W-trending F₃ folding which produced upright to inclined shallowly-plunging open folds (Macey et al., 2011). The S₃ foliation planes are commonly filled with 2–3-cm-thick un-deformed equigranular white to cream-coloured quartz-feldspar ± biotite ± magnetite leucosomes (Macey et al., 2011). Although S₂ and S₃ are roughly coaxial, the dip of S₃ with respect to S₂ is variable across the F₃ folds (Grantham, 2000a, 2000b; Macey et al., 2011).

The D₄ phase is associated with small-amplitude/large-wavelength, very-large-scale, NW-trending open folds which are monoclinical in places and in general have the appearance of gentle megascale warping (Albat, 1984). The D₄ deformation is restricted to folding of all previously existing structures, but did not result in the production of any new penetrative foliations.

2.2.4 The Hondekloof prospect

Figure 2.3 indicates the location of the Hondekloof prospect within the simplified geological map of the Bushmanland Subprovince.

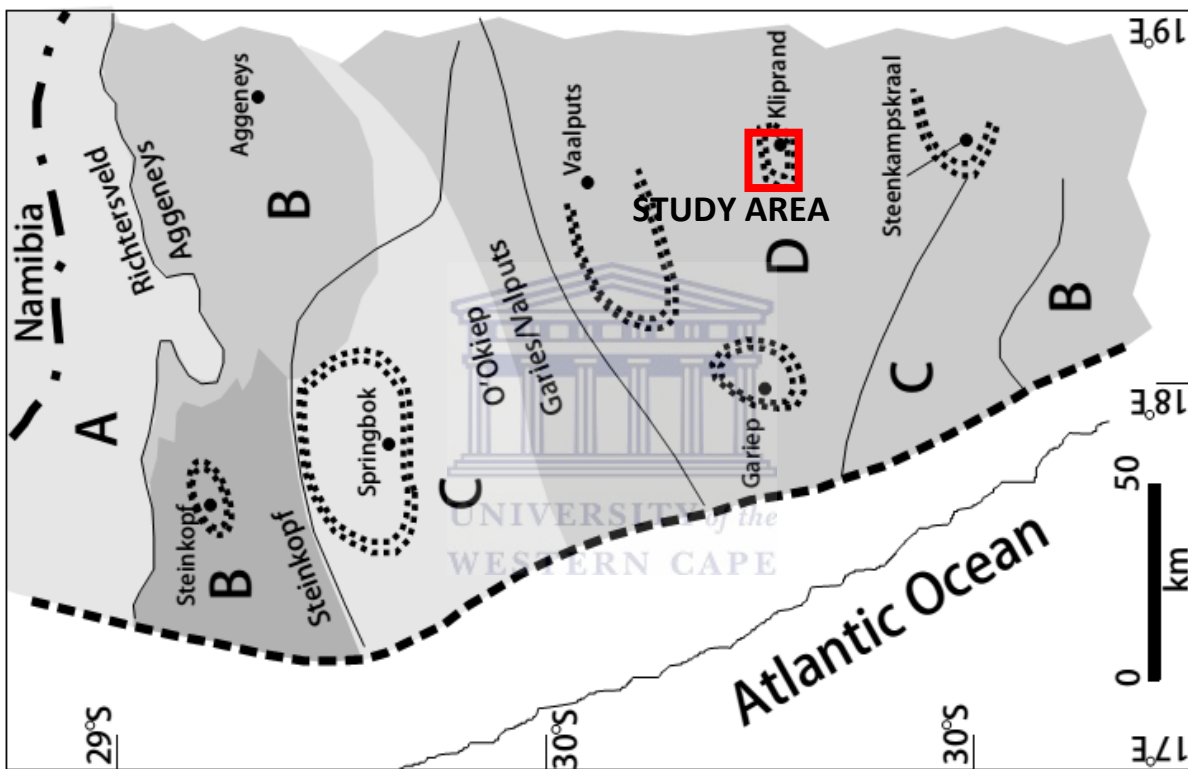


Figure 2-3: A simplified geological map of the southwestern and western portion of the Namaqua Sector (modified after Andreoli et al., 2006). Tectonic terranes are shown in variable shading. Double dotted lines indicate clusters of Koperberg suite and related mafic intrusions. Solid lines show metamorphic facies boundaries (A: greenschist, B: amphibolite, C: low-T granulite, D: high-T granulite). Short, dashed line near the coastline indicates staurolite zone (Pan African overprint). The study area is indicated by means of a red rectangle

The deposit sits within the moderate relief granitic hills which forms the heart of the Bushmanland plateau (Andreoli et al., 1991a; Hamman et al., 1996). The geology of the Hondekloof deposit and surroundings was investigated and broadly described by Taylor (1990), Andreoli and Moore (1991), and Hamman et al. (1996). Following the interpretation of these authors, the Hondekloof

deposit, on the surface, is marked by a series of fourteen to fifteen discontinuous gossan outcrops extending 200 m wide and 3.5 km long. These gossans are reported to have been spatially associated with small attenuated and flattened mafic bodies forming part of the Nuwefontein Suite and Oorkraal Suite (Albat, 1984; Taylor 1990). According to Bekker (1980) and Albat (1984) these rocks are part of the pre- to syn-tectonic intrusive rocks metamorphosed to granulite facies conditions, and tectonically deformed during the main isoclinal structural event of the Namaquan Orogeny.

As illustrated in Fig. 2.3, the Kliprand area falls under the spinel + quartz upper granulite facies domain (D in Fig. 2.3) within the six metamorphic facies domains established by Waters (1991) (see explanation of the facies in Fig. 2.3). Because of that, it has been interpreted to represent a deeper crustal level than its neighbouring blocks around the Springbok (Maier et al., 2013, Fig. 2.3). The deposit is underlain by large bodies of megacrystic charnockite and charnockitic orthogneiss, mafic two-pyroxene granulites of the Oorkraal Suite (Table 2.1; de Beer et al., 2002) and an easterly-trending belt of predominantly supracrustal rocks which consists of calc-silicate rocks, metapelites, biotite-garnet gneisses, quartzite and ferruginous rocks belonging to the Kamiesberg Subgroup (de Beer et al., 2002; Albat 1984; Moore 1989). According to Andreoli and Moore (1991) the deposit is generally hosted in small attenuated and flattened regional fabric-parallel noritoid bodies, which, according to these authors, are not well characterized.

3. CHAPTER III

METHODOLOGY

3.1 Introduction

This project seeks to examine the petrography, petrology and whole rock geochemistry of the host rocks to the Hondekloof prospect and thereby constrain and characterize both the deposit and its host rocks. It involves firstly logging and sampling of key exploration boreholes which have intersected sulphide mineralization of significance and secondly make a meaningful contribution based on analysing, evaluating and interpreting the data generated from petrographic and geochemical studies.

3.2 Data collection

Six exploration boreholes were logged, sampled and examined at the deposit site in Kliprand. Logging was carried out in each borehole employing such criteria as: (1) changes in grain size, (2) fabrics or textures, (3) colour, (4) litho-types, and type of contacts, (5) contact angle and (6) additional remarks, to establish and classify the different varieties of the lithology encountered in the boreholes. Sampling was also carried out concurrently and the representative specimen (of ca. 20 cm length) for each lithology measured was sampled.

3.3 Petrography

A total of forty-five polished thin section slides were prepared and examined using a number of in-house transmitted and reflected light petrographic microscopes. The physical working conditions and the standards of the microscopes used are described in detail in Raith et al. (2012), and are also illustrated in Figure 3.1. The rocks are described in two sections, firstly as they appear in the cores and secondly as they appear in thin section. The estimated mineral mode for each lithology has been reported, with their abundances being given as a range (e.g. from - to ~ wt. %).

3.4 Geochemistry

A total of forty-two samples plus three duplicates were prepared for XRF and Laser Ablation-ICP-MS analyses. The samples were crushed and milled according to the standard geochemical sample preparation procedures. The major element compositions were analysed by X-ray fluorescence

(XRF) spectrometry on fused glass beads prepared from 5 g per sample. The XRF spectrometer employed a Rh tube at a power output of 3 kW prepared with La-free flux. Loss On Ignition (LOI) calculations, which determine the amount of volatiles in a sample, is calculated by determining the weight difference after ignition to 1000°C. The XRF spectrometer uses the combination of both a gas-flow proportional counting detector and a scintillation detector to cover the analysis of all major elements. Detection limits for the XRF spectrometer are typically lower than 0.5 ppm (0.00005%), and a wide range of international (NIST®) and national (SARM®) standards were used in the calibration procedures.

Complimentary to the major element analysis by XRF spectrometry, a complete suite of trace and rare earth element (REE) analyses were determined using Laser Ablation ICP-MS. In this technique, a Resonetics 193nm Excimer laser was connected to an Agilent 7500 ICP-MS for laser ablation work with a solution of 0.9L/min Argon + 0.004L/min Nitrogen as carrier gas. The samples were analysed on the same polished pressed powder pellets (mounts) previously prepared for XRF fusion. Accuracy and precision were monitored through the repeated analyses of in-house and international standards and duplicate samples. Effort was made to report analytical errors in the relevant tables in chapter 5 of the geochemistry. Detection limits of most trace elements analysed were equal to, or less than 0.1 ppm, except for Th and Co (0.2 ppm), Sr (0.5 ppm), Sc and Zn (1 ppm), and V (8 ppm). Most of the REE had detection limits less than or equal to 0.05 ppm, with the exceptions being Nd (0.3 ppm), and La and Ce (0.1 ppm).

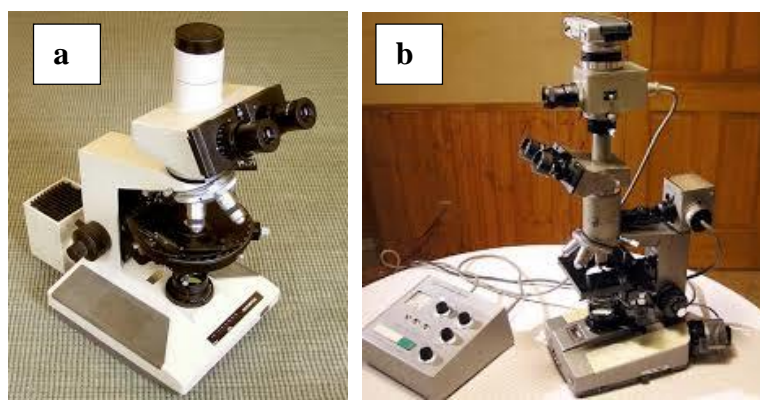


Figure 3.1 Illustration of the polarized microscope used for petrographic study. (a): Reflected light

4. CHAPTER IV

LITHOLOGICAL DESCRIPTION

4.1 Introduction

The results obtained from core and petrographic observations are reported together in order to avoid duplication. A summary of the borehole locations within the extensions of the orebody are shown both in Figure 4.1 and listed in Table 4.1.

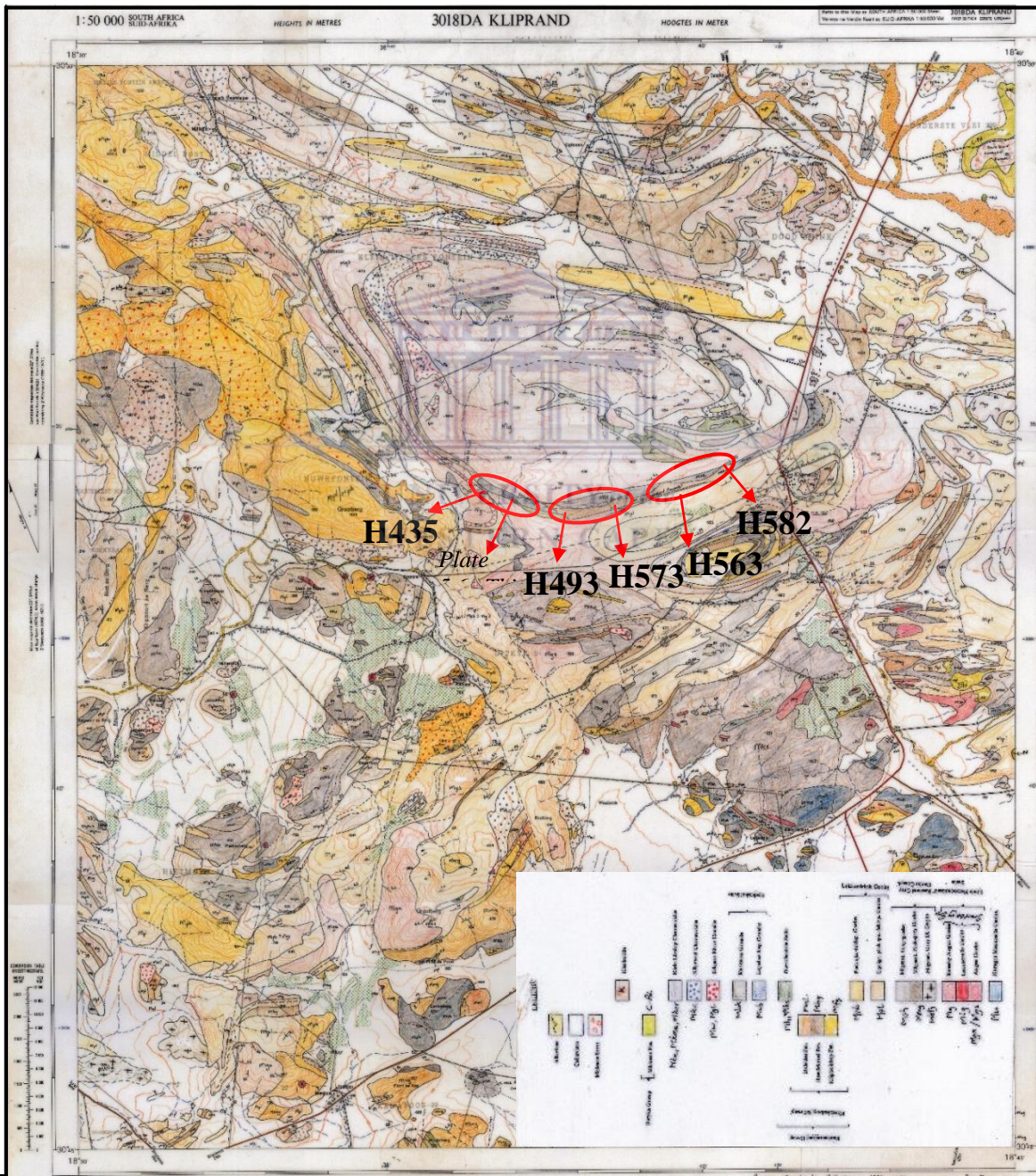


Figure 4-1: Three lenses of the Hondekloof prospect on the simplified geological map of the Kliprand area. (Modified after Macey et al., 2011).

Table 4-1: List of boreholes examined and their location within the orebody

Location:	Borehole ID
Eastern extension:	H563, H582
Central extension:	H493, H573
Western extension:	H435, H445

Figure 4.1 is a schematic map showing the surface delineation of the Hondekloof prospect and the locations of the three gossanous outcrops for which the lateral extensions of the Hondekloof orebody (on the surface) is defined (Macey et al., 2011). The lithologies are firstly described individually in order to give their characteristics and are secondly shown on simplified modelled strip logs in order to relate their vertical distribution in various boreholes. The classification and nomenclature of the lithologies are based on the criteria specified in chapter 3. Effort was also made to summarize the petrographic descriptions (mineral composition, grain size, textures etc.) of all the lithologies in Table 4.2. To achieve a more meaningful description of lithologies and acknowledge their highly metamorphosed nature, the rocks are named in accordance with the classification scheme of the British Geological Survey (Robertson, 1999) as adopted by Bailie et al. (2010b).

4.2 Meta-gabbronorite

4.2.1 Core description

The meta-gabbronorite shows a weak to moderate foliation as well as numerous variations in the way in which it occurs in the different boreholes. Four varieties are present in the boreholes listed in Table 4.1.

Certain varieties display a dark-brown to green colouration in which the biotite content is high (20-25 Wt.%) (Plate 4.1a). Other varieties, especially those hosted in borehole H582, have a generic dark green colouration and contain a large amount of pyroxene (25-30 Wt.%) (Plate 4.1b). Some are also highly mineralized (sulphide content = 20-35 wt.%), with greater amounts of pyrrhotite and pyrite as well as lesser amounts of pentlandite and chalcopyrite (Plate 4.1c). An

additional variety, here termed a meta-norite (Plate 4.1d), is also present, which specifically occurs in borehole H193.



Plate 4-1: Core photographs of the meta-gabbronorite. Photos a, b and c show the different varieties of the meta-gabbronorite. Photo d shows the variety described as meta-norite.

4.2.2 Petrographic description

The meta-gabbronorite is dominated by two pyroxenes, with hypersthene, which hosts several inclusions of hornblende, biotite and opaque minerals, the more abundant. Two metamorphic textures, firstly granoblastic, and secondly decussate, consistently occur in the meta-gabbronorite. There are also two generations of biotite with different grain shapes, a euhedral and an embayed type of biotite. The latter type is uncommon and, together with hornblende, occurs as replacement products of orthopyroxene. Hornblende alone also replaces the orthopyroxene locally. A sample reported as meta-norite (Plate 4.2a) from borehole H493, is characterized by only having a single

type of pyroxene (orthopyroxene) (Plate 4.2a) rather than two types (orthopyroxene and clinopyroxene) which are seen in the meta-gabbronorite samples (Plate 4.2b).

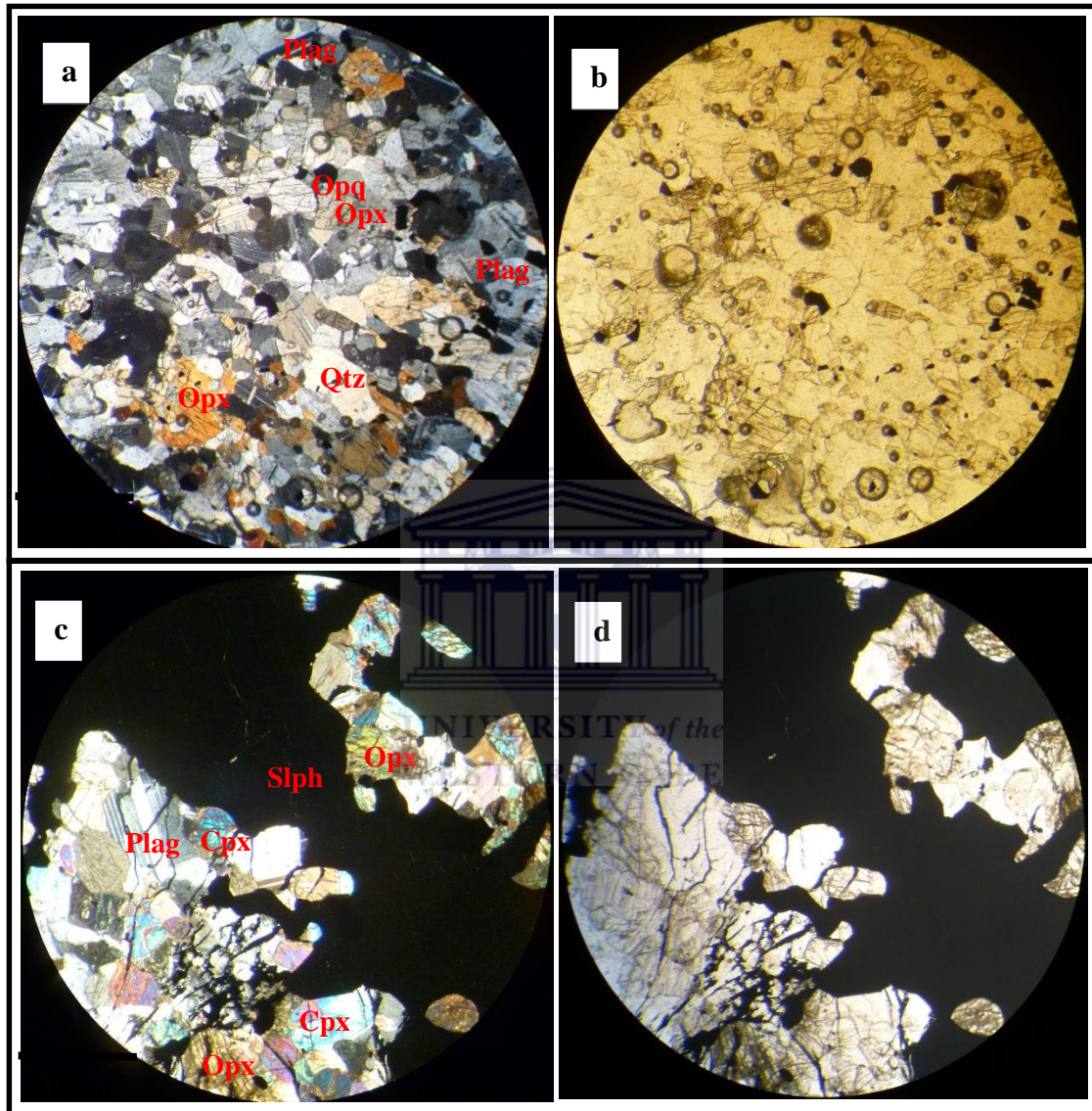


Plate 4-2: a and b: Thin section photomicrographs of a meta-norite at the Hondekloof deposit. Notice the lack of clinopyroxene in the thin section (a). Granoblastic texture (nearly equigranular-equidimensional crystals) (taken in crossed polarized light). c and d)-Thin section photomicrographs of a mineralized metagabbronorite. Notice how sulphides account for between 40 and 45 % of the rock volume. Opx: orthopyroxene, Cpx: clinopyroxene, Plg: plagioclase, Qtz: quartz. Opq: opaque mineral. Coloured photographs (a and c) are taken in crossed polarized light, and black and white photographs (b and d) in plane polarized light.

Table 4-2: Summarized petrographic descriptions of the host lithologies to the Hondekloof deposit

Litho-type	Mineral assemblage in vol.%	Textures, alteration & grain sizes	Boreholes
Meta-gabbronorite	<p>Primary: orthopyroxene (15-20 vol.%) and clinopyroxene (5-8 vol.%), plagioclase (30-35 vol.%), biotite (10-15 vol.%)</p> <p>Secondary: hornblende (\pm 4-5 vol.%), quartz (\pm 4-5 vol.%), phlogopite (\pm 1-2 vol.%), andalusite (\pm 2-3 vol.%) and opaque minerals (\leq 2-3 vol.%)</p> <p>Accessories: Sphene (titanite) and epidote</p>	<p>Textures: granoblastic, decussate and poikiloblastic, weakly foliated</p> <p>Alterations: uralitization, biotitization</p> <p>Grain size: coarse grained (1.0 to 9.0 mm)</p>	H582, H573, H563, H493, H445, H435
Garnetiferous quartzofeldspathic rock	<p>Primary: quartz (25-30 vol.%), alkali feldspar (orthoclase) (20-25 vol.%), garnet (almandine) (20-23 vol.%), plagioclase (5-6 vol.%), cordierite (5-6 vol.%), biotite (5-8 vol.%)</p> <p>Secondary: muscovite (3 vol.%), microcline (\pm 2-3 vol.%) opaque minerals (\pm 1-2 vol.%), sillimanite (2-3 vol.%)</p> <p>Accessories: chlorite and sericite</p>	<p>Textures: porphyroblastic and poikiloblastic</p> <p>Alterations: Sericitization and chloritization</p> <p>Grain size: coarse grained (\geq 7.0-9.0 mm)</p>	H563, H493, H445, H435
Biotite gneiss	<p>Primary: alkali feldspar (orthoclase) (25-30 vol.%), quartz (20-25 vol.%), cordierite (8-10 vol.%), biotite (10-12 vol.%)</p> <p>Secondary: garnet (10-13 vol.%), plagioclase (5-6 vol.%), andalusite (\pm 1-2 vol.%) and opaque minerals (1-2 vol.%)</p> <p>Accessories: epidote and sericite</p>	<p>Textures: foliation, granoblastic, poikiloblastic, recrystallized and intracrystalline deformation textures</p> <p>Alterations: Sericitization, chloritization and saussuritization</p> <p>Grain size: fine to medium grained (1.5 to 0.1 mm)</p>	H582, H563, H493, H445, H435

Table 4.2 (Cont.) Summarized petrographic descriptions of the host lithologies to the Hondekloof deposit

Litho-type	Mineral assemblage in vol.%	Textures, alteration & grain sizes	Boreholes
Feldspathic biotite garnet gneiss	Primary: garnet (15-17 vol.%), orthoclase (22-26 vol.%), quartz (26-32 vol.%), biotite (8-10 vol.%). Secondary: sericitized plagioclase (4-7 vol.%), microcline (1-2 vol.%), staurolite (3-4 vol.%), cordierite (3-4 vol.%) Accessories: calcite, apatite, pyrophyllite	Textures: foliation, poikiloblastic, granoblastic and vermicular textures Alterations: Sericitization Grain size: fine to medium (2.3 to 3.0 mm)	H563
Pink gneiss	Primary: orthoclase (30-35 vol.%), quartz (15-20 vol.%), biotite (20-25 vol.%), cordierite (10-13 vol.%), Secondary: microcline (\pm 2-3 vol.%), garnet (\pm 5-6 vol.%), sericitized plagioclase (\pm 5-6 vol.%) and opaque minerals (\pm 1-2 vol.%). Accessories: N/A	Textures: foliation Alterations: Sericitization, plagioclase alteration to clay minerals Grain size: fine to medium grained (\leq 2.5 to 1 mm)	H582, H573, H563
Meta-syenite	Primary: alkali feldspar (60-65 vol.%), biotite (10-12 vol.%), sericitized plagioclase (5-10 vol.%), orthopyroxene (3-5 vol.%), quartz (3-5 vol.%), hornblende (\pm 5-10 vol.%), Secondary: opaque minerals (\leq 1-1.5 vol.%) Accessories: chlorite and epidote	Textures: interlocking, decussate Alterations: chloritization, uralitization and saussuritization. Grain size: coarse grained (5 to 6 mm)	H573, H435
Enderbite	Primary: plagioclase (30-35 vol.%), orthoclase (35-40 vol.%), orthopyroxene (5-10 vol.%) Secondary: microcline (3-4 vol.%), quartz (4-5 vol.%), sulphides (5-10 vol.%). Accessories: epidote	Textures: interlocking, decussate and poikiloblastic Alterations: Sericitization and saussuritization. Grain size: coarse grained (2.0 to 6 mm)	H582, H493

4.3 Garnetiferous quartzofeldspathic rock

4.3.1 Core description

The garnetiferous quartzofeldspathic rock is a light coloured, coarse grained, garnet-rich unit. Garnet porphyroblasts commonly occur in large (2-3 cm) aggregates and give the rock a conspicuous, spotted appearance (Plate 4.3a). The garnet porphyroblasts, furthermore, host various inclusions of biotite, muscovite and, locally, sillimanite, and are characteristically poikiloblastic (Plate 4.3b). Mafic minerals, such as pyroxenes and amphibole, are lacking and the rock has the largest grain size of all the lithologies encountered in the different boreholes. Consequently, it is consistently porphyroblastic throughout. Although quartz and alkali feldspar are the major minerals present, locally they may constitute less than 45wt.% in some boreholes (Plate 4.3b); in these cases garnet constitutes up to 50wt.% of the rock volume. Many of the varieties of this garnetiferous quartzofeldspathic rock commonly occur as thickened veins (melt products) within the other reported litho-types.



Plate 4-3: Core photograph of the two varieties of the garnetiferous quartzofeldspathic rock.

4.3.2 Petrographic description

The garnetiferous quartzofeldspathic rock is characterized by containing remnants of several minerals (such as orthoclase and biotite) which have cannibalized to form almandine garnet (Plate 4.4). The garnet has also grown much larger than the other minerals (a poikiloblastic texture) (Plate 4.4a). Polygonization texture is also common, especially in quartz-dominated samples. Undulose extinction is consistent and well displayed where quartz and orthoclase are abundant. Orthoclase porphyroblasts show internal fracturing indicating intracrystalline deformation. Nearly all the minerals are angular to sub-angular in shape, with the exception of

garnet, which is euhedral (Plate 4.4a). Weathered orthoclase is sericitized (Plate 4.4a), whilst chlorite replaces biotite (Plate 4.4a).

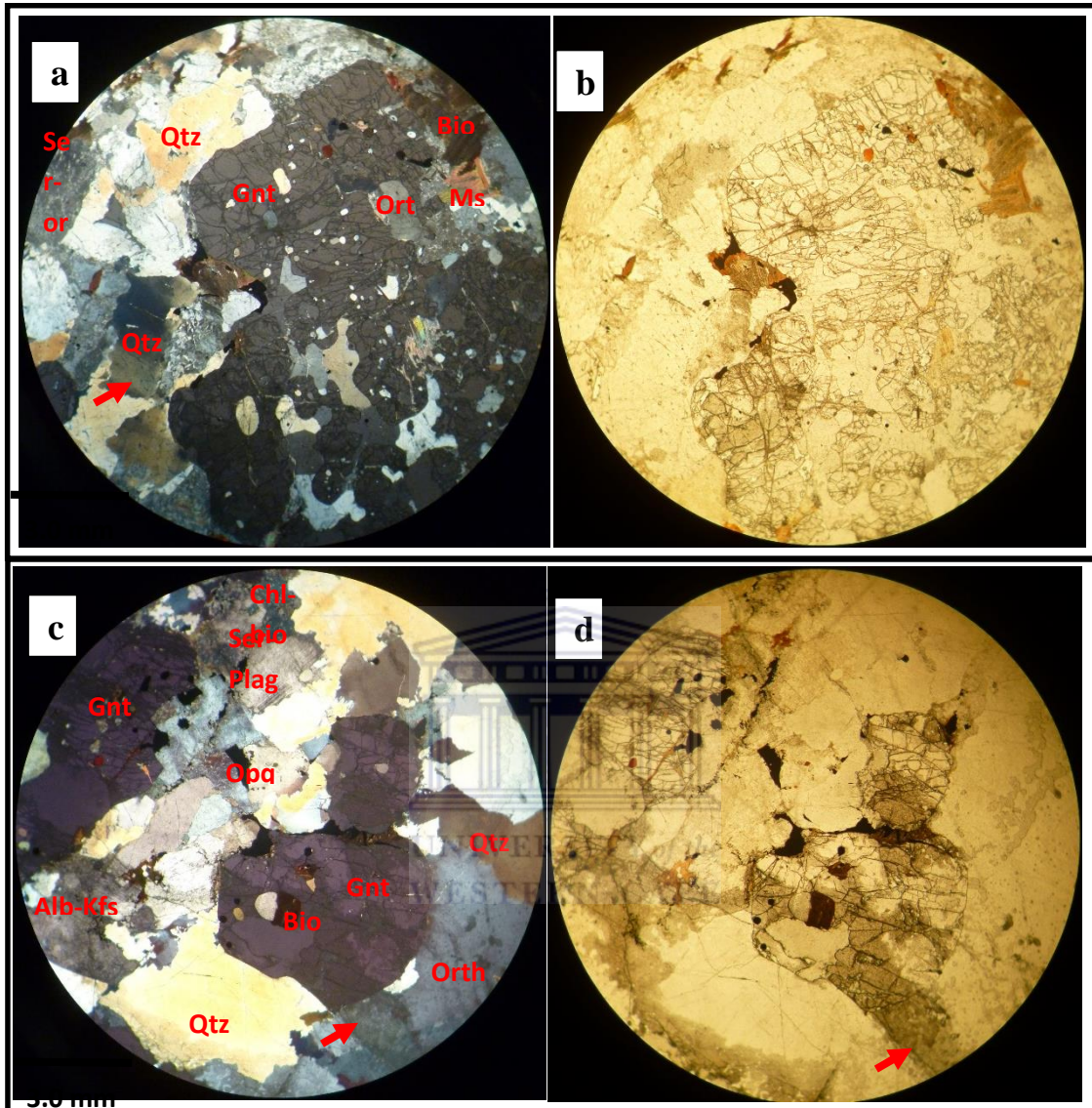


Plate 4-4: Thin section photomicrographs of a garnetiferous quartzo-feldspathic rock from the Hondekloof deposit. Notice how the garnet porphyroblasts define both the porphyroblastic and poikiloblastic metamorphic textures in the rock (a). The red arrow in photo a indicates undulose extinction in quartz. The red arrow in photo c indicates how almandine garnet ($(\text{Mg}, \text{Fe}, \text{Mn})_3\text{AlSi}_3\text{O}_{12}$) has been overgrown by orthoclase (KAlSi_3O_8). Two alteration processes are well displayed in photo c: (1) biotite \rightarrow chlorite and (2) Plagioclase \rightarrow sericite. Abbreviations: Gnt: garnet, Bio: biotite, Qtz: quartz, opq: opaque mineral, Ser-plg: sericitized plagioclase, Orth: orthoclase. Ser-orth: sericitized orthoclase. Photos a and c (cross polarized light), and b and d (taken in plan polar).

4.4 Biotite gneiss

4.4.1 Core description

The biotite gneiss is a banded, quartzofeldspathic gneiss showing distinctive leucocratic and melanocratic sets of bands. The leucocratic bands comprise quartz and alkali feldspar, and the melanocratic bands are composed of biotite, hornblende and epidote. There are four varieties of this biotite gneiss (established on the basis of distinctive foliation styles). The first variety shows a unique type of up-dip folding foliation fabric (with symmetrical micro-limbs on the folds) (Plate 4.5a). The second variety displays a simple type of streaky foliation fabric in which there is a clear segregation between the felsic and mafic minerals (quartz + alkali feldspar vs. biotite + hornblende, respectively) (Plate 4.5b). The third variety shows open box-like fold foliation fabrics in which the biotite content decreases incrementally up-dip as compared to the first two varieties (Plate 4.5c). The fourth variety has poorly developed folding foliation bands as well as having a lower biotite content compared to the third variety, but, in addition, has variable amounts of garnet porphyroblasts present (Plate 4.5d). There are also sections, locally, where some varieties of this biotite gneiss, as well as those of the feldspathic biotite garnet gneiss, show some melt segregations within them.

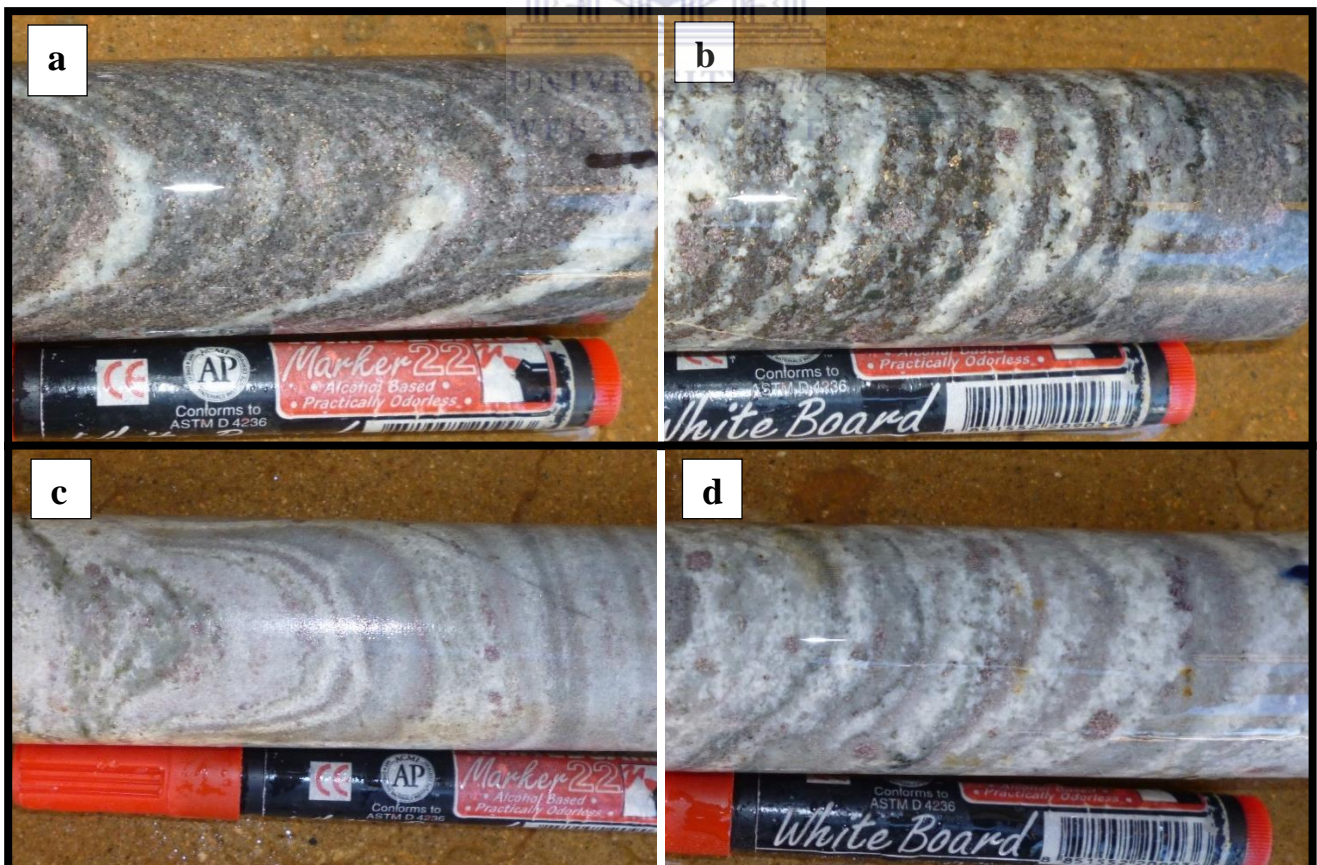


Plate 4-5: Core photographs showing the varieties of the biotite gneiss. .a. variety 1; b. variety 2; c. variety 3; d. variety 4

4.4.2 Petrographic description

The biotite gneiss contains similar type of orthoclase and cordierite which are dusty and are showing speckled microscopic appearances. Sericitization is common, in which the alkali feldspars have been variably altered to sericite. Saussuritization, with epidote replacing plagioclase, also occurs. Biotite is chloritized to varying degrees but less pervasively than the other alterations reported. A penetrative foliation fabric is evident and common in most samples, and is defined by the elongation and alignment of the biotite grains (Plate 5.6a & b). A granoblastic texture is also common, with the garnet and andalusite being characteristically poikiloblastic. Minerals appear to have been strained and have been subjected to recrystallisation, as indicated by the amalgamation of small strained sub-grains to generate a coalesced texture in some samples. An intracrystalline deformation texture is also pervasive, as indicated by the presence of internal fracturing within the alkali feldspars (orthoclase). Furthermore, andulose extinction is also common as evidence of the fact that the minerals have been strained.

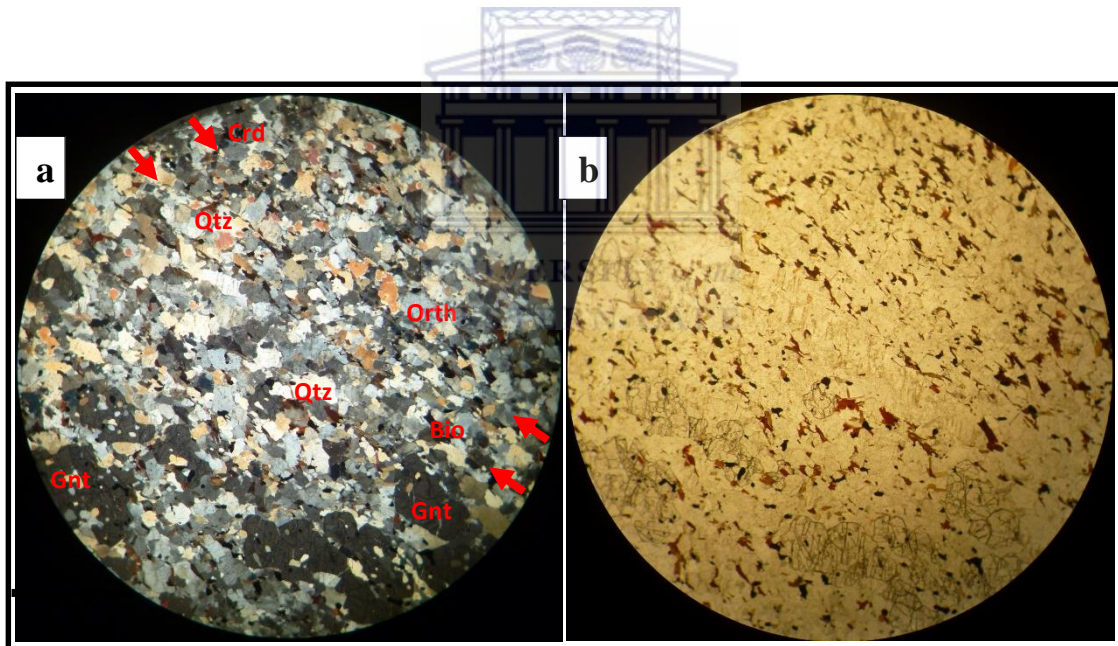


Plate 4-6: Thin section photomicrographs of a biotite gneiss from the Hondekloof deposit. The red arrows in photo c indicate a coalescence texture where strained-sub-grains recrystallized to form large strain free quartz grains. Notice how each sub-grain goes extinct at a different angle. Photograph a) and b) are shown in cross polarized light and plane polarised light respectively. Grt: garnet, Qtz: quartz, Bio: biotite, Orth: orthoclase, Crd: cordierite.

4.5 Feldspathic biotite garnet gneiss

4.5.1 Core description

The feldspathic biotite garnet gneiss preserves several features, such as post-tectonic garnet porphyroblasts which overgrew the foliation texture defined by the biotite. The garnet grains are generally clustered together with inclusions of both quartz and alkali feldspar as well as biotite. There are four varieties of this biotite gneiss among which different characteristics are described in the different boreholes (Plate 4.7a-d). One of these varieties has large amounts of both alkali feldspar and biotite and displays a weathered brown colouration (Plate 4.7a). Some, especially those hosted in boreholes H445 and H435, have penetrative fabrics as well as large and well-developed garnet porphyroblasts (Plate 4.7b). Other equivalents also have a conspicuous, spotted appearance with lower biotite contents and greater alkali feldspar contents (Plate 4.7c and d). The latter variety is also coarse grained, and furthermore have garnets which are sparsely distributed.



Plate 4-7: : Core photographs showing different variations of the feldspathic biotite garnet gneiss. Variety 1 (a), variety 2 (b), variety 3 (c), variety 4 (d).

4.5.2 Petrographic description

The feldspathic biotite garnet gneiss preserves features that are similar to the biotite gneiss. It has sections with large amounts of almandine garnet which indicate syn-kinematic growth (rotation) (Plate 4.8a). There are crystals of plagioclase and quartz which have cannibalized to form myrmekitic intergrowth with vermicular textures (Plate 4.8b). Garnet is characteristically poikiloblastic, hosting quartz, sulphides (pyrrhotite) and pyrophyllite as inclusions (Plate 4.8a). Fine-grained calcite grains occur within small tension gashes and are associated with apatite as accessory minerals. Most samples show alteration of alkali feldspars (such as orthoclase) which are severely sericitized. Metamorphic textures, notably granoblastic and vermicular, locally occur in sections which are garnet-poor.

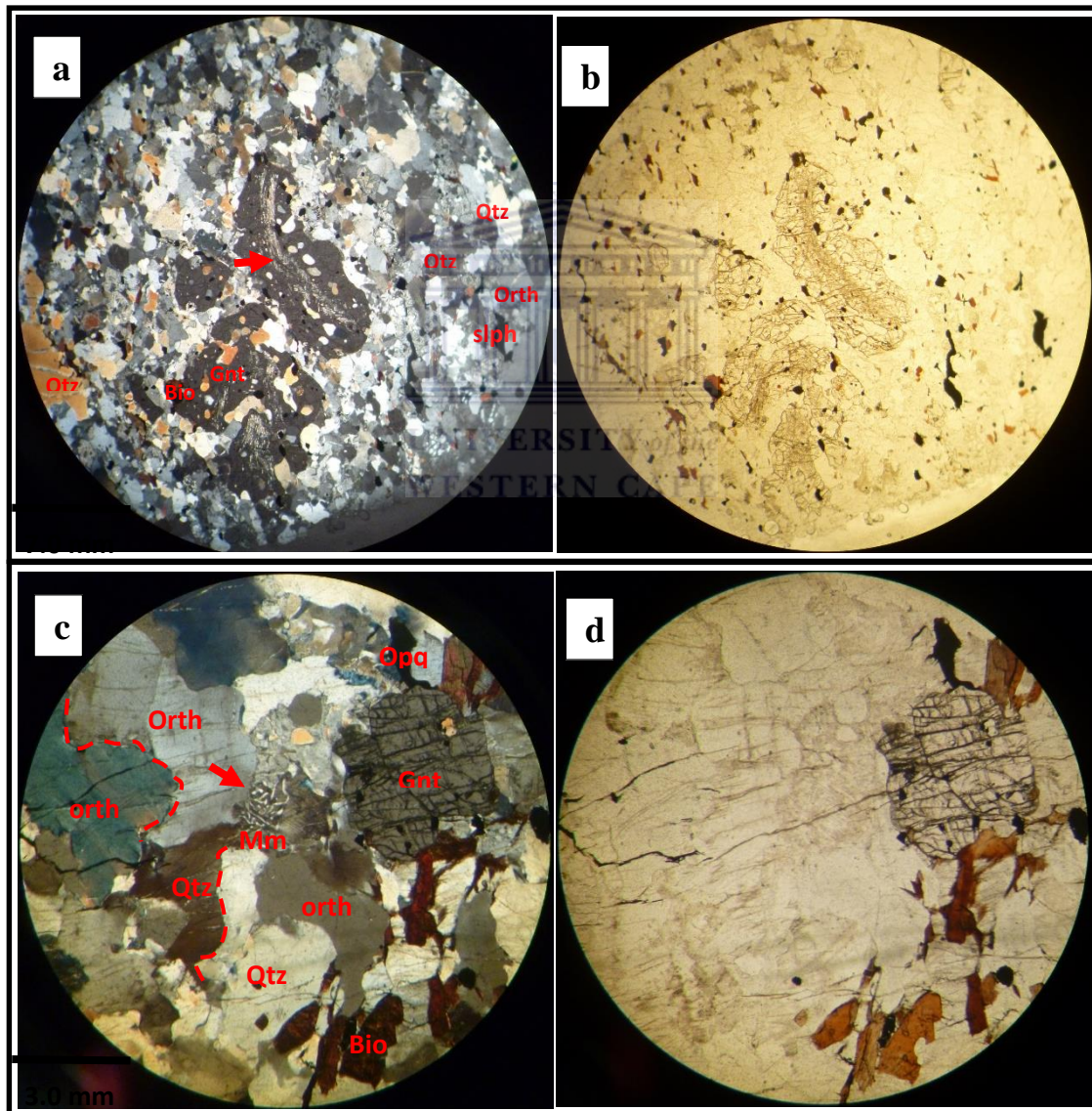


Plate 4-8: Thin section photomicrographs of the feldspathic biotite garnet gneiss from the Hondekloof deposit. The red arrow shown in photo a shows rotation as sign of a syn-kinematic growth. That in photo (c) shows the development of vermicular texture of a myrmekite. Orth: orthoclase, Qtz: quartz, Bio: biotite, Mk: mermekite, Grt: garnet, slph: sulphide.

4.6 Pink gneiss

4.6.1 Core description

The pink gneiss is a pink coloured, equigranular, granoblastic, foliated quartzofeldspathic gneiss. The foliation is defined by quartz and alkali feldspar that are flattened (Plate 4.9a). Alkali feldspar grains are heterogeneously distributed, particularly in terms of the grain size distribution. For example, the grains become fine-grained where the biotite content is high, and medium to coarse grained as the biotite content decreases. Biotite also exhibits some intrafolial foliation fabrics as they folded between the foliation bands (Plate 4.9b). The pink gneiss only occurs in two varieties. The first is medium grained and has a pink colouration (Plate 4.9a), with the other fine grained and having a pink to weathered brown colouration (Plate 4.9b).

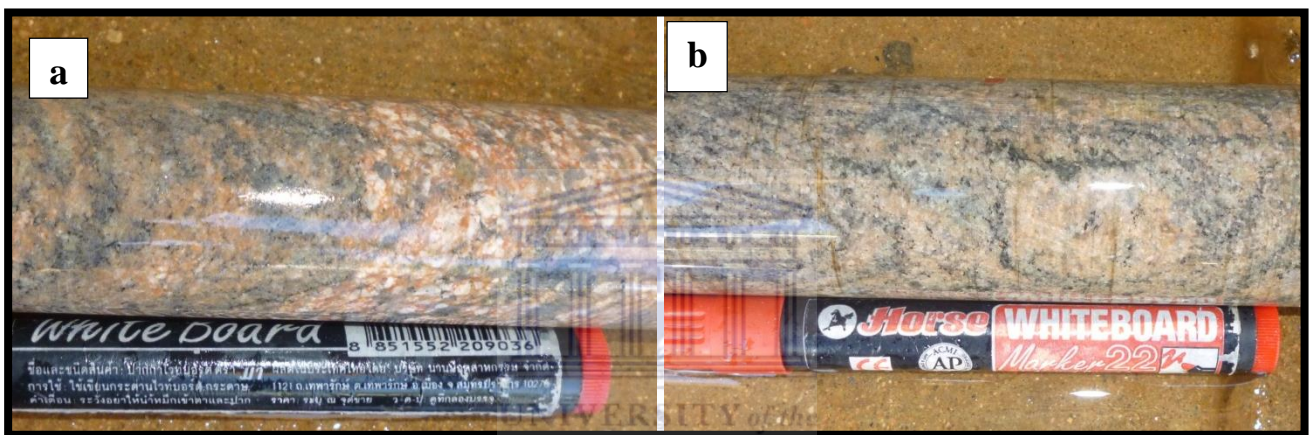


Plate 4-9: The two varieties of pink gneiss; a. variety 1 and b. variety 2.

4.6.2 Petrographic description

The pink gneiss is marked by the absence of mafic minerals, such as amphibole, and by the absence of biotite in some samples. This results in a high quartz, alkali feldspar (orthoclase) and cordierite content in samples where biotite is absent, or present in minor amounts (Plate 4.10a). Sericitic alteration is common and occurs as an alteration of plagioclase and alkali feldspar in different samples. Plagioclase alteration to clay minerals is also seen, but is localized and less common. The pink gneiss, however, does not show as much textural variation as shown by the other gneisses investigated, with the foliation remaining consistent in both hand specimen and thin section (Plate 4.10a). Two foliation fabrics are present, one defined by mineral recrystallization into smaller grain aggregates (Plate 4.10a), and the second by localised mineral elongation and alignment of biotite grains (Plate 4.10d). In addition, where biotite becomes less abundant the grain size also becomes progressively equi-dimensional

(Plate 4.10c). Undulose extinction in both quartz and orthoclase indicate strain in these mineral grains. The grain size also varies from fine to coarse grained (with a bi-modal grain size distribution) in biotite-rich samples (Plate 4.10a), and is more typically medium grained (with an equi-dimensional grain size distribution) in samples which are biotite-poor (Plate 4.10c)

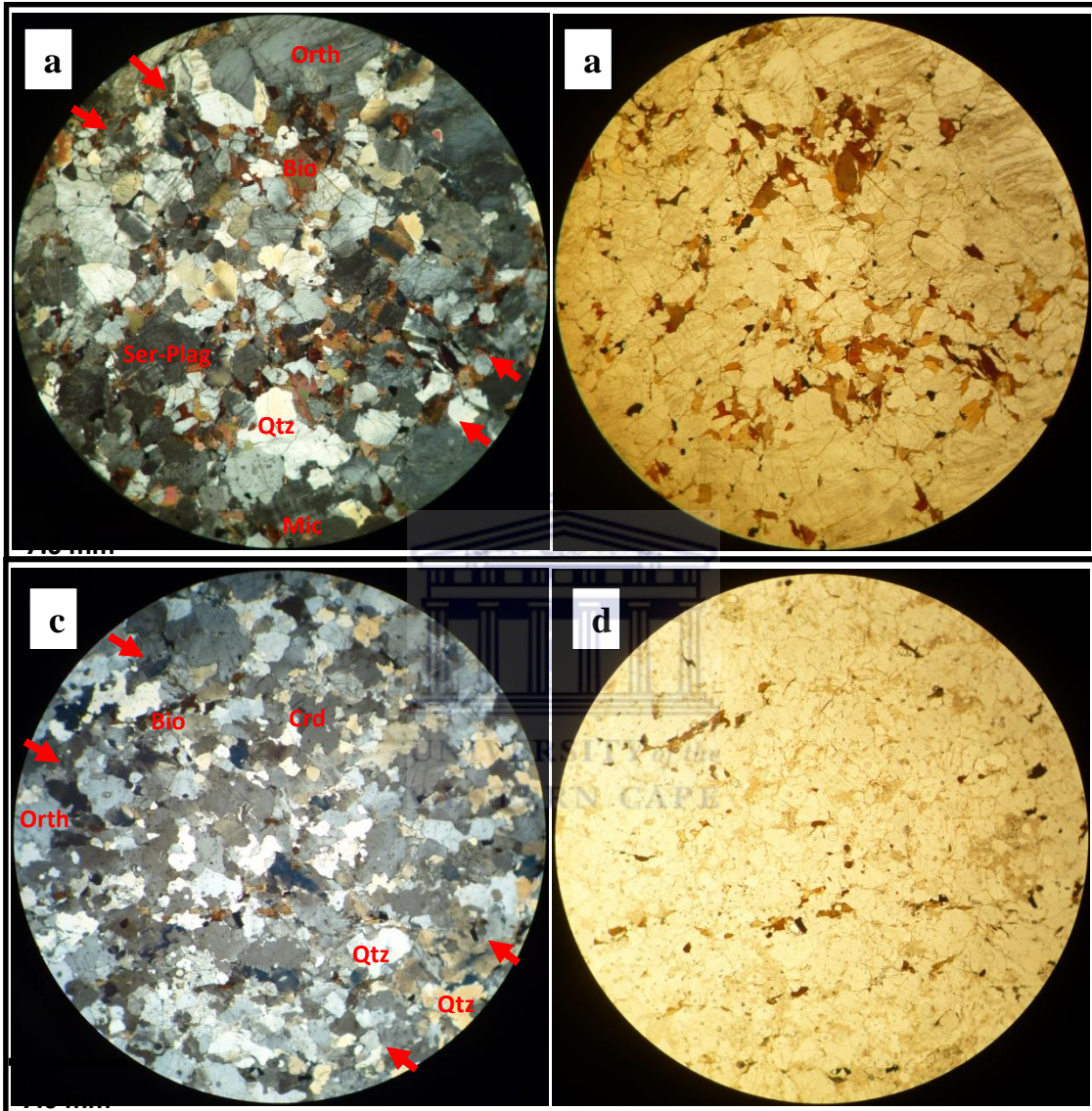


Plate 4-10: Thin section photomicrographs of a pink gneiss from the Hondekloof deposit. The red arrows indicate the plane of foliation marked by mineral recrystallization into smaller grains (in photo a), and that marked by mineral elongation and alignment (in photo c). Ser-plg: sericitized plagioclase, Qtz: quartz, Bio: biotite, Mic: microcline. Crd: cordierite, Orth: orthoclase. Photos a and c are taken in crossed polars and b and d in plane polarized light.

4.7 Meta-syenite

4.7.1 Core description

The meta-syenite is a leucocratic rock consisting of more than 60 wt.% of alkali feldspar (Plate 4.11a). The alkali feldspar occurs in association with quartz, plagioclase and biotite, and lesser amounts of hornblende and pyroxene. The alkali feldspar is typically euhedral and characteristically translucent. The rock furthermore displays fracturing of the alkali feldspar crystals and is generically coarse grained. Two varieties are shown in Plate 4.11a and b, and are different based on their distinctive colouration (pink and green, respectively). Both varieties are thin, and occur as thin layers of between 0.9 and 1 m within the meta-gabbronorite (and most especially in borehole H435).



Plate 4-11: Core photographs showing the meta-syenite of the Hondekloof deposit. a. variety 1; b. variety 2.

4.7.2 Petrographic description

Orthoclase phenocrysts display an interlocking texture which is indicative of extensive recrystallization (Plate 4.12a). The orthoclase phenocrysts have angular to sub-angular shape, whereas plagioclase, biotite and hornblende display embayments (Plate 4.12a). The texture is generally decussate, with fracturing within orthoclase (Plate 4.12a). Undulose extinction is present, but is localized within individual grains of plagioclase and quartz. Partial alteration of hornblende to biotite is seen but is uncommon and localized (Plate 4.12a & b). Alteration involving hornblende, biotite and chlorite is shown in Plate 4.12. There is also fracturing present within individual orthoclase grains with a sense of shear (rotation).

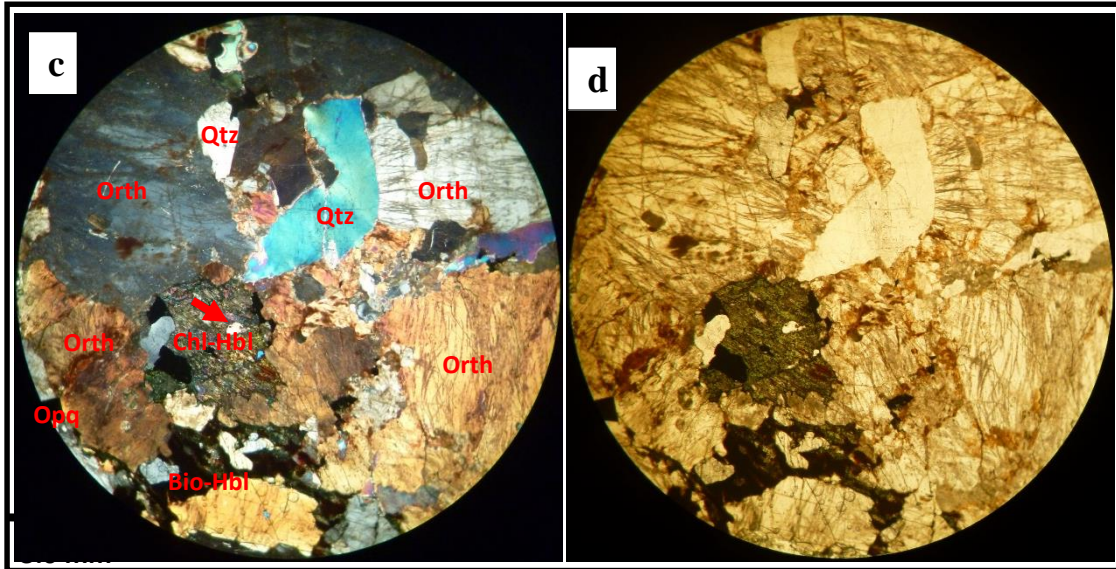


Plate 4-12: Thin section photomicrographs of the meta-syenite of the Hondekloof deposit.. Orth: orthoclase, Qtz: quartz, Bio-Hbl: hornblende → biotite, Chl-Hbl: hornblende → chlorite.

4.8 Enderbite

4.8.1 Core description

The enderbite is a recrystallized, megacrystic, leucocratic, sulphide-rich rock occurring as a vein. It consists of alkali feldspar, quartz and plagioclase along with minor amounts of orthopyroxene, with or without hornblende and biotite. Some varieties, especially those examined in borehole H 582, are devoid of hornblende and biotite (Plate 4.13a). Generally it is coarse grained, with heterogeneous granoblastic textures, and consists of large alkali feldspar grains alongside quartz grains which are randomly oriented. This enderbite, furthermore, displays both a spotted appearance and a pegmatitic texture, and occurs, to some extent, as a pegmatite (Plate 4.13b). Sulphides, mostly in the form of pyrite, are present, but are mostly disseminated and may occur in volumes of between 10 to 20wt. % in some borehole intervals (Plate 4.13a). This lithology, like the garnetiferous quartzofeldspathic rock (see section 4.13) occurs as a product of partial melting (as it occurs as a vein with a large amount of coarse grain quartz and alkali feldspar).

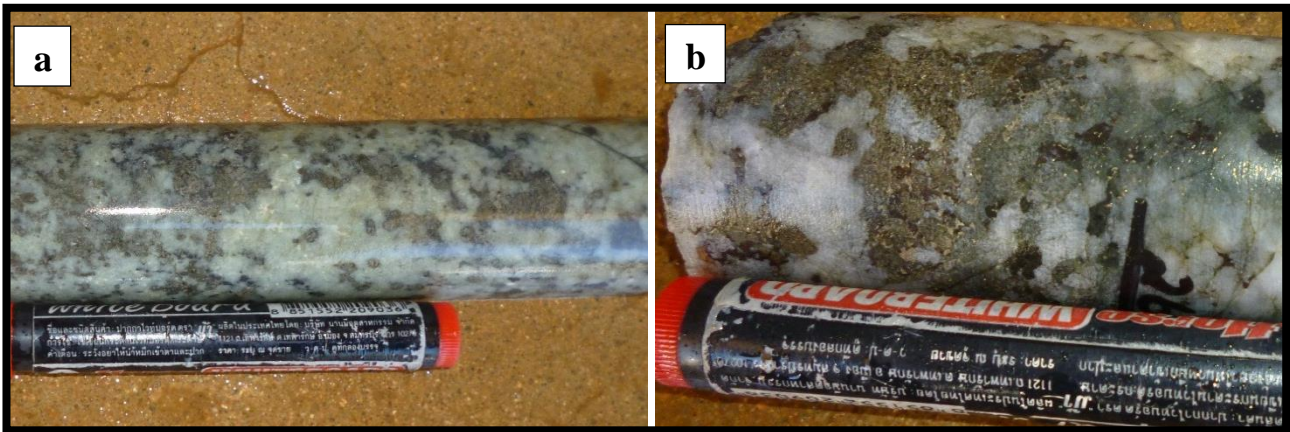


Plate 4-13: Core photographs displaying the enderbite of the Hondekloof deposit.

4.8.2 Petrographic description

Saussuritization is common in which plagioclase has altered into epidote. Sericitization is pervasive as both alkali feldspar and plagioclase are altered to varying degrees to form sericite. Pyroxene porphyroblasts are poikiloblastic and contain inclusions of fine grained orthoclase (Plate 4.14a). Most grains of plagioclase are between 2.0 to 10 mm, with some being as large as 15mm. A coarse-grained interlocking texture is present due to the angular and elongated plagioclase grains. The plagioclase grains also display decussate and poikiloblastic textures which are common but localized (Plate 4.14a). The two samples of the enderbite have different mineralogical compositions in terms of felsic and mafic minerals. One has high alkali feldspar contents and is less mineralized (borehole H 582), whereas the one in borehole H493 is orthopyroxene-rich and is mineralized.

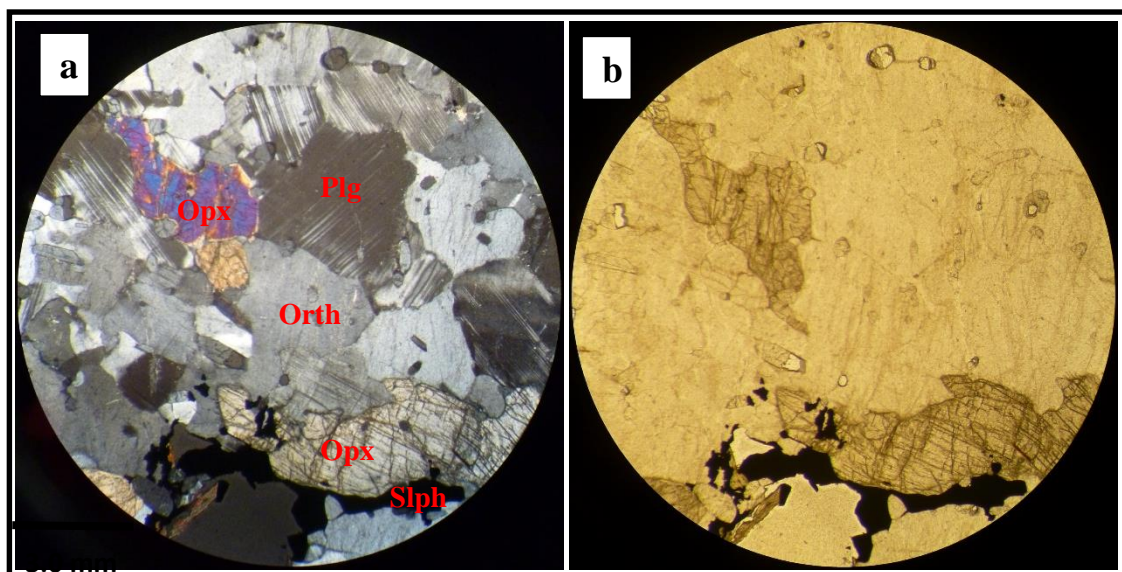


Plate 4-14: Thin section photomicrographs of the enderbite from the Hondekloof deposit. Notice the even distribution of the feldspars (plagioclase and alkali feldspar). Opx: orthopyroxene, Orth: orthoclase, Plg: plagioclase, Sph: sulphide. Photo a is shown in crossed polars and b in plane polarised light.

4.9 Summary

Strip logs (Fig. 4.2) are given in order to illustrate the distribution of the various lithologies in the different boreholes. Additional description of the geology of the borehole locations is provided in section 2 of the appendices.

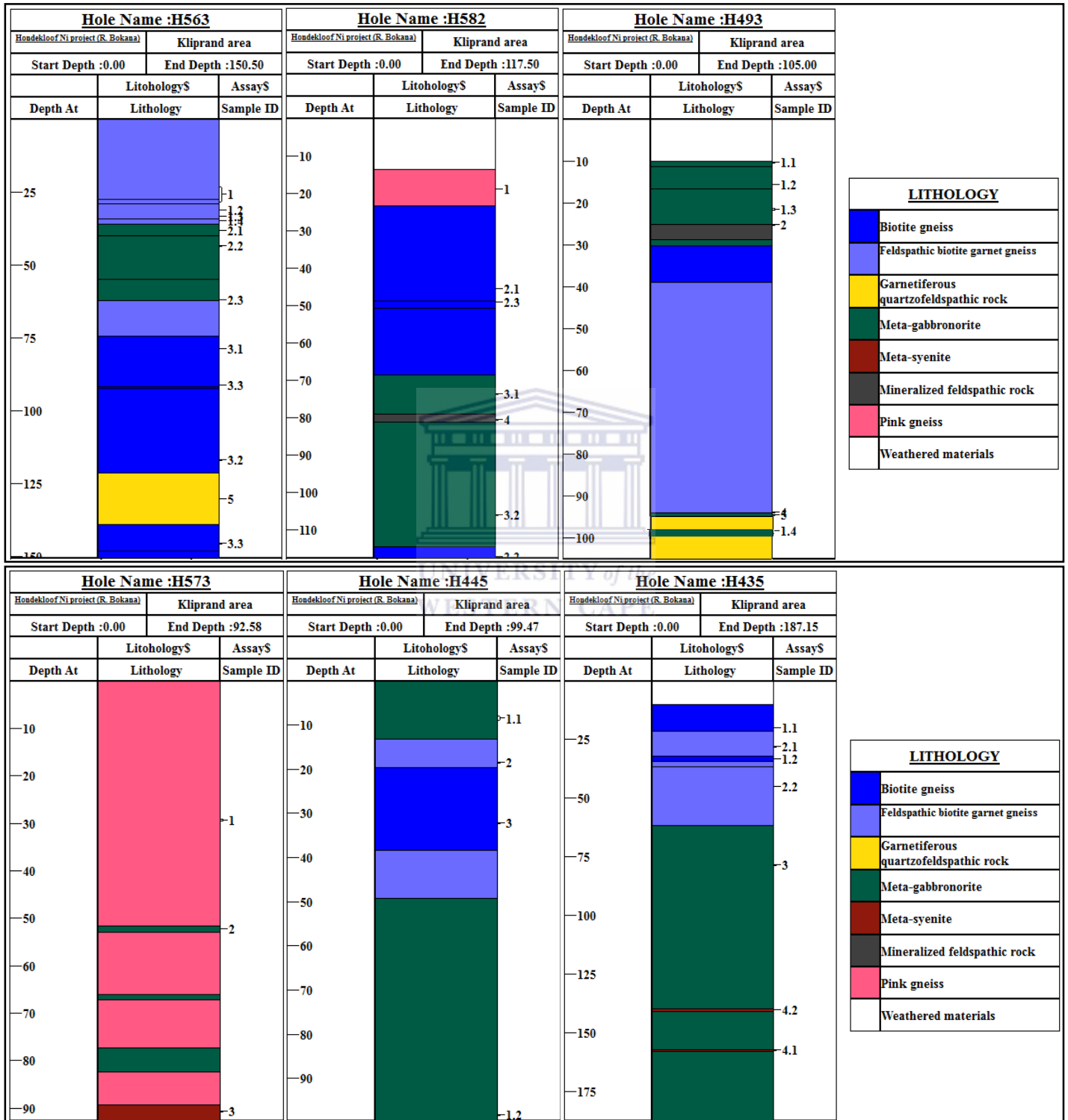


Figure 4-2: Strip logs showing the vertical distribution of the different lithologies examined in the different boreholes.

4.10 Estimation of the metamorphic grade

Evidence obtained from core and petrographic examination (Table 4.2) clearly indicates that most of the lithologies have undergone severe degrees of metamorphism. Previous studies by Albat (1984) and Waters (1986b, 1989) all point to the temperature and pressure conditions attaining granulite facies and partial melting conditions (P-T of 750–870°C and 4.5-6 kbar). The metamorphic petrogenesis guide of Bucher and Grapes (2011) (Fig. 4.3), employed in this study to estimate the metamorphic pressure-temperature (P-T) conditions, likewise estimated similar granulite facies conditions. The estimation of the temperature and pressure conditions, as well as the metamorphic mineral assemblages that formed by prograde and retrograde reactions, is shown by red and green ellipses, respectively, for rocks of mafic composition, namely the metagabbro, as determined from geochemical analyses, found in the study area (Fig. 4.3).

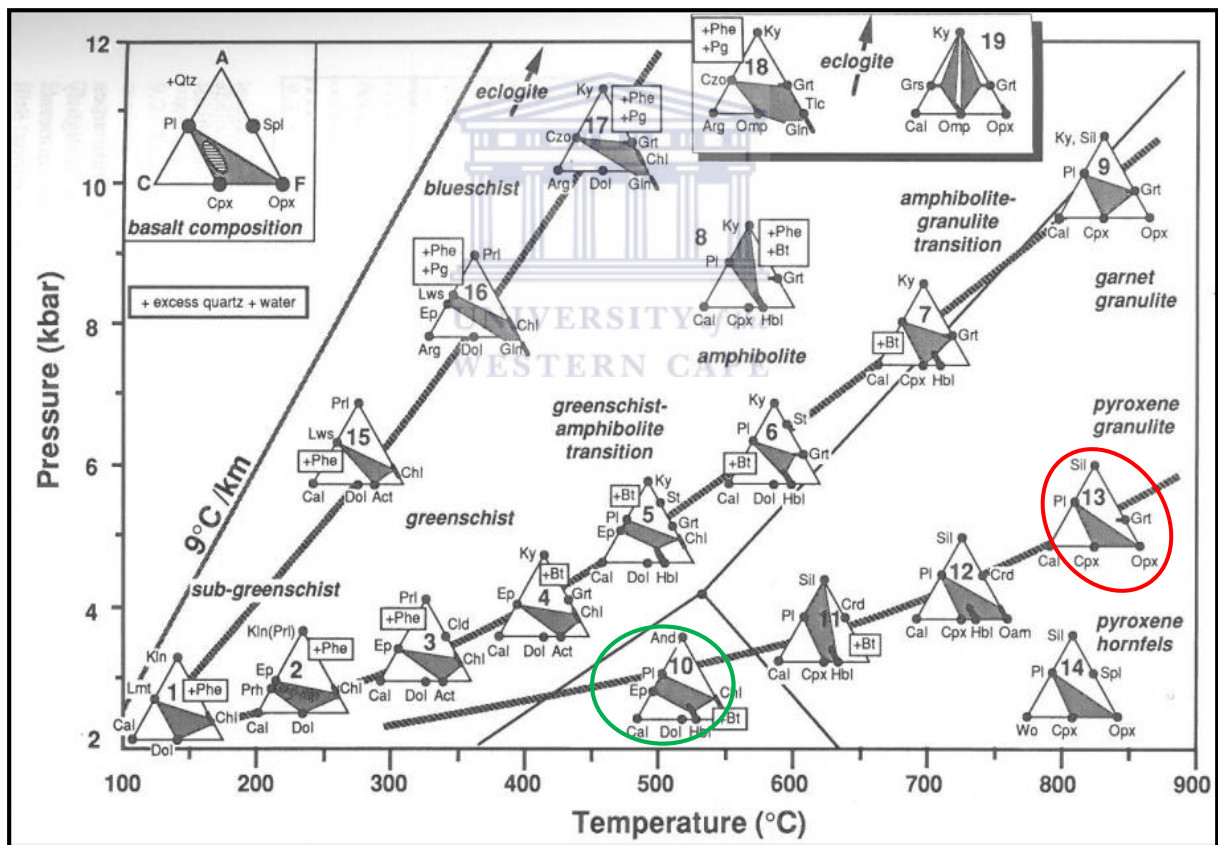
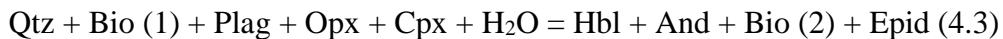


Figure 4-3: A generalised pressure and temperature petrogenesis phase diagram used to estimate the degree of metamorphism from the meta-gabbro of the Hondekloof deposit (after Bucher and Grapes, 2011). The triangular diagrams are ACF diagrams showing the predominant metamorphic assemblages (shaded) at varying degrees of pressure and temperature (P-T) conditions. The ACF diagram in the red circle is the representative or estimated prograde metamorphic conditions (based on mineralogy), and the corresponding prograde mineral assemblage (ACF diagram in the green circle – based on overprinting retrograde assemblages) for the meta-gabbro. Temperature: ~ 750-870°C; Pressure: ~4-6 kbar. The green ellipse represents the approximate P-T conditions for the retrograde assemblages (Temperature: 450-550°C, and Pressure: 2-3.5 kbar). Note that the metamorphic grade is estimated here by comparing the mineral paragenesis.

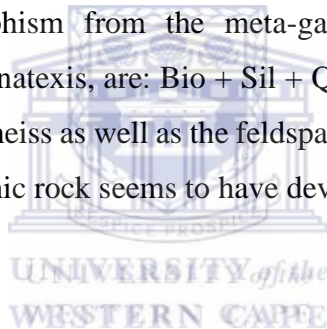
The prograde assemblages likely formed by a reaction, such as:



The above reaction corresponds to the series of metamorphic reactions proposed by Waters and Whales (1984) for the granulite facies and anatexis conditions in the southwestern section of the Namaqua Sector. Similar reactions of metamorphic anatexis are also suggested by Stevens et al. (1997). The retrograde assemblage for the meta-gabbro norite likely formed by such a reaction as:



during cooling. Evidence of a prograde dehydration reaction, such as those suggested by Waters and Whales (1984), for example: $\text{Bio} + \text{Plag} + \text{Qtz} = \text{Opx} + \text{Cpx} + \text{Plag} + \text{H}_2\text{O}$ (4.4) are applicable in the present study for the case of the enderbite and meta-gabbro norite (based on reaction 4.4). It is thus assumed that the enderbite likely formed as a melt product of prograde dehydration metamorphism from the meta-gabbro norite. Similar examples of metamorphic reactions marking anatexis, are: $\text{Bio} + \text{Sil} + \text{Qtz} + \text{Plag} = \text{Grt} + \text{Kfs} + \text{H}_2\text{O}$ (4.5) which is produced in the biotite gneiss as well as the feldspathic biotite garnet gneiss for which the garnetiferous quartzofeldspathic rock seems to have developed as a melt product.



5. CHAPTER V

GEOCHEMISTRY

5.1 Introduction

The representative major and trace element analyses of the examined samples were obtained (Table 5.1 & 5.2) and used to determine the chemical composition of the rocks as well as infer their origins (source or provenance), protoliths and tectonic settings. However, because of the high grade metamorphism experienced by the investigated rocks in the study area, most elements, particularly some of the major elements, such as SiO₂, MgO, the alkalis and CaO, along with the large ion lithophile elements (LILE), were used with caution knowing that their present concentrations in the rocks likely may not reflect their initial concentrations in the protoliths. It is likely that the rocks have experienced some compositional changes due to elements mobility during metamorphism (Rollinson, 1993; Bailie et al., 2010). Consequently many of the elements were used with care and a greater reliance was placed on the high field strength (HFS) and transition elements (Ti, Zr, Hf, Nb, Th, Ta, Y, Cr, P, Ni, Sc), as well as the Rare Earth Elements (REE), as most of these are typically treated as being immobile during metamorphic processes (e.g. Winchester and Floyd, 1977; Pearce, 1982, 1996; Jenner, 1996; Hollings and Wyman, 2005), and therefore can be considerably useful for seeing through the effects of metamorphism or metasomatism. Nonetheless, the effects of element mobilization may still be influential on the results.

5.2 General classification

All the varieties of gneisses examined, namely the biotite gneiss, feldspathic biotite garnet gneiss and pink gneiss, as well as the meta-syenite generally have high SiO₂, Na₂O, and P₂O₅, moderate to high K₂O, intermediate to high Al₂O₃, and low MgO, CaO and TiO₂, and show variability in trace element concentrations (Fig. 5.1 and b). The meta-gabbro, in contrast, shows moderate to high MgO, intermediate to high Fe₂O₃ and CaO, high TiO₂ and Cr₂O₃, and low SiO₂, Na₂O, and K₂O contents (Table 5.1 and 5.2). In addition, some of the meta-gabbro samples examined (H 563-3c and H493-1a, Table 5.2) have high Th (339.16-345.38 ppm), and high U (8.93-9.61 ppm) contents, indicating that they are highly radioactive. The enderbite and garnetiferous quartzofeldspathic rock consistently show a significant range in some of their major and trace element concentrations, but only two samples were analysed for each of them (Table 5.2). The two samples of enderbite differ in terms of their major

element concentrations, with one sample (H 493-2) being felsic (having high SiO₂ (75.74 wt.%), low Fe₂O₃ (5.26 wt.%) and fairly low CaO (3.28 wt.%) contents, with the other (H582-5) being more mafic in composition (with high Fe₂O₃ (10.57 wt.%), fairly high CaO (6.56 wt.%) and low SiO₂ (50.75 wt.%) contents) (Fig. 5.1). The two garnetiferous quartzofeldspathic rock samples also show high variability in terms of Fe₂O₃ (6.63-18.24 wt.%), SiO₂ (56.62-63.61 wt.%) and K₂O (0.81-4.56 wt.%) contents (Fig. 5.1).

Figure 5.1 & 5.2 show multiple bivariate plots using MgO as an abscissa plotted against all the major oxide-elements (Na₂O, K₂O, Al₂O₃, CaO, Fe₂O₃, P₂O₅ and TiO₂), as well as MgO plotted against some of the selected trace and transition elements (Cr, Ni, Rb, Sr, Y, Zr, Ba, La, and Ce). It is worth noting that the specific set of bivariate diagrams plotted with MgO as the abscissa may, however, not be as useful a discriminant function for some of the lithologies investigated (e.g. all the gneisses), as it is for the meta-gabbromorite.

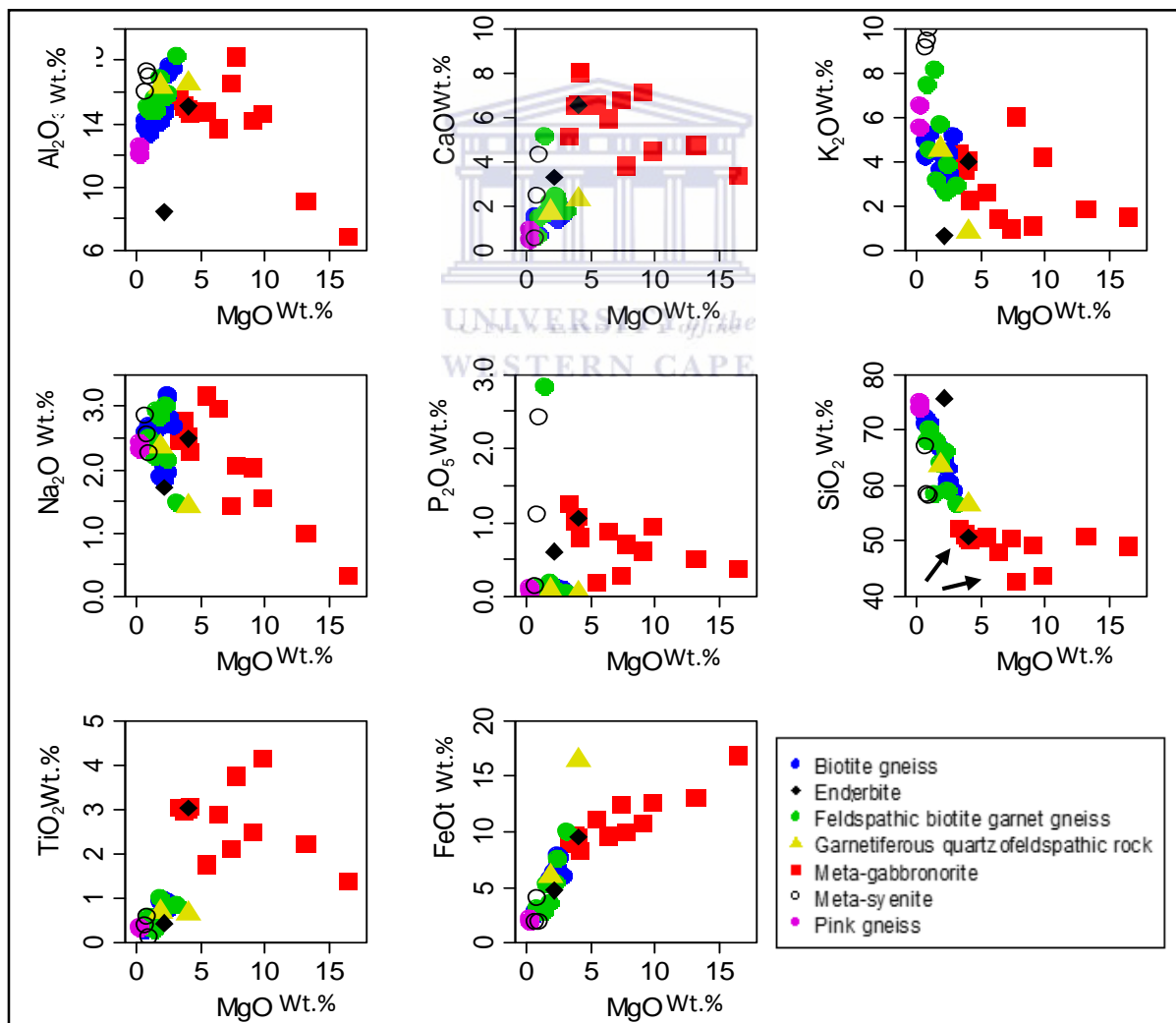


Figure 5-1: Bivariate plots using MgO in wt% as the abscissa plotted against all the major oxides. The arrows indicate the low silica sample for both the meta-gabbromorite (H 582-6, H 493-1c) and enderbite (H582-5).

Linear relationships, with negative correlations between MgO and the majority of the major and trace elements (SiO₂, Al₂O₃, CaO, K₂O, Na₂O, P₂O₅, Rb, Sr, Y, Ba and Ce), along with a positive correlation for such elements as FeO_{total}, Cr, Ni and Mg# are clearly shown on Figure 6.1a and b respectively. The negative correlations, as indicated by such elements as Al₂O₃, CaO and K₂O, as well as Na₂O, P₂O₅ and SiO₂, correspond with the presence of two pyroxenes in the meta-gabbronorite (Table 4.2), particularly as some of these elements would act incompatibly toward such minerals, whilst MgO would act in a compatible manner toward them. FeO_{total}, in turn, shows a positive correlation with MgO in the meta-gabbronorite, as does TiO₂ (Fig.5.1). Furthermore, some samples of the meta-gabbronorite (H 582-6, H 493-1c) also show very low silica (35.87 wt.%), and fairly high MgO (13.20 wt.%) contents, and fairly intermediate Mg# (100MgO/(FeO_{Total} + MgO)) (40-60), indicating an overall primitive composition as compared to the other samples investigated (Fig. 5.1; Table 5.1).

A collective trend is also shown on the plots of SiO₂ vs. MgO, Na₂O vs. MgO and K₂O vs. MgO, along with positive trends for the Fe₂O₃ vs. MgO plot (Fig. 5.1), for the gneisses, meta-syenite, enderbite and garnetiferous quartzofeldspathic rock. There is a sharp negative correlation between SiO₂ and MgO, a sharp positive correlation between MgO and Fe₂O₃, and increasing Na₂O and K₂O with decreasing MgO (Fig. 6.1). Furthermore, there is also a strong relationship (or good association) between some of the meta-gabbronorite samples and those of the enderbite (particularly the more mafic one, H 582-5) in many of the bivariate plots shown on Fig. 5.1 and 5.2.

Cr and Ni show some degree of positive correlation with MgO for the meta-gabbronorite samples (Fig. 5.2). In addition, positive correlations were also obtained when plotting Mg# vs. MgO, and negative correlations between MgO and Rb, Sr, Ba, La, Ce and Zr for the meta-gabbronorite samples (Fig. 5.2). Figure 5.1b also displays all the samples of the gneisses, meta-syenite and garnetiferous quartzofeldspathic rock. These rocks display Zr, Ce, Y and Rb increasing sharply with decreasing MgO content. However, the meta-syenite alone shows a high Sr, Rb, La, Ba and low Cr and Ni content. The gneisses, including the garnetiferous quartzofeldspathic rock, have a relatively high Zr content.

Note that sample H 582 has been excluded from the geochemical classification diagrams because it sulphide-rich and therefore affect the geochemical classification of the meta-gabbronorite.

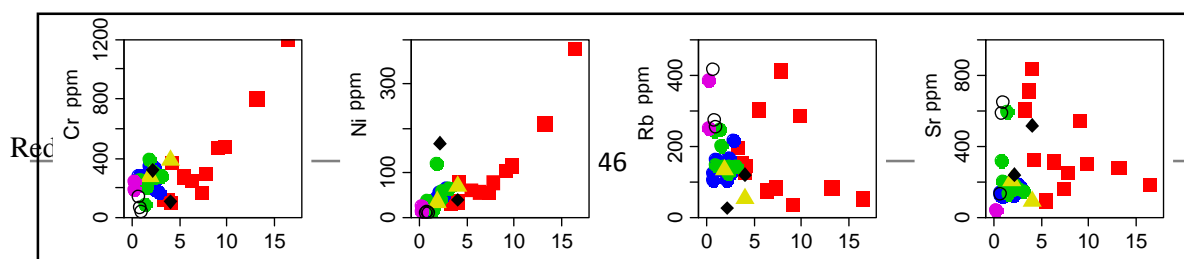


Figure 5-2: Bivariate plots with MgO in wt.% as the abscissa plotted against some selected trace elements

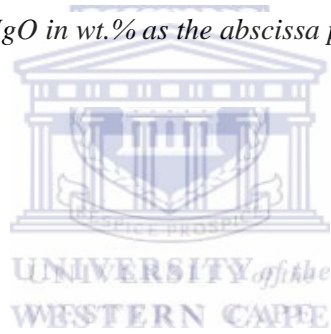


Table 5-1: Major element composition of the host rocks to the Hondekloof deposit

Lithology	Sample ID	SiO ₂	Al ₂ O ₃	TiO ₂	Fe ₂ O ₃	MgO	CaO	Na ₂ O	K ₂ O	MnO	P ₂ O ₅	Cr ₂ O ₃	L.O.I.	Total
Meta-gabbronorite														
	H582-4	47.98	13.67	2.89	10.67	6.36	5.95	2.96	1.42	0.17	0.88	0.03	7.12	100.1
	H582-6	35.87	8.39	2.09	35.9	7.08	4.29	1.29	1.03	0.17	0.56	0.05	4.16	100.88
	H573-2	50.54	14.73	1.75	12.3	5.5	6.55	3.16	2.61	0.22	0.19	0.04	1.73	99.32
	H563-3a	49.12	6.85	1.39	18.7	16.42	3.39	0.33	1.48	0.25	0.37	0.17	0.75	99.22
	H563-3b	50.37	14.6	3.07	9.2	4.18	8.02	2.28	2.26	0.12	0.8	0.05	4.29	99.24
	H563-3c	42.76	18.2	3.75	11.09	7.78	3.8	2.07	6.01	0.05	0.7	0.04	1.32	97.57
	H493-1a	43.64	14.61	4.14	14.04	9.78	4.47	1.56	4.2	0.11	0.95	0.07	0.86	98.43
	H493-1b	49.28	14.15	2.49	11.92	9.11	7.15	2.03	1.11	0.15	0.61	0.06	1.33	99.39
	H493-1c	50.83	9.13	2.23	14.56	13.2	4.73	1	1.85	0.19	0.51	0.11	1.08	99.42
	H493-1d	50.48	16.54	2.11	13.8	7.34	6.75	1.42	0.96	0.19	0.28	0.02	0.16	100.05
	H445-1a	51.18	15.06	2.97	10.73	3.81	6.54	2.76	3.66	0.14	1.01	0.01	0.95	98.82
	H445-1b	52.26	15.5	3.03	9.98	3.32	5.13	2.44	4.36	0.11	1.24	0.01	1.75	99.13
	H435-3	50.48	14.92	2.99	10.56	4.05	6.55	2.53	4.04	0.16	1.08	0.01	0.81	98.18
Biotite gneiss														
	H582-2a	66.71	14.02	0.6	6.32	1.96	1.61	2.66	3.59	0.08	0.08	0.04	1.39	99.06
	H582-2b	63.04	15.77	0.92	7.4	2.53	1.8	3.14	3.44	0.11	0.07	0.04	0.84	99.1
	H582-3	71.31	13.26	0.37	3.12	1.02	0.67	2.68	5.19	0.06	0.07	0.03	1.4	98.87
	H563-4a	60.53	17.63	0.88	8.5	2.63	2	2.81	3.45	0.12	0.07	0.03	0.94	99.59
	H563-4b	64.9	14.55	0.95	6.99	2.2	1.57	1.84	4.11	0.09	0.05	0.03	2.16	99.44
	H563-4c	65.35	15.04	0.92	6.71	2.19	1.68	2.05	2.74	0.12	0.06	0.03	2.75	99.64
	H563-4d	72.28	13.76	0.27	2.83	0.74	1.36	2.46	4.88	0.09	0.06	0.03	0.7	99.46
	H563-4e	71.06	14.21	0.29	3.08	0.76	1.52	2.58	4.19	0.08	0.07	0.03	1.22	99.09
	H493-3	60.93	17.13	0.75	7.45	2.42	1.89	3.16	4.3	0.1	0.11	0.03	0.92	99.19
	H445-3	60.03	17.04	0.89	8.77	2.46	1.38	1.96	4.45	0.14	0.07	0.02	1.96	99.17
Errors (1 Std. deviation)(in wt.%)		0.05	0.29	1.31	0.16	0.72	0.04	1.92	3.26	1.25	1.22	0.05	2.45	99.33

Table 5-1 (cont.) Major element composition of the host rocks to the Hondekloof deposit

Lithology	Sample ID	SiO ₂	Al ₂ O ₃	TiO ₂	Fe ₂ O ₃	MgO	CaO	Na ₂ O	K ₂ O	MnO	P ₂ O ₅	Cr ₂ O ₃	L.O.I.	Total
Biotite gneiss														
	H435-1a	59.03	17.54	0.86	6.72	2.85	1.62	2.68	5.15	0.04	0.1	0.02	2.67	99.28
	H435-1b	66.74	14.5	0.94	5.86	1.86	1.87	1.88	3.31	0.06	0.09	0.03	2.23	99.37
Feldspathic biotite garnet gneiss														
	H563-2a	67.87	15	0.35	3.44	0.95	0.62	2.36	7.42	0.06	0.11	0.03	1.02	99.23
	H563-2b	67.92	14.76	0.48	5.85	1.56	1.67	2.94	3.17	0.12	0.05	0.04	0.89	99.45
	H563-2c	66.05	15.62	0.82	5.96	2.28	2.42	3.01	2.61	0.11	0.05	0.03	0.66	99.62
	H563-1	63.81	16.85	1.02	4.01	1.91	2.16	2.82	5.71	0.03	0.19	0.03	1.04	99.58
	H493-4a	59.09	15.89	0.82	8.38	2.49	2.23	2.15	3.82	0.13	0.07	0.03	4.19	99.29
	H445-2	58.44	15.55	0.28	3.04	1.55	5.14	2.2	8.12	0.05	2.83	0.01	1.43	99.64
	H435-2a	70.03	14.78	0.57	3.08	1	1.44	2.5	4.5	0.05	0.11	0.02	1.53	99.61
	H435-2b	56.72	18.28	0.85	11.11	3.18	1.79	1.49	2.93	0.19	0.04	0.03	2.41	99.02
Garnetiferous quartzofeldspathic rock														
	H563-5	56.62	16.52	0.66	18.24	4.07	2.27	1.42	0.81	0.58	0.05	0.05	0.12	101.41
	H493-4b	63.61	16.35	0.7	6.63	1.92	1.72	2.37	4.56	0.14	0.08	0.04	1.5	99.62
Pink gneiss														
	H582-1	73.68	12.6	0.32	2.14	0.38	0.48	2.3	6.55	0.01	0.12	0.03	0.77	99.38
	H573-1	74.89	12	0.36	2.45	0.39	0.91	2.42	5.53	0.03	0.06	0.02	0.43	99.49
Mineralized feldspathic rock														
	H582-5	50.75	15.09	3.03	10.57	4.08	6.56	2.49	4.01	0.16	1.06	0.01	0.85	98.66
	H493-2	75.74	8.44	0.44	5.26	2.18	3.28	1.72	0.66	0.05	0.61	0.04	1.17	99.59
Meta-syenite														
	H573-3	67.01	15.97	0.4	2	0.76	0.55	2.84	9.1	0.01	0.13	0.02	0.76	99.55
	H435-4a	58.35	17.25	0.59	4.42	0.93	2.47	2.54	9.47	0.03	1.11	0	1.1	98.26
	H435-4b	58.19	16.99	0.12	1.99	1.04	4.28	2.26	9.97	0.03	2.41	0	1.04	98.32
Errors (1 Std. deviation)(in wt.%)		0.05	0.29	1.31	0.16	0.72	0.04	1.92	3.26	1.25	1.22	0.05	2.45	99.33

The lithogeochemical characterization-Hondekloof Ni mineralization

Table 5-2: Trace element composition of the host rocks to the Hondekloof deposit

Lithology	Sample ID	Sc	V	Cr	Co	Ni	Cu	Zn	Rb	Sr	Y	Ta	Nb	Mo	Cs	Ba	Zr	Hf	
Meta-gabbro																			
	H582-4	25.34	L	249	32.16	56.34	10.42	150	74.37	309.4	39.73	1.17	17.36	1.66	1.83	665.6	377.4	8.93	
	H582-6	21.57	150.8	420.4	453.1	6897	621.2	234.1	27.49	301.7	24.51	0.79	10.24	6.55	0.59	540.1	278.1	7.03	
	H573-2	33.81	231.5	273	40.37	61.76	27.32	135.1	300.2	94.39	114.9	1.54	12.54	10.43	30	138.8	200.6	6.25	
	H563-3a	30.42	167	1198	68.13	377.9	29.92	414.9	50.89	183.9	25.38	0.46	6.98	2.71	3.71	501.2	274.2	5.89	
	H563-3b	25.29	192.1	370.5	31.01	80.32	46.25	255.7	146.4	323.8	43.27	1.51	23.17	6.23	3.91	638.9	772.2	19.36	
	H563-3c	20.09	260	296.7	35.05	77.79	16.3	234.9	412.1	251.3	62.44	2.44	41.37	2.84	10.4	1553	469.2	13.25	
	H493-1a	27.34	274.4	476.7	46.33	114.6	21.77	236.5	284.7	299.6	72.58	1.58	35.45	2.64	7.31	1247	450.1	10.81	
	H493-1b	27.8	197.9	471	42.76	105	20.02	151.2	33.48	545.2	30.06	0.68	10.19	3.01	0.88	786	385.7	8.21	
	H493-1c	32.15	207.7	795.4	62.16	210.1	46.92	169.3	83.13	275.3	36.37	0.74	10.87	3.54	2.12	740.2	480.9	16.7	
	H493-1d	34.85	277	167.8	46.58	55.57	14.36	239.5	81.51	159.2	30.92	0.54	8.18	4.59	8.87	141.3	184.2	5	
	H445-1a	33.33	220.8	121.3	24.67	35.12	20.97	155.6	151.3	709.9	79.6	1.95	33.38	4.91	1.21	1829	737.1	18.04	
	H445-1b	25.2	208.3	119.9	20.75	31.06	24.43	192.1	195.9	601.2	72.52	2.53	40.57	6.24	3.3	2284	468.7	13.05	
	H435-3	33.98	227.4	102.9	26	34.78	26.99	159	129.1	836.8	66.06	2.09	34.52	4.35	1.2	2587	809.9	19.73	
Biotite gneiss																			
	H582-2a	22.49	111.8	336.2	14	41.71	51.46	86.59	140.4	174.9	75.15	0.69	10.19	20.31	1.77	640.3	391.5	12.04	
	H582-2b	23.4	148.7	330.5	16.82	45.84	53.01	130.3	135.9	165.4	49.2	0.86	15.27	17.91	3.95	688.6	304	9.13	
	H582-3	13.04	70.02	274.3	4.39	16.52	10.99	73.39	161	117.4	44.43	0.41	6.93	15.88	1.36	530.1	427.1	10.28	
	H563-4a	25.94	156.3	245.5	19.36	49.57	34.43	151.4	123.5	186.3	56.76	1.05	14.7	20.74	3.96	679.8	309.2	8.48	
	H563-4b	19.77	135.2	250.1	19.12	54.86	52.95	125.1	161.8	162.7	49.36	0.67	12.73	15.41	3.88	828.6	528.3	17.46	
	H563-4c	26.04	148.1	276.4	15.75	46.37	35.02	127.9	103.6	125.1	70.05	0.86	15.46	17.67	2.74	494.6	437.2	13.93	
	H563-4d	13.99	46.91	277	4.36	16.01	10.92	44.15	123.2	139.2	62.96	0.32	7.89	15.2	1.4	579.6	355.1	11.08	
	H563-4e	14.92	58.84	248	7.05	26.3	24.66	43.73	104.1	123.3	56.57	0.37	4.08	18.5	1.3	495.6	332.8	5.25	
	H493-3	21.86	143.4	255.3	17.2	45.95	42.24	139.5	163.1	172.4	54.74	0.95	13.89	16.88	3.89	728.3	305	11.08	
	H445-3	27.23	162.5	182.1	20.16	50.33	45.17	158.2	162.4	166.7	68.46	1.02	14.88	14.02	4.3	808.7	258.8	7.37	
	H435-1a	18.29	219.6	166.9	21.58	65.83	91.02	151.2	214	166.4	30.58	1	14	20.44	5.63	848.5	274.4	8.34	
	H435-1b	17.95	121.9	248.7	13.81	38.42	35.23	114	130	139.8	47.76	0.65	14.29	11.23	1.93	599.3	330	9.64	
Detection Limits																			
	Instrument DL	0.05	0.02	0.89	0	0.16	0.35	0.3	0	0	0	0	0	0	0	0	0	0	
	Fusion method DL	0.53	0.23	8.93	0	1.63	3.53	2.96	0	0	0	0.03	0	0	0	0	0	0	

Table 5-2 (cont.) Trace element composition of the host rocks to the Hondekloof deposit

Lithology	Sample ID	Sc	V	Cr	Co	Ni	Cu	Zn	Rb	Sr	Y	Ta	Nb	Mo	Cs	Ba	Zr	Hf
Feldspathic biotite garnet gneiss																		
	H563-2a	11.37	143.9	245	8.75	37.17	21.47	127.2	239.8	314.2	26.7	0.73	14.14	12.69	3.63	1812	511.7	12.76
	H563-2b	16.73	57.76	205.5	4.15	20.15	12.31	45.72	199.6	133.4	70.46	0.63	5.88	12.1	1.57	801.6	212.2	7.36
	H563-2c	24.95	94.06	308.3	11.33	39.22	28.65	79.94	122.1	177.6	89.49	0.45	7.74	18.25	3.24	596.4	318.6	9.94
	H563-1	22.92	128.6	383.9	13.12	118.4	18.47	95.58	141.9	193.9	86.17	21.54	14.76	11.43	5.14	452.7	387.7	10.81
	H493-4a	21.29	148.1	263.3	23.07	56.88	64.23	260.7	140.4	159.1	49.29	0.79	13.55	20.39	3.12	776.7	364	9.69
	H445-2	13.29	31.44	86.62	5.48	15.6	7.95	66.09	245.9	589.6	144.9	0.3	3.87	4.73	3.26	2495	230	7.32
	H435-2a	13.08	53.7	247.5	6.08	30.81	11.48	146.4	146	198.7	31.62	0.7	11.82	12.52	1.93	840.7	260.2	7.11
	H435-2b	34.8	168.2	272.1	25.5	63.85	51.44	156	142.3	147.7	83.02	1.34	18.47	20.99	5.5	599.5	504	11.89
Garnetiferous quartzofeldspathic rock																		
	H563-5	85.16	189.9	387	27.15	71.24	36.73	145.6	54.1	93.87	52.94	1.07	12.4	29.03	6.04	111.2	493.3	15.21
	H493-4b	25.77	105.6	279.9	11.82	35.19	25.46	114.6	132.7	204.6	71.72	0.59	10.59	16.91	2.09	988.4	247.5	9.37
Pink gneiss																		
	H582-1	8.95	45.77	241.7	3.43	11.27	10.46	51.31	249.9	39.41	17.82	0.27	3.98	14.95	1.82	245.2	315.5	8.56
	H573-1	10.59	41.03	181.5	4.39	25.66	11.55	45.39	384.2	37.43	40.89	1.1	10.53	12.08	8.98	189.8	281.2	9.32
Mineralized feldspathic rock																		
	H582-5	25.74	135.7	107.6	27.09	40.05	16.48	187.3	119.9	517	113.3	2.41	38.44	3.29	2.94	2274	90.78	1.42
	H493-2	14.75	82.45	318.2	28.41	167	67.13	72.04	26.94	240.3	26.73	0.6	5.28	17.37	2.81	217.1	107.7	3.06
Meta-syenite																		
	H573-3	7.52	47.84	137.3	3.95	9.9	6.56	58.68	414.4	133.3	21.4	0.25	6.85	8.54	5.79	879.5	18.51	0.62
	H435-4a	7.73	62.36	68.39	6.44	12.21	10.19	83.81	273.2	585.4	55.82	0.28	4.13	4.73	2.88	2902	100.9	2.65
	H435-4b	7.28	13.57	40.88	3.96	10.29	8.14	26.5	251.4	643.2	98.33	0.188	1.56	2.64	2.32	2588	5.42	4.5
Detection Limits																		
	Instrument DL	0.05	0.02	0.89	0	0.16	0.35	0.3	0	0	0	0	0	0	0	0	0	0
	Fusion method DL	0.53	0.23	8.93	0	1.63	3.53	2.96	0	0	0	0.03	0	0	0	0	0	0

Table 5-2 (cont.) Trace element composition of Host rocks to the Hondekloof deposit

Lithology	Sample ID	La	Ce	Pr	Nd	Sm	Eu	Gd	Tb	Dy	Ho	Er	Tm	Yb	Lu	Pb	Th	U	
Meta-gabbronorite																			
	H582-4	44.37	103.1	13.73	58.42	13.28	2.76	11.76	1.74	8.59	1.6	3.99	0.5	3.09	0.5	8.84	2.4	1.11	
	H582-6	28.67	63.71	8.18	35.19	7.28	1.98	6.1	0.97	4.83	0.97	2.74	0.38	2.29	0.33	29.53	1.29	0.68	
	H573-2	42.34	109.9	13.85	52.79	13.66	1.61	14.62	2.57	17.11	3.88	12.19	2	14.52	2.24	15.35	12.05	8.94	
	H563-3a	27.98	65.25	8.42	34.87	7.22	1.65	6.4	0.92	5.08	0.94	2.64	0.4	2.54	0.38	7.94	6.18	1.84	
	H563-3b	87.48	209.3	26.26	107.5	21.39	2.59	18.64	2.27	10.13	1.81	3.94	0.67	4.06	0.64	17.65	34.1	2.56	
	H563-3c	617.9	1231	151.8	577.5	101.5	3.29	65.94	6.32	21.44	2.7	3.84	0.46	2.16	0.32	50.52	345.4	9.61	
	H493-1a	610.7	1225	152.6	577.2	101.9	3.3	68.97	6.73	23.93	2.97	5.38	0.53	3.08	0.38	44.45	339.2	8.93	
	H493-1b	34.18	73.71	9.65	39.48	8.93	2.69	7.52	1.11	5.52	1.26	3.2	0.48	2.78	0.54	11.78	1.05	0.51	
	H493-1c	36.04	85.79	11.22	47.98	9.8	2.42	8.42	1.31	7.16	1.6	3.89	0.56	3.55	0.61	9.82	6.28	1.85	
	H493-1d	14.79	37.58	5.21	23.71	6.93	1.56	7.58	1.16	6.61	1.19	3.27	0.48	3.09	0.49	13.27	2.53	1.52	
	H445-1a	97.84	232.6	30.49	123.7	24.75	3.85	20.14	3.09	16.35	3.15	8.01	1.13	6.52	0.93	24.35	2.07	0.48	
	H445-1b	82.97	195.4	24.81	102.7	21.77	3.71	18.94	2.72	14.67	2.8	7.07	0.97	5.71	0.8	41.27	2.88	1.07	
	H435-3	98.17	227	29.14	120.1	23.17	3.96	18.1	2.48	13.69	2.54	6.69	0.88	5.59	0.71	31.86	3.34	0.65	
Biotite gneiss																			
	H582-2a	55.94	119.5	14.52	57.61	10.85	1.52	10.95	1.94	12.74	2.96	8.7	1.45	10.61	1.51	32.26	22.98	2.67	
	H582-2b	49.7	103.8	12.41	48.5	9.33	1.71	8.49	1.35	8.43	1.85	5.37	0.84	5.93	0.86	26.33	16.8	2.7	
	H582-3	48.37	109.5	12.33	44.94	7.85	1.38	6.81	1.02	6.54	1.53	4.88	0.87	5.59	0.83	42.86	20.88	2.98	
	H563-4a	55.22	111.7	13.49	50.28	10.67	1.79	9.06	1.63	9.87	2.15	6.69	0.95	6.79	0.99	29.63	17.65	2.49	
	H563-4b	59.77	134.6	17.02	62.15	12.09	1.72	10.96	1.39	8.51	1.83	5.43	0.9	6.04	0.89	35.33	26.14	2.19	
	H563-4c	58.76	130.1	15.07	57.77	11.18	1.55	11.06	1.79	12.8	2.74	8.21	1.28	8.86	1.19	29.86	24.85	2.25	
	H563-4d	45.72	101.6	11.19	39.66	6.5	1.48	7.97	1.47	9.7	2.05	6.54	1.18	7.98	1.2	42.46	20.41	2.36	
	H563-4e	47.64	113.4	13.29	49.29	10.51	1.11	9.07	1.63	10.1	2.25	5.74	0.79	6.88	0.94	39.61	22.48	2.21	
Detection Limits																			
	Instrument DL	0	0	0	0	0	0	0	0	0.01	0	0	0	0	0	0.01	0	0	
	Fusion method DL	0	0	0	0	0	0	0	0	0.13	0	0	0	0	0.04	0.09	0	0	

The lithogeochemical characterization-Hondekloof Ni mineralization

Table 5-2 (cont.) Trace element composition of Host rocks to the Hondekloof deposit

Lithology	Sample ID	La	Ce	Pr	Nd	Sm	Eu	Gd	Tb	Dy	Ho	Er	Tm	Yb	Lu	Pb	Th	U	
Biotite gneiss																			
	H493-3	56.93	119	14.13	56.65	11.35	1.7	9.56	1.46	10.21	2.44	5.65	0.92	5.46	0.94	35.02	19.8	3.24	
	H445-3	51.99	108.6	13.22	49.72	10.19	1.82	10.37	1.87	11.76	2.53	7.46	1.15	8.3	1.22	41.48	17.92	1.91	
	H435-1a	53.57	114.3	13.29	50.85	9.7	1.98	8.47	1.17	6.3	1.21	3.14	0.44	2.73	0.49	34.44	20.52	3.43	
	H435-1b	52.07	108.3	13.2	50.38	10.51	1.69	9.11	1.47	8.52	1.69	5.09	0.66	4.78	0.7	30.13	18.69	2.86	
Feldspathic biotite garnet gneiss																			
	H563-2a	60.76	132	15.69	63.12	13.33	2.26	10.59	1.18	6.33	1.01	2.37	0.35	1.97	0.29	44.83	24.45	3.35	
	H563-2b	82.82	188.2	22.94	88.21	16.26	1.86	13.49	1.84	12.07	2.46	8.55	1.37	9.49	1.46	52.11	48.93	4.21	
	H563-2c	35.25	66.62	6.87	25.96	5.82	1.62	6.88	1.71	13.51	3.22	9.93	1.48	10.68	1.57	37.15	8.23	1.76	
	H563-1	67.98	139.1	16.02	57.77	11.59	1.92	10.56	2.08	14.87	3.16	9.22	1.43	8.71	1.31	32.6	30.11	2.96	
	H493-4a	48.7	97.98	11.32	42.8	8.53	1.76	7.77	1.3	8.6	1.82	5.82	0.8	5.74	0.88	1693	15.01	1.36	
	H445-2	224.5	536.3	70.36	283.2	53.29	5.87	49.66	6.43	32.51	5.63	14	1.56	9.42	1.32	51.07	16.44	2.45	
	H435-2a	59.31	129.9	16.07	60.57	13.71	1.86	10.73	1.55	7.37	1.28	3.49	0.51	3.34	0.45	35.61	34.05	3.7	
	H435-2b	56.99	118.6	14.39	54.78	10.83	1.57	12.41	1.97	13.29	3.15	9.1	1.5	10.5	1.54	33.67	26.51	2.72	
Garnetiferous quartzofeldspathic rock																			
	H563-5	24.97	52.08	5.85	21.55	7.75	1.02	21.75	6.89	69.43	19.26	67.8	11.27	81.03	11.83	10.35	10.15	4.16	
	H493-4b	75.94	163.2	19.52	74.85	14.22	2.2	11.41	1.8	12.38	2.67	7.66	0.94	6.77	1.09	63.36	34.91	1.61	
Pink gneiss																			
	H582-1	18.83	40.53	4.52	16.51	3.46	0.69	3.25	0.56	3.2	0.69	1.7	0.24	1.39	0.24	36.19	7.77	1.86	
	H573-1	44.79	102.9	11.13	38.89	8.48	0.64	7.14	1.26	7.47	1.65	4.25	0.67	3.83	0.59	33.06	30.04	6.88	
Mineralized feldspathic rock																			
	H582-5	93.62	246.1	34.52	157.4	39.11	3.94	38.42	5.13	26.58	4.33	9.26	1.06	5.72	0.69	29.92	3.56	1.97	
	H493-2	31.05	73.12	9.96	42.4	10.08	1.48	9.14	1.19	5.79	1.03	2.06	0.27	1.76	0.23	10.72	2.15	1.79	
Meta-syenite																			
	H573-3	220.5	501.5	57.66	207.3	35.61	1.83	21.89	2.02	7.44	0.82	1.42	0.12	0.64	0.08	78.36	136.5	5.7	
	H435-4a	94.74	217.2	27.86	111.5	23.49	3.49	20.1	2.48	12.77	2.09	4.75	0.49	2.68	0.36	54	6.86	0.71	
	H435-4b	153.3	431.1	44.81	183.9	37.46	4.68	25.64	4.25	21.15	2.94	8.83	1.01	5.55	0.5	51.53	10.13	1.07	
Detection Limits																			
	Instrument DL	0	0	0	0	0	0	0	0	0.01	0	0	0	0	0	0.01	0	0	
	Fusion method DL	0	0	0	0	0	0	0	0	0.13	0	0	0	0	0.04	0.09	0	0	

5.3 Determination of protoliths

In order to interpret the tectonic and metamorphic history of the rocks hosting the deposits, it is essential to determine their protoliths. This firstly involve determining whether they were sedimentary or magmatic in origin prior to metamorphism. Using the immobile element geochemical discriminant diagram of Winchester and Max (1982), where Ni is plotted against Zr/Ti (Fig. 5.3) as a discriminant function, as a method successfully applied by Yigitbas et al. (2008) and Cardona et al. (2010), would therefore yield reliable results for resolving this problem. This diagram mainly relies on a rational relationship that exists between two immobile elements, Zr and Ti. In general, Zr contents are much higher, on average, in immature sedimentary rocks (e.g. greywacke, 140–800 ppm) than in felsic igneous rocks (e.g. granite 140–175 ppm and syenite 100-500 ppm) (Mielke and Winkler, 1979; Watson and Harrison, 1983). Ti, by contrast, has a concentration which is 10 times greater (≥ 2.0 wt.%) in mafic igneous rocks than the maximum concentration values which are found in mafic sedimentary rocks (≤ 0.25 wt.%) (Mielke and Winkler, 1979; Nicollet and Andriambololona, 1980). Consequently, the Zr/Ti ratio may yield a reasonably reliable estimate as to the nature of the protoliths of the metamorphic rocks. In this diagram, however, one must be aware that the line separating igneous and sedimentary boundary is interpreted as a maximum value for igneous rocks. Meaning that sedimentary rocks directly derived from limited weathering and erosion of an igneous provenance, or which were originally volcaniclastic rocks with a large magmatic component, can also plot below the discriminant line, within the igneous field. One must therefore be mindful of this possibility when interpreting the results obtained from the diagram.

A discriminant line for separating the igneous and sedimentary fields has been drawn, taking two values of 0.10 ppm and 0.05 ppm for the Zr/Ti ratio (Winchester and Floyd, 1987) and extrapolated accordingly,. The meta-gabbro and the meta-syenite, as well as the enderbite, plot exclusively within the igneous field (Fig. 5.3), clearly confirming a derivation from magmatic precursors. The biotite gneiss as well as the feldspathic biotite garnet gneiss and the garnetiferous quartzofeldspathic rock, in turn, plot variably within both the igneous and sedimentary fields. These rocks, therefore, broadly reflect the compositions of a hybrid nature which suggests either that: 1) the sedimentary protolith experienced relatively little effects of weathering of an igneous provenance, or 2) the parent rocks were originally volcaniclastic with a significant magmatic component, or 3) rocks of different parentage were mixed together during deformation and metamorphism.

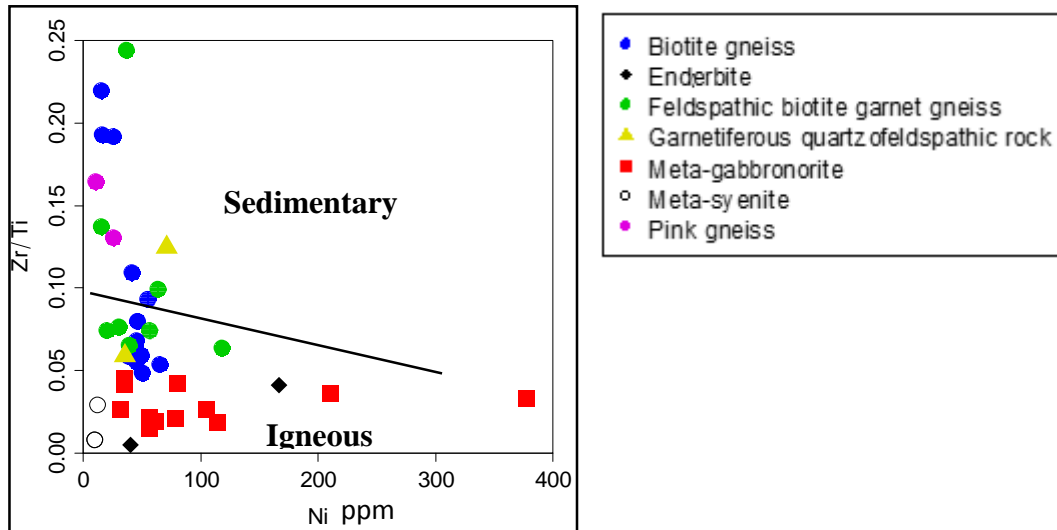


Figure 5-3: Discrimination diagram to determine sedimentary and igneous precursors (after Winchester and Max, 1982).

The pink gneiss plots exclusively within the sedimentary field, implying a derivation from a sedimentary precursor. Two classification discriminant diagrams using immobile high field strength element (HFSE) data Y/Nb vs. Zr/TiO₂ (Fig. 5.4a), and the combination of trace and major element data, Zr/TiO₂ vs. SiO₂ (Fig. 5.4b) respectively, as proposed by Winchester and Floyd (1977), have been used to classify the protoliths to the metamorphosed magmatic rocks as well as to determine the average composition of the provenance for the metamorphosed sedimentary rocks (Fig. 5.4a & b). On these diagrams, two groups of protoliths with contrasting compositions are distinguished, one being felsic (plotting within the rhyolitic and dacitic fields), and the other being mafic (plotting within the basaltic field) (Fig. 5.4a and b). The felsic group includes all the various gneisses, the meta-syenite and the garnetiferous quartzofeldspathic rock. The mafic group, in turn, only includes the meta-gabbro samples. The two analysed samples of the enderbite plot separately, having one in each group, this implies that one of them is felsic and another is mafic. The explanation for this is discussed in chapter 6.

The meta-gabbro samples plot within the basaltic field in both diagrams (Fig. 5.4a and b). Those of the remaining lithologies falling in the felsic group are scattered variably from the rhyodacitic to dacitic fields (Fig. 5.4a), as well as some within the andesitic to the rhyolitic fields (Fig. 5.4b). This variability may be the result of the degree of reworking or weathering or compositional variability in the materials forming these rocks. The meta-syenite, because it contains more plagioclase than quartz, has most likely a protolith of rhyodacitic composition (Fig. 5.4a). There are two analysed samples of the meta-syenite which compared to the other

samples have relatively low SiO₂ contents, and relatively moderate Zr/TiO₂ ratios (Fig. 5.4b); these samples plot towards the andesite field (Fig. 5.4a and b). The majority of the syenite samples, however, plot much closer to the rhyolite fields in both diagrams of Winchester and Floyd (1977) (Fig. 5.4a & b). The compositional changes, in this case, possibly means that the chemistry of the rocks may have been influenced to some degree, and that furthermore the rock might possibly have experienced element-depletion (e.g. SiO₂ and Zr) during metamorphism. Additionally, the location of the analysed specimen as being close to the meta-gabbronorite interval may also play a role in influencing the composition of the meta-syenite by affecting the concentrations of SiO₂ and Zr. Similar protolith compositions indicate a derivation from felsic to intermediate provenances for all the metasedimentary rocks i.e. the biotite gneiss, feldspathic biotite garnet gneiss and pink gneiss.

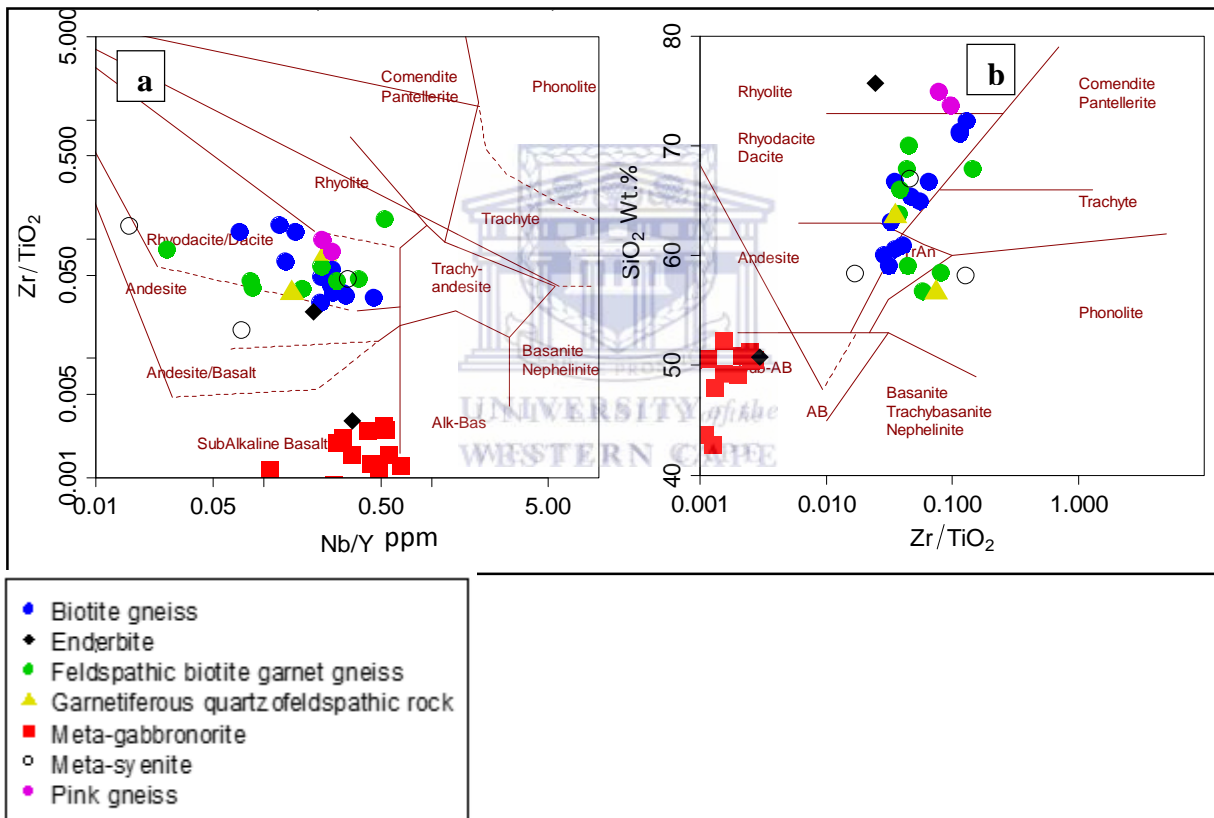


Figure 5-4: Comparative classification diagrams for protoliths and provenance composition (after Winchester and Floyd 1977), (a) Nb/Y vs. Zr/TiO₂ and (b) Zr/TiO₂ vs. SiO₂. Alk-Bas: Alkaline basalt, SB-AB: Sub-alkaline basalt.

5.3.1 Magmatic precursors

From the discriminant diagram of Winchester and Max (1982) (Fig. 5.3), the meta-gabbronorite, meta-syenite and enderbite, indicate the majority of magmatic rocks as their

precursors. Little to none is known about the characteristics of the enderbite's precursors because of the erratic distribution shown on the majority of its samples. The discrimination diagram of silica vs. the alkalis (Middlemost, 1975) places both the meta-gabbronorite and meta-syenite fully within the alkaline field (Fig. 5.5a). In addition, the plot on which the alkalis are displayed exclusively (the Na₂O vs. K₂O plot) places the samples of the meta-syenite within the high K-alkaline series, and those of the meta-gabbronorite within the K- and Na series (Fig. 5.5b). There is, however, a large discrepancy between the results obtained from Fig. 5.5a and Fig. 5.5b, and those reported earlier on and displayed in Fig. 5.4a and Fig 5.4b, with regards to the positions of the meta-gabbronorite samples. In the former diagrams (Fig. 5.4a & b), it is shown that the meta-gabbronorite samples plot exclusively within the sub-alkaline field, whilst in the latter diagrams (Fig. 5.5a, b & c) the same samples plot exclusively in the alkaline field. The mobility of the alkalis and silica used in Fig. 5.5a and b should be taken into account. However, Fig. 5.5c, where the immobile element, Zr, was used, also produced a similar result as where the alkalis and silica were used in Fig. 5.5. The AFM plot of Irvine and Barger (1971) (Fig. 5.5d), plots the samples predominantly within the tholeiitic field.

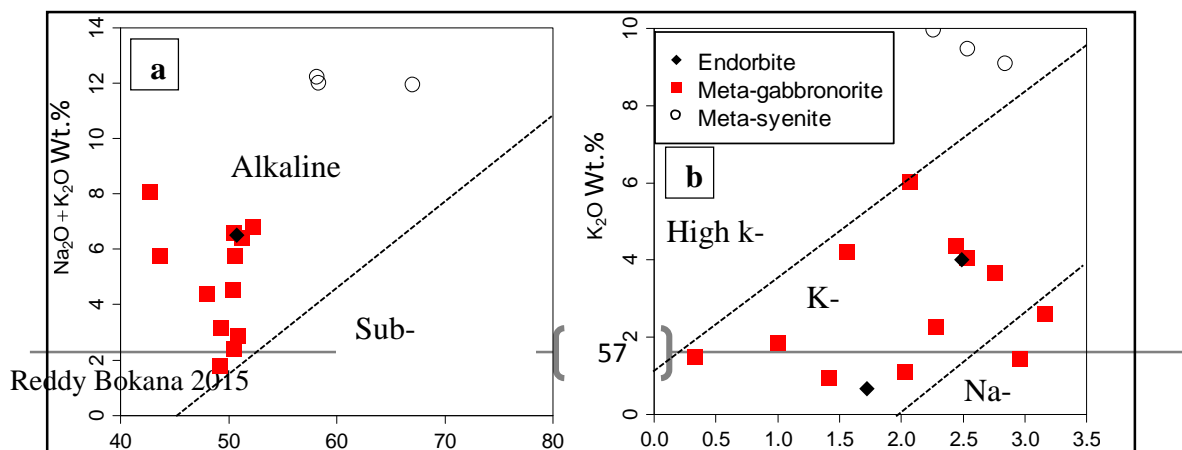
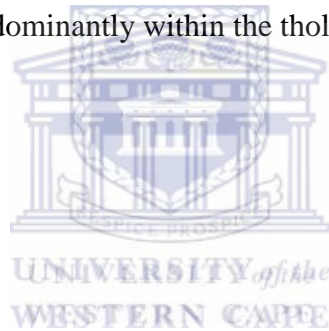


Figure 5-5 (previous page): (a) Total alkali vs. silica diagram for separating the alkaline and sub-alkaline basalts, (b) Na_2O vs. K_2O diagram for subdividing the alkaline magmas (after Middlemost 1975), (c) Zr vs. P_2O_5 diagram (after Winchester and Floyd, 1976) for separating the alkaline and tholeiitic basalts, (d) AFM diagram (after Irvine and Barager, 1971)

Classification of the meta-gabbronorite using two discriminant diagrams of Saunders et al. (1992), using the immobile elements ratios, La/Nb vs. La/Ba (Fig. 5.6a) and Zr/Y vs. Ti/Y (Fig. 5.6b) also helped to see through the meta-gabbronorite's melt source. The majority of the samples show the signature of an asthenospheric source by occupying the space in which both La/Nb vs. La/Ba ratios increase thus showing affinity to an asthenospheric melt (Fig. 5.6a). Figure 5.6b, on which MORB and OIB are separated based on Zr/Y vs. Ti/Y ratios display the samples occupying the space in which the MORB mantle melt are generally represented (Saunders et al., 1992; de Kock et al., 2014).

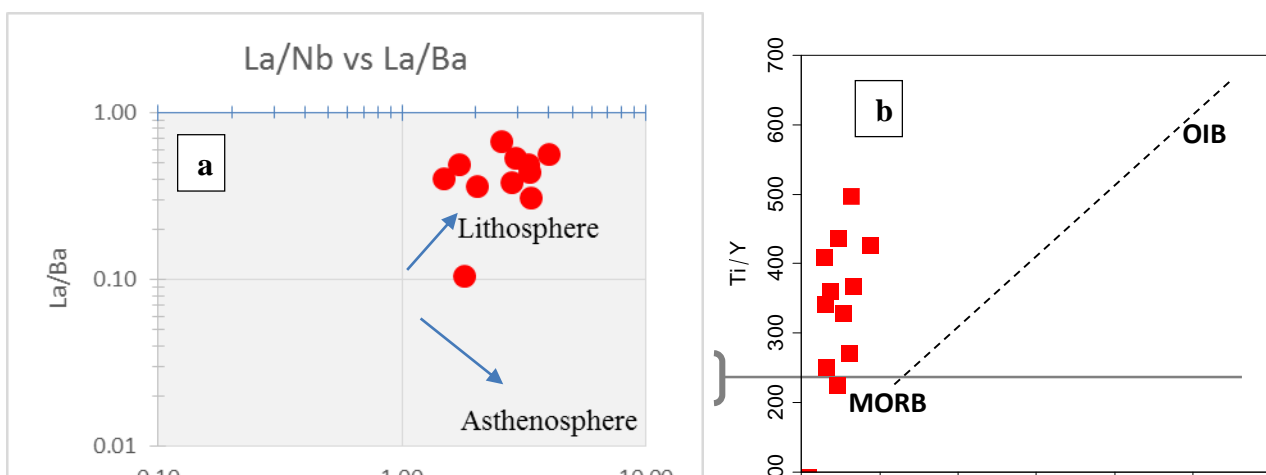


Figure 5-6: (a) La/Ba vs. La/Nb diagram displaying asthenospheric and lithospheric mantle sources, and (b) Zr/Y vs. Ti/Y showing the MORB and OIB characteristics of the mantle melt for the meta-gabbronorite (after Saunders et al., 1992).

The five sets of tectonic discriminant diagrams of Verma et al. (2006) (Fig. 5.7), along with ten newer multi-dimensional plots of Verma et al. (2013) (Fig. 5.8), integrating both major and trace element data, as well as two additional older tectonic discriminant diagrams, namely the Zr-Ti-plot of Pearce (1982), and the Zr-Zr/Y-plot of Pearce and Norry (1979), are used to infer the tectonic setting of the meta-gabbronorite. It must be remembered that the effects of element mobility, as noted above, may be influential in affecting the compositions of these rocks. Using only single element diagrams, particularly for the determination of tectonic settings, may result in spurious results. Therefore, using the combination of multi-element diagrams, as well as mathematical ratios, as applied by Verma et al. (2006, 2013) may help to minimize those effects.

The tectonic setting diagrams of Verma et al. (2006 and 2013) rely on a collective number of discriminant functions calculated based on mathematical and logarithmic ratios (e.g. DF1 and DF2). Each diagram in the set makes use of two selected independent discriminant functions calculated independently. Basaltic rocks forming in island arc (IA), continental rift (CR) and continental arc (CA) settings, along with those in ocean island arc (OI) and collisional systems (Col), are all displayed in their different fields. The suffix B in the annotations, particularly in Figure 5.7, simply stands for basalt. The deducible tectonic setting is therefore obtained on the basis of the reproducibility of the results (meaning that the samples would consistently plot in the same setting or field in each of the five diagrams reported).

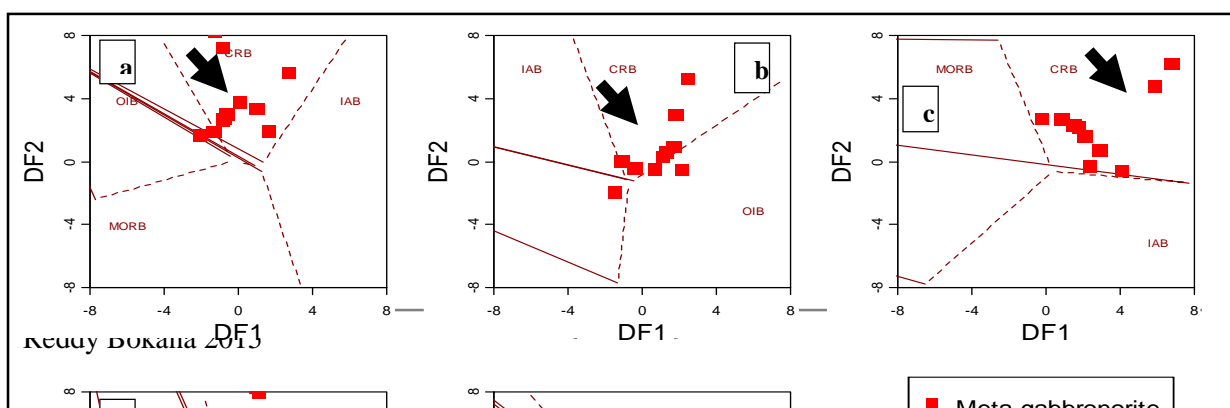




Figure 5-7 (previous page): (a)- (e) Discrimination diagrams showing different tectonic settings based on natural logarithm transformation of major-element ratio (Verma et al., 2006). Note that of the five diagrams, one will consistently not show a particular tectonic setting. This should be noted and borne in mind. DF1 and DF2 stand for the discriminant function. Field of island arc basalt (IAB), continental rift basalt (CRB), ocean-island basalt (OIB) and mid-ocean ridge basalt (MORB) are shown in their respective positions. Tectonic setting diagrams (f) after Pearce (1982) and (g) Pearce and Norry (1979), showing different fields of Island Arc, Mid-Oceanic Ridge and Within Plate Basalts. Black. The black arrow showing the predominant field where samples are represented.

As shown in Fig. 5.7 (a-d), the meta-gabbro-norite plots consistently and repeatedly within the field of continental rift, indicating that this rock was emplaced in a rifting or crustal extension setting. In addition, two comparable tectonic discriminant diagrams of Pearce (1982) and Pearce and Norry (1979) strongly agree with each other, indicating a within plate tectonic setting. These diagrams, along with the multi-element diagrams of Verma et al. (2006) (Fig. 5.7a-g), suggest that the metagabbro-norite was emplaced in a rift or crustal extensional regime. Three outlier samples, which suggest an oceanic island arc setting, are also shown in Fig. 5.7a, b & e. Given that the tectonic setting is an extensional setting, then the island arc setting shown

by these outlier samples may be suggesting some relationship to an arc and relating the setting of the meta-gabbro to a back-arc type environment.

The ten newer multi-dimensional diagrams of Verma et al. (2013), in contrast, yield a different result to the one obtained above. These diagrams, on the grounds of using: 1) the combination of major and trace element data (Fig. 5.8), and 2) strictly immobile trace element data (Fig. 5.9) plot the samples consistently in the continental arc field; suggesting that the meta-gabbro was likely emplaced in a subduction-related complex. Some samples also plot in the field of island arc as well as in that of a collisional setting (particularly in the one case where the field of continental arc is not shown) (e.g. Fig.5.8d and Fig. 5.9d). The possibility of the latter environments (island arc or collisional) are discounted based on the minority of the samples showing such results. Alternatively, these possible tectonic settings could also be related to the likely adjacent settings to the continental arc (within the overall subduction complex). It, however, should be noted that two possible tectonic settings, i.e. one being a rifting or crustal extensional environment, and the other being a continental arc environment, are suggested for the study area. The interpretation of which setting is more suitable, will be discussed in the next chapter.

Conclusive results were also obtained using the combination of multi-element spider diagrams and the REE-diagrams with trace element data. On multi-element spider plots, based on primitive mantle normalization, and plotted according to the element order and values of McDonough and Sun (1995), the meta-gabbro shows a slightly flat to negatively sloping pattern (Fig. 5.10a), in which the LILE are highly enriched relative to the HFSE, as is Zr, whereas Sr, Eu, Ti and P and the HFSE are depleted. A prominent Nb-Ta trough is also evident. The LILE are also showing variable patterns that are indicative of either igneous fractionation, crustal contamination or element mobility.

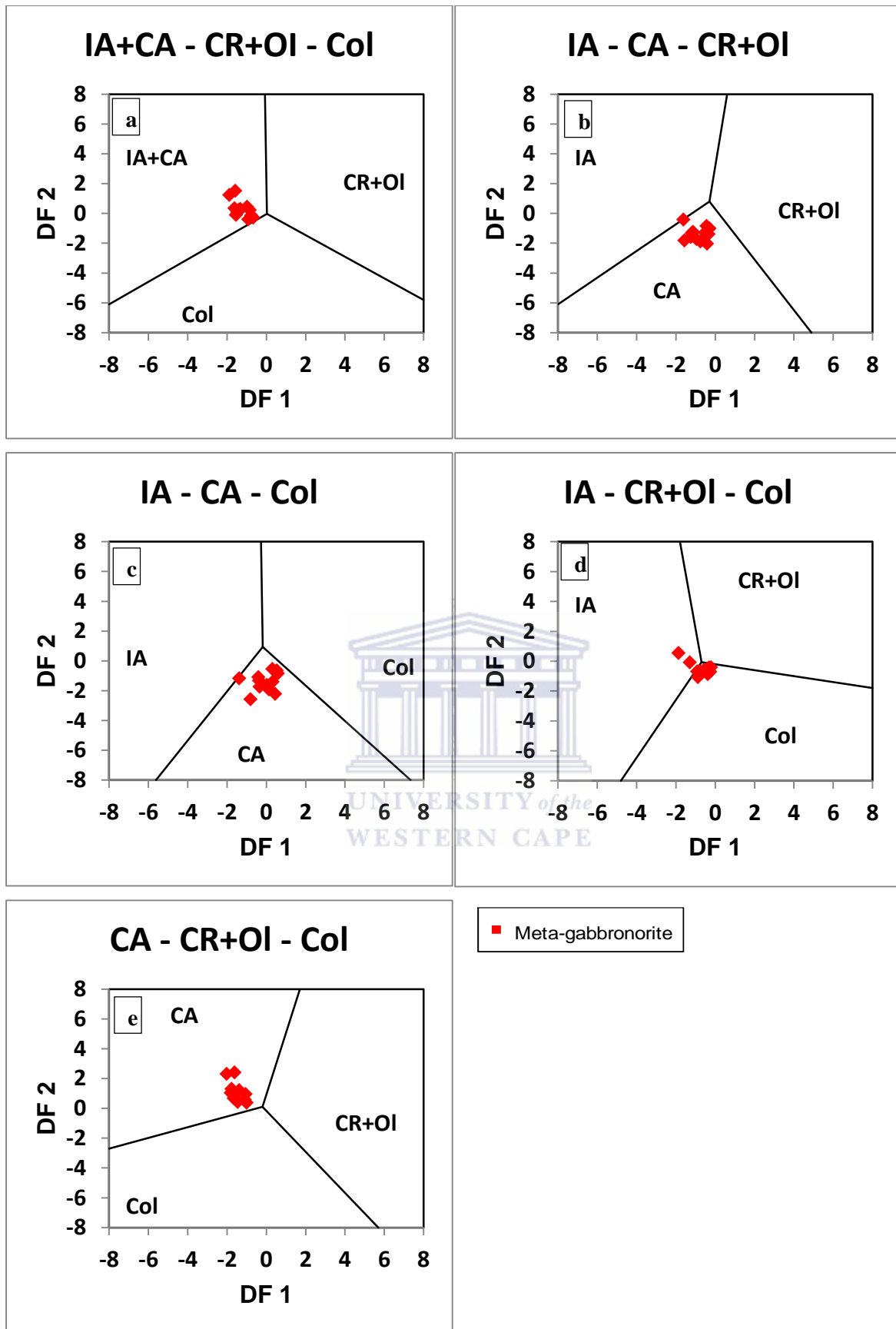


Figure 5-8: Mafic samples of the meta-gabbro in five new multidimensional diagrams based on log-ratios of major and trace elements (TiO_2 , MgO , P_2O_5 , Nb, Y and Zr) for discrimination of island arc (IAB), continental rift (CRB), ocean island (OIB), and mid-ocean ridge (MORB) tectonic settings (Verma et al. 2013).

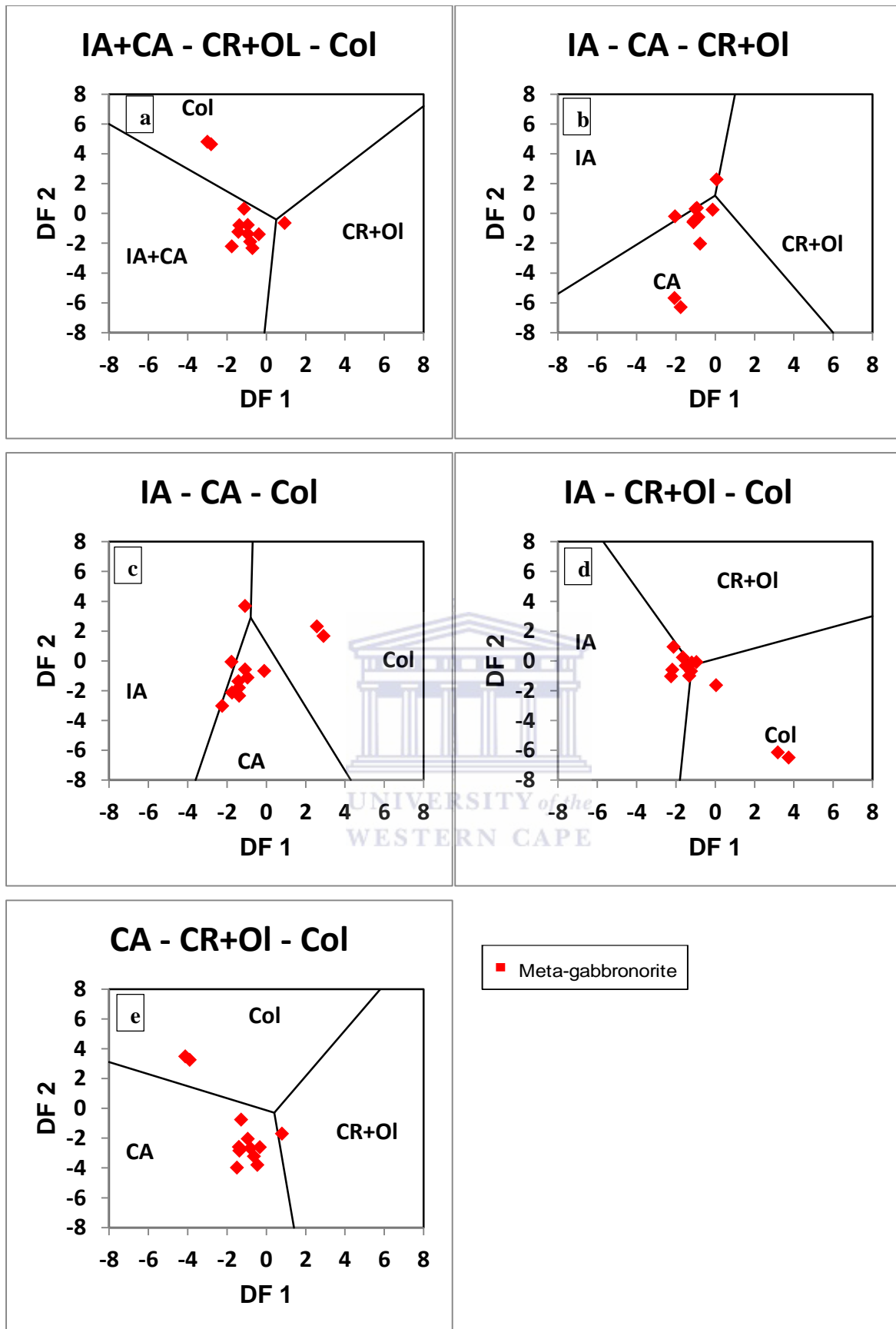


Figure 5-9: Mafic samples of the meta-gabbro in five new multidimensional diagrams based on log-ratios of immobile trace elements (Yb, La, Ce, Sm, Nb, Th, Y and Zr) for discrimination of island arc (IAB), continental rift (CRB), ocean island (OIB), and mid-ocean ridge (MORB) tectonic settings (Verma et al. 2013).

On the REE plot, normalized relative to chondrite and plotted in the order of Nakamura (1974) (Fig.5.10b), the meta-gabbro displays light rare earth element (LREE)-enrichment, and heavy rare earth element (HREE)-depletion, with a gently negative sloping REE pattern. The majority of the samples also show moderate to strong negative Eu anomalies [$(Eu/Eu^*)_N = 1.00-0.12$] a flattening towards Lu, with high HREE fractionation ($Gd_N/Yb_N = 1.92-24.69$), weak to no LREE fractionation ($La_N/Sm_N = 0.38-2.67$) and a range of $\Sigma LREE/\Sigma HREE$ ratios, ranging between 3.36 to 10.72, confirming the influence of crustal components in the meta-gabbro. One sample of the meta-gabbro (H 582-6) (Fig. 5.10b) displays a typical horizontal REE pattern. The ratio for LREE fractionation relative to the HREEs, given by $(La/Lu)_N$, is between 1.96 and 20.21 for all the meta-gabbro samples.

The meta-syenite samples, being felsic, display an overall highly fractionated patterns in the multi-element spider plots (Fig. 5.10c). The samples are characterised by strong positive anomalies of Th, Pb, and the LREE (Nd, Sm and Dy), as well as strong negative anomalies of Cs, Nb, Ta, Sr, Eu as well as P and Ti. The REE plot also shows a strongly sloping pattern, with LREE-enrichment relative to the HREE (Fig. 5.10d). The meta-syenite samples furthermore display large negative Eu anomalies ($(Eu/Eu^*)_N = 0.20-0.49$), with a pattern steepening towards Lu, low to moderate fractionation within the LREE ($La_N/Sm_N = 2.53-3.88$) and moderate to strong fractionation within the HREE ($Gd_N/Yb_N = 3.73-27.45$), as well as large values for $\Sigma LREE / \Sigma HREE$ (10.39-29.71).

The two enderbite samples show a rather more erratic pattern on the multi-element spider diagram (Fig. 5.10e) than that of the meta-syenite. The one sample (H 582-5), with a higher overall trace element content (Fig. 5.10e), shows moderate to high LILE-enrichment relative to the HFSE, fairly pronounced positive Rb, Ba, Ta, , Pb, , P, and LREE anomalies, and low contents/anomalies and troughs in Th, Sr and Ti. The sample with the lower overall trace element content (H 493-2) (Fig. 5.10e) shows peak anomalies for U, La, Pb, Nd, Sm, and Dy, along with negative anomalies for Nb, Sr and Ti, and is seemingly less fractionated compared to sample H582-5. Both samples display fairly similar negatively sloping patterns on the REE plot (Fig. 5.9f), showing overall pronounced negative Eu anomalies ($(Eu/Eu^*)_N = 0.31-0.47$), a degree of moderate fractionation within the HREE ($Gd_N/Yb_N = 4.20-5.42$), relatively flat LREE patterns ($La_N/Sm_N = 1.51-1.94$), and show relatively similar ranges in terms of $\Sigma LREE/\Sigma HREE$ (6.26-7.76), with quite strong LREE enrichment compared to the HREE.

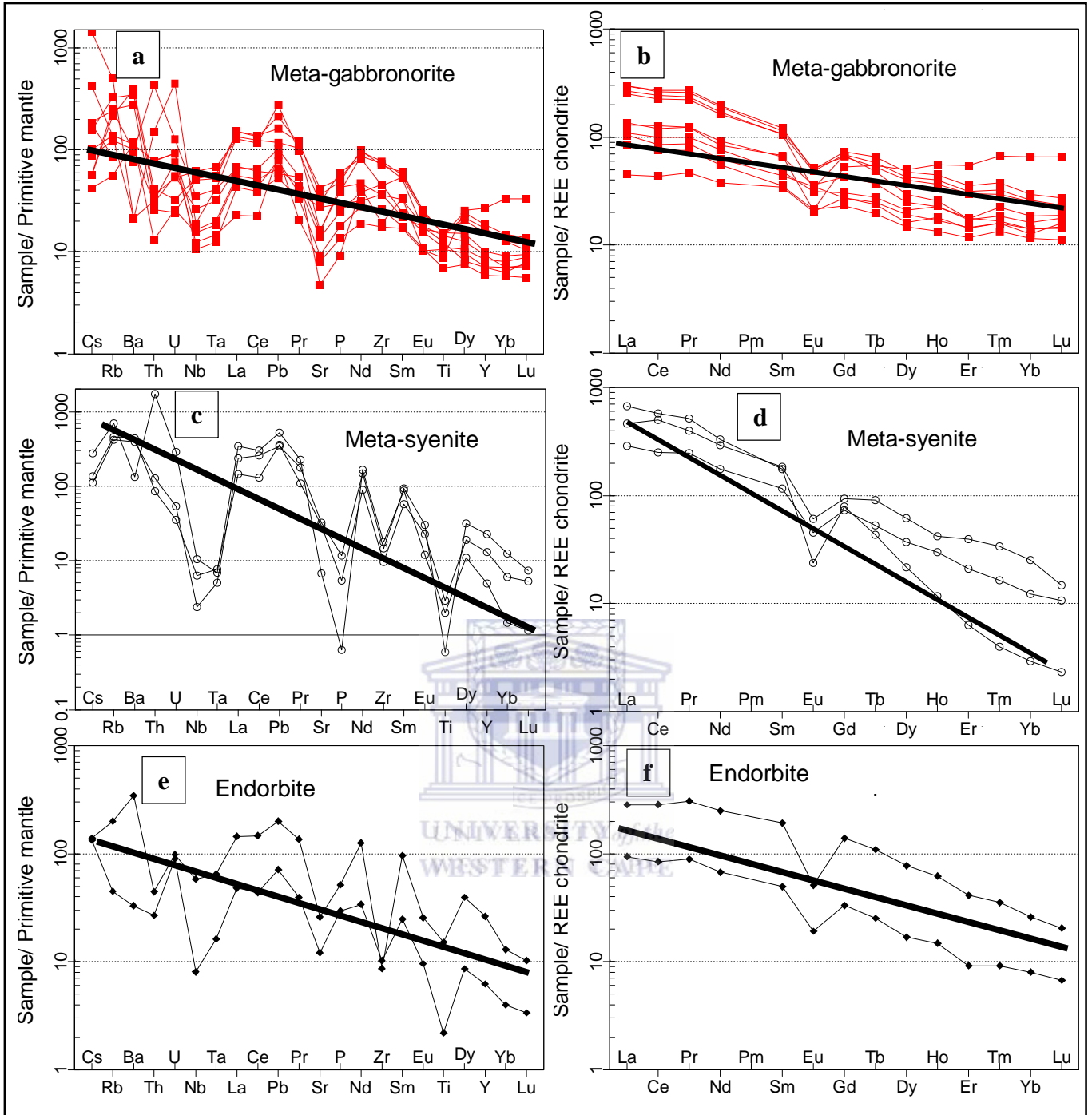


Figure 5-10: Multi-element spider diagrams normalized to primitive mantle (after McDonough and Sun, 1995) and REE plots normalized to the chondritic values of Nakamura (1974) for various meta-magmatic rocks of the western Namaqua Sector. Diagrams dealing with particular rocks are shown. The black line in each diagram is drawn for visualization of a general trend in the diagram.

5.3.2 Sedimentary precursor

The samples of the biotite gneiss, feldspathic biotite garnet gneiss and garnetiferous quartzofeldspathic rock, straddle the boundary between the sedimentary and igneous fields on the protolith discrimination diagram of Winchester and Max (1982) (Fig. 5.3). The pink gneiss, by contrast, plots exclusively within the field of sedimentary protoliths (Fig. 5.3). As highlighted in Chapter 4, some of these units, particularly the garnetiferous quartzofeldspathic rock, seem to occur as the product of partial melt. Some of the other lithotypes, for example the biotite gneiss and the feldspathic biotite garnet gneiss, also contain some remnant of partial melt products. Consequently, given the origin of the garnetiferous quartzofeldspathic rock as a melt segregation product, irregularity in its composition is to be expected. However, in order to facilitate the interpretation, all the units mentioned, including the pink gneiss, have all been classified as having been derived from different varieties of sedimentary protoliths. The assumption was made that the samples of a particular lithology, such as the biotite gneiss, that plot in the igneous field should be regarded as having compositions that have either undergone a small degree of weathering of an igneous provenance, or show a significant magmatic component to their protolith, such as a volcanoclastic. The garnetiferous quartzofeldspathic rock is however treated as a different case for its random geochemical distribution and also for it being considered as product of partial melt product.

5.3.2.1 Weathering in the source area

Source area weathering is one of the most important processes which affect the mineralogical and chemical composition of the siliciclastic sediments or rocks (Taylor and McLennan, 1985). The effects of weathering, i.e. element-depletion (particularly of the alkali and alkali earth elements) and element-enrichment (particularly, for example, of Al_2O_3) is often captured in the chemistry of the siliciclastic sediments (Nesbitt et al., 1980; Grandstaff et al., 1986; Harnois, 1988), so that the chemistry (both major and trace element composition) of the sediments (i.e. either modern or ancient metamorphosed sediments) derived from various sources, can be used to quantify the intensity of weathering of their source areas (e.g. Nesbitt et al., 1980; Bailie et al., 2007; Abu El-Enen, 2011; Grisolia and Oliveira, 2012).

An evaluation of the extent of source area weathering can be quantified using parameters such as the weathering index, WI (Nesbitt et al., 1980), which may be given by two parameters:

1. Chemical index of alteration ($\text{CIA} = \frac{1}{4}100[\text{Al}_2\text{O}_3 / (\text{Al}_2\text{O}_3 + \text{CaO}^* + \text{Na}_2\text{O} + \text{K}_2\text{O})]$), or

2. Chemical Index of Weathering ($CIW = 100[Al_2O_3 / (Al_2O_3 + CaO + Na_2O)]$),

calculated based on molecular proportions. CaO^* is defined as the amount of CaO contributed by silicate minerals in the system (Nesbitt and Young, 1982). The CIA is a quantitative measure of the amount of chemically weathered materials added into the siliciclastic sediments or rocks during weathering, and therefore reflects the chemical weathering intensity in the source areas (Grisolia and Oliveira, 2012). In general, unweathered, fresh basaltic and granitic rocks usually have CIA values ranging between 30 to 45, and 45 to 55, respectively (Nesbitt, 2003). Intensely weathered rocks, on the other hand, which produce secondary minerals such as clays with high kaolinite and/or gibbsite contents, generally reflect CIA values closer to 100 (Nesbitt, 2003; Abu El-Enen, 2011).

The CIA values obtained range from 60.10 to 67.25 for the biotite gneiss, 50.15 to 74.64 for the feldspathic biotite garnet gneiss and 57.43 to 57.46 for the pink gneiss (Table 5.2). Their CIW values, in the same order, are ranged from 76.15 to 83.61 for the biotite gneiss; 67.93 to 84.79 for the feldspathic biotite garnet gneiss; and 78.28 to 81.92 for the pink gneiss. These CIA values, therefore, collectively indicate that the provenance to the gneisses certainly underwent some degree of low to moderate chemical weathering; except for the feldspathic biotite garnet gneiss which has CIA indices ranging up to 74.64, reflecting quite an extensive degree of weathering.

Additional results were also obtained using the Index of Compositional Variability, ICV ($ICV = (Fe_2O_3 + K_2O + Na_2O + CaO + MgO + TiO_2) / Al_2O_3$) of Cox et al. (1995). This index, however, only estimates the abundance of alumina contents relative to the other major cations in siliciclastic sediments or rocks, and is, therefore, applicable in reflecting the degree of maturity of mud rocks or pelitic rocks delivered to a sedimentary basin (Cox et al., 1995). Immature pelitic rocks, with a high content of non-clayey silicate minerals, commonly occurring in tectonically active settings, i.e. in arc settings or rifting basins (van de Kamp and Leake, 1985), usually have ICV values of close to, or more than 1 (Cox et al., 1995), whereas more mature pelitic rocks, enriched in clay minerals, which tectonically characterize by quiescent or cratonic environments (Weaver, 1989) where recycling and weathering are active, usually have much lower values of ICV ($\ll 1$) (Cox et al., 1995).

The examined rocks collectively have ICV values ranging from 0.89 to 1.25, with an average of 1.10 (Table 5.3) suggesting that the materials forming the protoliths likely were derived either from immature pelitic sediments or from semi-pelitic sediments. Figure 5.11a, which

uses alumina and alkalis vs. silica, also suggests that the detritus that gave rise to the parent materials was deposited in an arid climatic zone (an area characterized by less intense chemical weathering due to the limited, or lack of, rainfall and precipitation) (Fig. 5.11a). Note that the latter diagrams are set up to record the climatic conditions present during deposition of the sediments and thus useful for recording the paleoclimatic environment.

Table 5-3: Discriminant ratios for determining the chemical characteristics of sedimentary rocks

Lithology	Sample ID	100TiO ₂ /Zr	K ₂ O/Al ₂ O ₃	Al ₂ O ₃ /TiO ₂	Cr/Zr	Th/Sc	CIA	CIW	ICV
Biotite gneiss									
	H582-2a	0.15	0.26	23.37	0.86	1.02	64.08	76.65	1.19
	H582-2b	0.30	0.22	17.14	1.09	0.72	65.30	76.15	1.22
	H582-3	0.09	0.39	35.84	0.64	1.60	60.83	79.83	0.98
	H563-4a	0.28	0.20	20.03	0.79	0.68	68.10	78.57	1.15
	H563-4b	0.18	0.28	15.32	0.47	1.32	65.93	81.01	1.21
	H563-4c	0.21	0.18	16.35	0.63	0.95	69.92	80.13	1.08
	H563-4d	0.08	0.35	50.96	0.78	1.46	61.26	78.27	0.91
	H563-4e	0.09	0.29	49.00	0.75	1.51	63.16	77.61	0.87
	H493-3	0.25	0.25	22.84	0.84	0.91	64.69	77.23	1.17
	H445-3	0.34	0.26	19.15	0.70	0.66	68.63	83.61	1.17
	H435-1a	0.31	0.29	20.40	0.61	1.12	64.99	80.31	1.13
	H435-1b	0.28	0.23	15.43	0.75	1.04	67.25	79.45	1.08
	Average	0.21	0.27	25.48	0.74	1.08	65.34	79.07	1.10
Feldspathic biotite garnet gneiss									
	H563-2a	0.07	0.49	42.86	0.48	2.15	59.06	83.43	1.01
	H563-2b	0.23	0.21	30.75	0.97	2.93	65.48	76.20	1.06
	H563-2c	0.26	0.17	19.05	0.97	0.33	66.02	74.20	1.09
	H563-1	0.26	0.34	16.52	0.99	1.31	61.18	77.19	1.05
	H493-4a	0.23	0.24	19.38	0.72	0.70	65.96	78.39	1.25
	H445-2	0.12	0.52	55.54	0.38	1.24	50.15	67.93	1.31
	H435-2a	0.22	0.30	25.93	0.95	2.60	63.65	78.95	0.89
	H435-2b	0.17	0.16	21.51	0.54	0.76	74.64	84.79	1.17
	Average	0.19	0.31	28.94	0.75	1.50	63.27	77.64	1.10
Pink gneiss									
	H582-1	0.10	0.52	39.38	0.77	0.87	57.46	81.92	0.97
	H573-1	0.13	0.46	33.33	0.65	2.84	57.53	78.28	1.01
	Average	0.11	0.49	36.35	0.71	1.85	57.49	80.10	0.99

Figure 5.11b, which estimates the process of element-exchange in the silicate-bearing minerals (e.g. biotite, feldspars and clays, etc.) during chemical weathering, attests to the formation of some clay-minerals, particularly smectite, in these rocks. Together with the CIA and CIW

values, the ICV values conclusively suggest that the protoliths to these rocks likely formed from semi-pelitic to psammitic sediments.

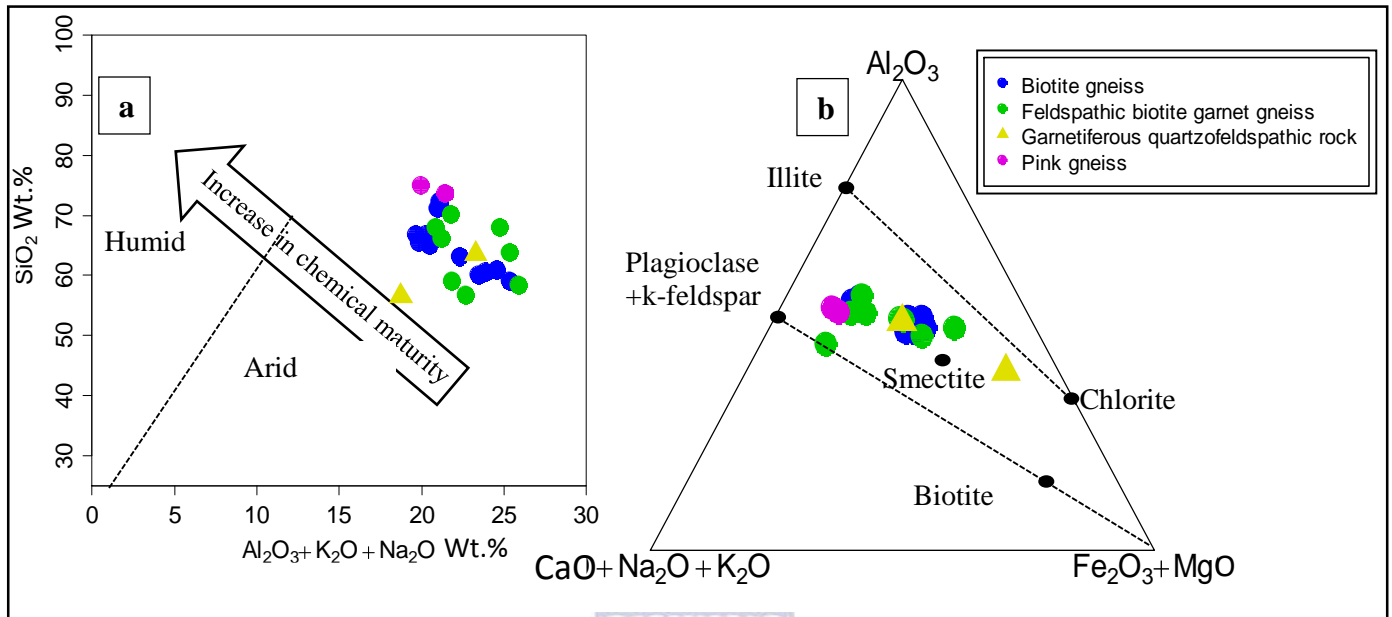


Figure 5-11: a. SiO₂ vs. Al₂O₃+K₂O+Na₂O paleoclimatic discriminant diagram, b CaO+Na₂O+K₂O-Al₂O₃-Fe₂O₃+MgO ternary plot for discriminating element exchange in the siliciclastic sediments during weathering.

5.3.2.2 Provenance

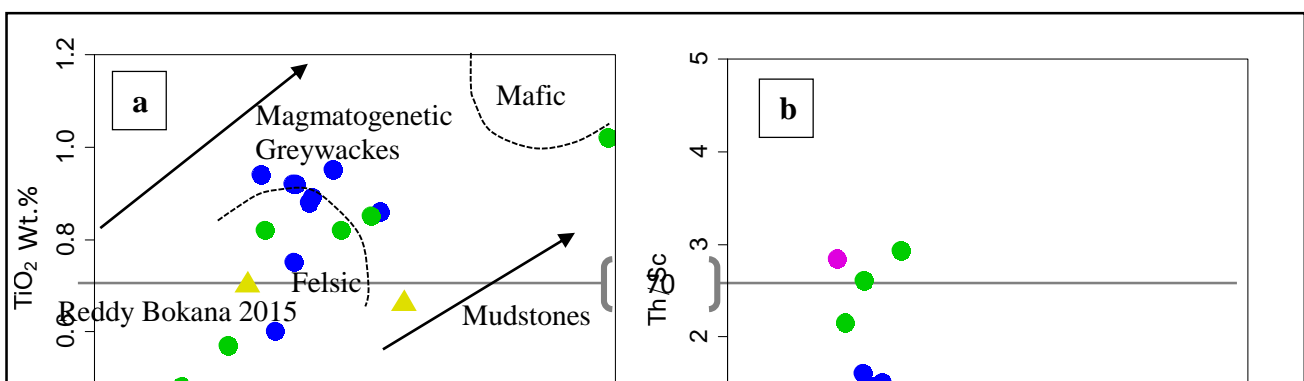
The Al₂O₃/K₂O ratios of Cox et al. (1995) is often used as a provenance indicator on the basis of the differential ratios determine by the presence of clay minerals (Al₂O₃/K₂O < 0.3) relative to the alkali feldspars (Al₂O₃/K₂O: 0.4-10) in the samples. Cox et al. (1995) proposed a specific value of this ratio, being Al₂O₃/K₂O = 0.5 in particular, to be a reliable discriminant function for determining the contribution of the alkali feldspars in the provenance. High and low ratios, i.e. Al₂O₃/K₂O > 0.5 and Al₂O₃/K₂O < 0.5 are denoted as being due to maximal or minimal contribution of the feldspars in the provenance. The maximum (0.52) and minimum (0.17), as well as average values (0.31) of the Al₂O₃/K₂O ratio yielded by the examined rocks collectively suggest that their parent rocks only had a minimal contribution of the alkali feldspar in their provenance. It was also borne in mind that this result may, however, be invalid in the event that the metamorphism was not isochemical (as the elements used as index, particularly K₂O, may be highly mobile during metamorphism).

The application of certain provenance ratios, particularly Al₂O₃/TiO₂, was also suggested by Girty et al. (1996) to discriminate the average provenance composition of pelitic rocks. Girty et al. (1996) effectively distinguished between sediments derived from mafic igneous rocks

($\text{Al}_2\text{O}_3/\text{TiO}_2 < 14$) from those derived from intermediate igneous precursors ($\text{Al}_2\text{O}_3/\text{TiO}_2 = 19$ -28) on the basis of using the specified values of the $\text{Al}_2\text{O}_3/\text{TiO}_2$ ratio. On that basis, therefore, the $\text{Al}_2\text{O}_3/\text{TiO}_2$ ratios of the examined rocks range from 15.43 to 55.54 with an average of 28.94. These results strongly suggest that the detritus forming the protoliths to the studied rocks likely derived from a provenance dominated by felsic to intermediate composition. Similar results were also obtained using Ni and TiO_2 as provenance index (Fig. 5.13a).

The Th/Sc ratio is regarded as one of the best provenance indicators available, i.e. for discriminating between a felsic and mafic provenance of the siliciclastic rocks (Taylor and McLennan, 1985; McLennan et al., 1990; Fedo et al., 1995). Scandium partitions preferentially into mafic minerals, such as the pyroxenes and amphiboles, whereas Th preferentially goes into felsic minerals, usually zircon and allanite (e.g. Rollinson, 1993). The overall moderate to high Th/Sc ratios of the majority of the samples (1-2.83) (Table 5.3), largely confirms the predominance of felsic materials in the provenance. However, the low Th/Sc ratio (0.33) yielded by one sample of the feldspathic biotite garnet gneiss (H- 563-2c) also attests to some contribution of mafic materials in the provenance. Figure 5.12b, which assesses the contribution of a mafic provenance (by indicating high Sc contents and low Th/Sc ratios) as opposed to a more felsic provenance which usually has low Sc contents and high Th/Sc ratios) also attests to the involvement of mafic components in the source area or provenance.

Cr and Zr also make reliable elements for a provenance indicator index (McLennan and Hemming, 1992; Fedo et al., 1995; Cox et al., 1995). Both elements, Cr and Zr, are used as proxies for the respective contents of chromite and zircon in the rocks. Chromium partitions strongly into mafic minerals or rocks, whilst zirconium partitions into felsic minerals or rocks. On this basis, therefore, Cr/Zr ratios should be able to reflect the relative contribution of either mafic or felsic igneous components in the source area. Consequently, the relatively low Cr/Zr ratios obtained from the examined samples (0.13 to 1.09, with an average of 0.75) suggest that the precursors to these rocks formed from materials derived from a provenance of felsic to intermediate composition. The protolith diagram of Reid (1997) (Fig. 5.12c), using the relative proportions of K_2O , MgO and NaO_2 , also suggests that variable types of arkoses are the most likely protoliths to these rocks.



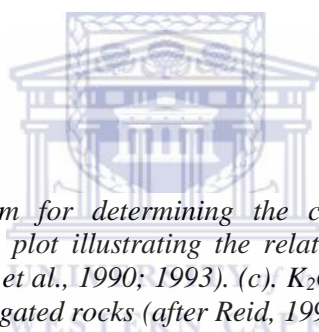


Figure 5-12: (a.) Discriminant diagram for determining the composition of the provenance to the metasedimentary rocks. (b) Th/Sc vs. Sc plot illustrating the relative contributions from mafic and felsic provenance to the rocks (after McLennan et al., 1990; 1993). (c). K_2O -MgO- Na_2O plot indicating the arkosic composition of the protoliths to the investigated rocks (after Reid, 1997).

The metasedimentary rocks have also been investigated by means of using multi-element distribution (with spider diagrams and REE plots). The elements in the spider plot are arranged in the order of McDonough and Sun (1995) and normalized to primitive mantle values. The biotite gneiss displays a typical LILE-enrichment and HFSE-depletion, along with positive anomalies for Rb, Th, and Pb, as well as Nd, U and Zr, and has low contents of Cs, Ba, Nb, Ta and Eu, with Sr, P and Ti showing strong depletion (Fig. 5.13a). The high LILE and Pb contents, along with low Ti and lower HFSE contents than the LILE, further suggests that their protoliths have some kind of crustal influence. The REE pattern, normalised to the chondritic values of Nakamura (1974), show LREE-enrichment and HREE-depletion, $La_N/Lu_N = 3.85$ -11.44, with large negative Eu anomalies [$(Eu/Eu^*)_N = 0.35$ -0.67], moderate fractionation within the LREE ($La/Sm)_N = 2.85$ -4.43) and a relatively flat to positively sloping HREE pattern ($Gd_N/Yb_N = 0.81$ -1.54), steepening from La to Eu and flattening towards Lu (Fig. 5.13b). The $\Sigma LREE/\Sigma HREE$ ratios range from 5.08 to 10.10.

The feldspathic biotite garnet gneiss shows an erratic distribution in the LILE, with high Rb, Th, Nd, and Zr contents, and low contents of Nb, Ta and P, coupled with Ti and Ba troughs (Fig. 5.13c). They furthermore display a negatively sloping REE pattern, with LREE-enrichment relative to HREE depletion ($La_N/Lu_N = 2.35-21.91$), and also showing an overall large and well pronounced negative Eu anomaly [$(Eu/Eu^*)_N = 0.35-0.78$] (Fig. 5.13d). There is one sample (H 445-2), which in the REE plot (Fig. 5.13d), has much higher REE contents than the others, and also has a well pronounced Eu anomaly [$(Eu/Eu^*)_N = 0.78$] which is much larger than that of the others.

The pink gneiss shows enrichments in Rb, Th, U, Pb, Nd and Zr, and depletion in Ba, Nb, Ta, Sr and Ti relative to the general trend of the trace element plot, along with a typical flattening towards the HFSE on the spider plot (Fig. 5.13e). The REE plot shows a negatively sloping pattern, with a typical LREE-enrichment and HREE depletion, with the $\Sigma LREE / \Sigma HREE$ ranging between 7.45-7.68, and having a characteristic negative Eu anomaly ($(Eu/Eu^*)_N = 0.25-0.63$). The Eu anomaly is well pronounced on one sample (H 573-1) [$(Eu/Eu^*)_N = 0.63$] plotting towards the upper field of the REE plot (Fig. 5.13f) and less so on the other sample (H 582-1) [$(Eu/Eu^*)_N = 0.25$] plotting on the lower field of the same plot.

Sample (H 563-5) in the spider plot shows enrichment in Rb, Th, La, Pb, and flattening towards Dy, Y, Yb and Lu in the HFSE, with depletion in Ba, Nb, Ta, Ce, P, Zr and Ti (Fig. 5.13g). It displays HREE-enrichment and LREE depletion ($La_N/Lu_N = 7.24$) and has a fairly pronounced negative Eu anomaly [$(Eu/Eu^*)_N = 0.53$] in the REE plot (Fig. 5.13h). The other sample (H 493-4), by contrast, shows high Cs, U, Ta, Pb, Na, and Sm contents, and ascending from Dy, Y to Yb, flattening towards Lu, with Ba, Nb, Ta, Ce, Zr, P and Ti showing troughs in the spider plot (Fig. 5.13g). The REE pattern, by contrast, shows normal LREE enrichment relative to HREE ($La_N/Lu_N = 0.22$), and has a smaller negative Eu anomaly [$(Eu/Eu^*)_N = 0.24$] in comparison to the one reported earlier. The garnetiferous quartzofeldspathic rock like the pink gneiss, has two samples showing contrasting patterns both in the spider diagram and the REE plot (Fig. 5.13g & h).

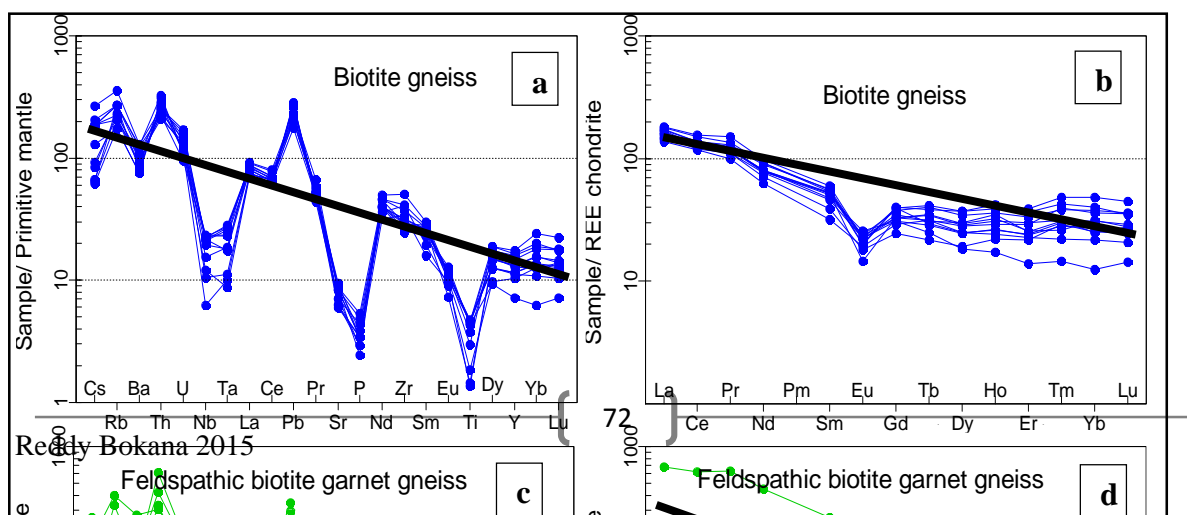
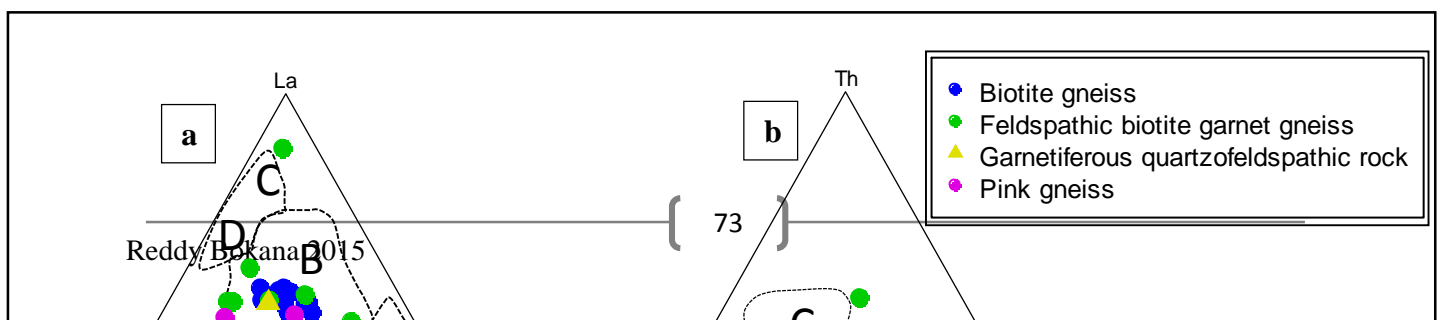




Figure 5-13: Spider plot normalized to the primitive mantle values of McDonough and Sun (1995), with the REEs normalised to the chondrite values of Nakamura (1974).

Th-Sc and La-Th-Zr/10 diagrams of Bhatia and Crook (1986) (Fig. 5.14a & b), were employed for tectonic discrimination of sedimentary rocks. Both diagrams (Figure 5.14a & b) show different fields in which modern and ancient sediments of various tectonic environments are determined. In both the La-Th-Sc plot (Fig. 5.14a) and the La-Th-Zr/10 plot (Fig. 5.14a & b), the majority of the samples plot within the field of continental island arc setting.



5.4 Geostatistical analysis

The geostatistical analyses, using R-mode cluster and stepwise discriminant analyses were employed on major and trace elements data in an attempt to establish the relationships that exist between the mineralization host and the country rocks. Particular attention was given to the meta-gabbronorite as it occurs as the actual host rock to the mineralization. Application of statistical techniques were employed in order to create meaningful geochemical patterns for which vectoring and element prediction can be developed. Most trace elements were, however, not useful because of their various distribution for developing vectors. Two clusters using major elements data were generated and are shown on dendrogram (Fig. 5.15). Each cluster is defined based on major element associations and lithological associations on the database.

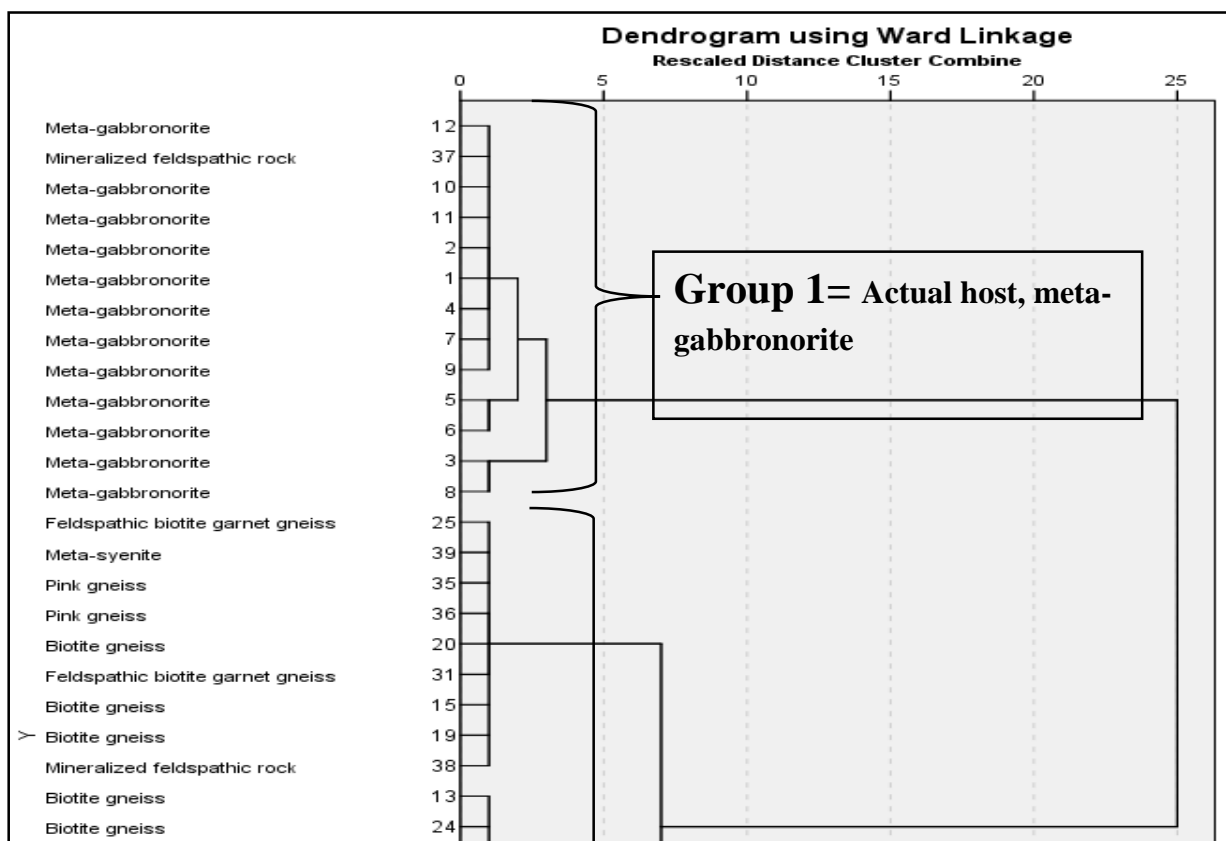


Figure 5-15: Dendrogram showing rock association groups based on the Ward method

Table 5.4a displays the element associations and the functionality of each cluster on the dendrogram:

- Group 1: actual host rock (the meta-gabbro ± enderbite)
Element association: TiO_2 , CaO , MgO , Fe_2O_3 , Cr_2O_3 , P_2O_5 , MnO and L.O.I.
- Group 2: country rocks
Element association: Al_2O_3 , Na_2O , K_2O and SiO_2

The two groups are characterized in terms of mafic and felsic element associations for group 1 and group 2 respectively. There are, however, only four elements (Al_2O_3 , CaO , MgO and TiO_2) in the database (Table 5.4b) which are significant for determining the classification of the groups. These results indicate that any sample in group 1, for example those of the meta-gabbro, would comprise of high TiO_2 , high CaO and high MgO but low Al_2O_3 contents. Those in group 2, by contrast, will show the opposite of those elements reported in group 1 (low TiO_2 , low CaO and low MgO but high Al_2O_3 contents). In addition, the samples falling in group 2 will also be characterized by high Na_2O , high K_2O and high SiO_2 , which otherwise are depleted in group 1.

The depletion in such elements as CaO, MgO and most especially TiO₂, and high contents of Na₂O, K₂O and SiO₂, and most especially Al₂O₃ should reflect the compositional differences, and contacts between the meta-gabbro and the other litho-types in the boreholes. Therefore, numerous geochemical indices, based on these compositional differences, could be developed and be used to monitor and visualize such contact using numerous bivariate plots (Fig. 5.15).

Table 5-4 Element discrimination function for determining the actual ore-host rock (the meta-gabbro) (group 1) and the associated host rocks (group 2)

a		b		c				
	Function		Function	Classification Results ^a				
	1		1		Ward Method		Predicted Group Membership	Total
					1	2		
TiO ₂	-.334	Al ₂ O ₃	-.514	Count	1	13	0	13
CaO	-.255	CaO	.789	Original	2	0	28	28
SiO ₂	.234	MgO	.578	%	1	100.0	.0	100.0
MgO	-.175	TiO ₂	.969		2	.0	100.0	100.0
Fe ₂ O ₃	-.149			A 100.0% of original grouped cases correctly classified.				
K ₂ O	.065							
Cr ₂ O ₃	-.055							
P ₂ O ₅	-.053							
MnO	-.047							
Na ₂ O	.040							
Al ₂ O ₃	.037							
L.O.I.	-.022							

a) General discriminant functions showing the two groups, with a positive association (indicating group 1) and a negative association (indicating group 2). b) Most significant element-discriminant functions in the groups. c) Eigenvalue indicating the accuracy and validity of the classification.

Figure 5.16 displays four typical examples in which such indices (namely Al₂O₃ vs. CaO; Al₂O₃ vs. MgO; Al₂O₃ vs. TiO₂; and Al₂O₃ vs. CaO+MgO+TiO₂) can be used to set aside the actual host rock (which is the meta-gabbro) to the large group of country rocks. Several indices with such kinds of examples are discussed further in Chapter 6. As also shown in Table 5.3c, the success rate of using these indices is quantified as being as 100 % accurate and applicable; implying that each indices can be applied with a fair amount of confidence for mapping the intervals where the meta-gabbro occurs within different boreholes. This technique can be used to aid to the logging technique to determine the position of the meta-gabbro in the boreholes (especially if conventional logging technique fail in case of the

presence of several alteration in the rocks). The application of these indices, for example, those shown in Figure 5.16, increases from index 1 (Fig. 5.16a) to index 4 (Fig. 5.16d), clearly indicating that the latter index (Fig. 5.16c) would be more useful than the former (Fig. 5.16a).

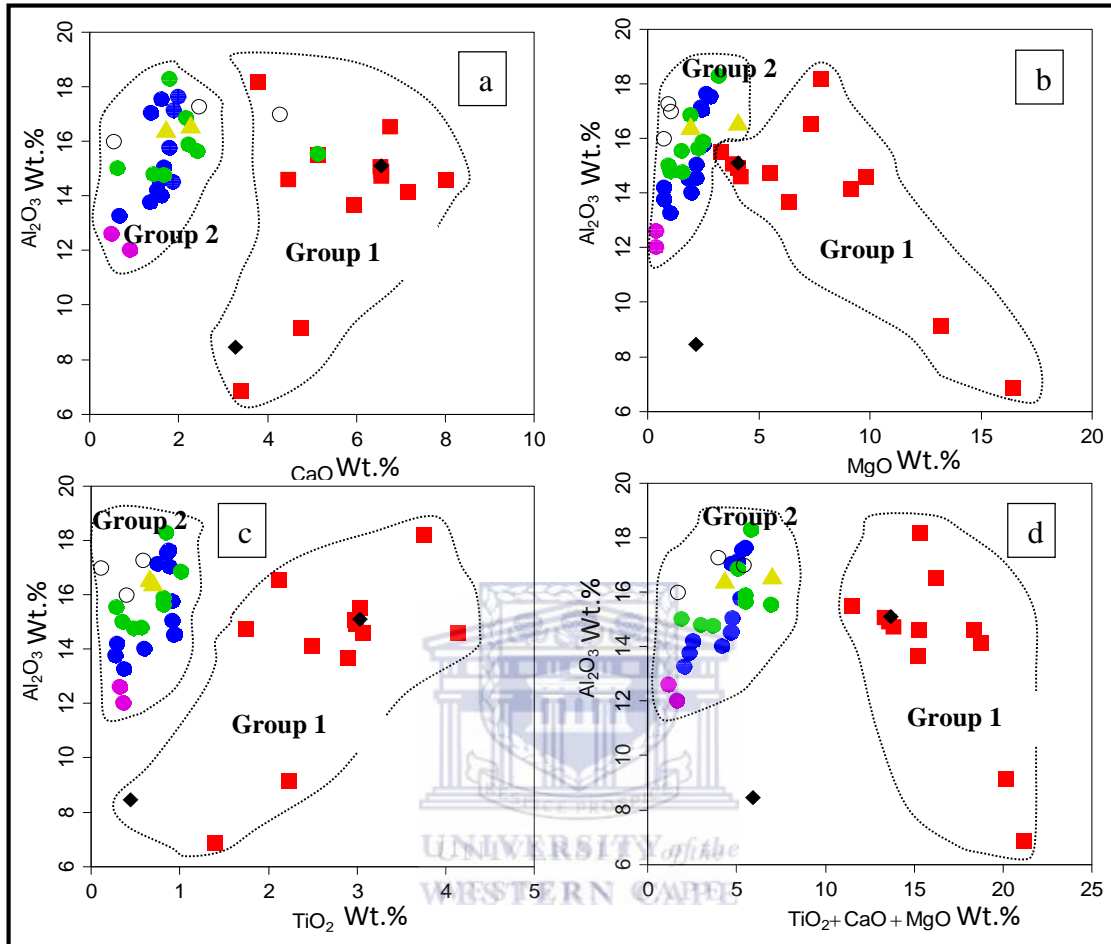


Figure 5-16: Indices to distinguish between the actual host-rock and the other associated host-rocks. Group 1 represents the meta-gabbro and group 2 all the other rock-types. TiO_2 vs Al_2O_3 and Al_2O_3 vs. $TiO_2+CaO+MgO$ provide the best differentiation between the two groups.

Table 5.5 also shows the results obtained from multivariate correlation analysis, of which the significance of the correlation matrix has been limited to 0.5, wherein the distribution and existing relationships among different elements, including the base metal sulphides (Ni, Cu, Zn and Co), have been investigated and highlighted. As clearly shown in Table 5.5, only values which are highlighted and those with two tails are considered as being the most useful correlation coefficients (as they fall within the significance of 0.05 as specified), and are also considered as the only values that show a meaningful measure of the nature (positive or negative), magnitude (high or low) and strength (strong or weak) of the relationships between the variables (elements, in this case) to be used for vectoring.

As mentioned earlier, significant correlations (or relationships) are highlighted on Table 5. 5. Certain elements, such as Al_2O_3 and Na_2O , showed a strong negative correlation with Ni, Cr,

Co, MgO and Fe₂O₃; Na₂O is negatively correlated with Zn. In the same order, Ni, Cr and Co also showed strong positive correlations with both MgO and Fe₂O₃ as well as among themselves. Zn, in turn, has only been positively correlated with Ni and Na₂O. Cu by contrast shows no significant correlation matrix in the dataset.

Table 5-5: correlation table showing element relationships in the dataset

Correlations													
	Al ₂ O ₃	CaO	Fe ₂ O ₃	K ₂ O	MgO	Na ₂ O	P ₂ O ₅	TiO ₂	Cr	Co	Ni	Cu	Zn
Al ₂ O ₃	1	.384	-.732**	.522	-.769**	.640*	.322	.600*	-.874**	-.745**	-.882**	-.507	-.467
CaO		1	-.613*	-.317	-.653*	.570*	.078	-.050	-.566*	-.498	-.603*	.047	-.510
Fe ₂ O ₃			1	-.400	.914**	-.841**	-.610*	-.541	.842**	.925**	.879**	.141	.656*
K ₂ O				1	-.396	.299	.581*	.711**	-.408	-.520	-.377	-.169	-.112
MgO					1	-.871**	-.558*	-.412	.939**	.956**	.927**	.250	.603*
Na ₂ O						1	.397	.301	-.816**	-.844**	-.839**	-.322	-.752**
P ₂ O ₅							1	.713**	-.493	-.727**	-.475	-.159	-.269
TiO ₂								1	-.465	-.540	-.510	-.233	-.226
Cr									1	.894**	.984**	.462	.676*
Co										1	.877**	.331	.550
Ni											1	.400	.746**
Cu												1	.178
Zn													1

** . Correlation is significant at the 0.01 level (2-tailed).
 * . Correlation is significant at the 0.05 level (2-tailed).
 The most significant correlations are highlighted in bold and the most significant correlations indicate two tails of which the number are either positive (where elements increase together) or negative (where the relationship becomes inverse).

Additional results obtained also indicate that Cr and Zr, together, correlate strongly with Ni, 98.1% of coefficient of determination (Table 5.5), with Cr alone providing 97% of the information of Ni. For all the host rocks combined, Cr provides 82.7%, Co 5.0% and Fe₂O₃ 1.3% of correlation with Ni. This result, therefore, indicates that Cr alone controls the distribution of Ni in all the host rocks and within the meta-gabbro. Co is controlled by MgO both in the meta-gabbro (90.9%) and in all the country rocks (89.9%). Similarly, the distribution of Zn in the meta-gabbro can be predicted using Na₂O (56.4%), followed by Co (64.1%) in the country rocks. Cu was, however, excluded in this investigation as the data revealed no correlation coefficient (Table 5.5) for it. Several geochemical indices are also developed and discussed further in chapter 6. Those indices are therefore considered as pathfinder elements with potential for pointing towards the mineralization. Table 5.6 shows different predictors for the mineralization both in the meta-gabbro and in all other country rocks altogether.

Table 5-6: Element predictors and their predictability percentage as pathfinders for Ni, Co and Zn in the meta-gabbro and in all the host-rocks

Element predictor for Ni	Percentage of prediction	Element predictor for Co	Percentage of prediction	Element predictor for Zn	Percentage of prediction
In the meta-gabbro					
Cr	97.0 %	MgO	90.9%	Na ₂ O	56.4%
Zn	1.1%	P ₂ O ₅	5.8%		
Total	98.1%				56.4%
In all country rocks altogether					
Cr	82.7%	MgO	89.9%	Co	61.4%
Co	5.0%	Cu	3.6%		
Fe ₂ O ₃	1.3%	CaO	2.4%		
Total	89.0%		95.9%		61.4%

Attached tables display both the coefficient of correlation (*R*) and the coefficient of determination (*R*-Square) and the potential predictors for each element of interest. Also shown are the results obtained while investigating the meta-gabbro in isolation and those for all the host-rocks combined.

6. CHAPTER VI

DISCUSSION, CONCLUSIONS AND RECOMMENDATIONS

6.1 Discussion

6.1.1 Introduction

Understanding the origins (source/provenance), protoliths and tectonic evolution of the highly metamorphosed and polyphase deformed rocks of the poorly-known Garies Terrane in the south-western section of the Mesoproterozoic Namaqua-Natal Metamorphic Province, and, in particular, the host lithologies to the Hondekloof mineralization, was the major focus of this study. Findings on the host lithological characteristics as well as a classification of the

mineralization type in view of the general and global classification of magmatic Ni sulphide mineralization, as defined by Naldrett (1999, 2004), Hronsky (2007), and Song et al. (2008, 2011) are discussed and addressed with particular attention on the Hondekloof prospect.

6.1.2 Origin and protoliths

There are a total of seven lithologies (namely the meta-gabbro-norite, biotite gneiss, feldspathic-biotite-garnet gneiss, pink gneiss, meta-syenite, enderbite and garnetiferous quartzofeldspathic rock) that are identified and among which only the meta-gabbro-norite occurs in association with the mineralization. The geochemical study conclusively revealed two overall precursor origins (magmatic and sedimentary) which allowed the characteristic natures of the protoliths of each lithology examined to be determined (Fig. 5.3). Lithologies of magmatic origin include the meta-gabbro-norite, meta-syenite, enderbite and the garnetiferous quartzofeldspathic rock. Those of sedimentary origin include the biotite gneiss, feldspathic biotite garnet gneiss, as well as the pink gneiss (Fig. 5.3).

The meta-gabbro-norite falls exclusively within the magmatic field on the classification diagram of Winchester and Max (1982) (Fig. 5.3) and has a basaltic composition on the protolith discrimination diagrams of Winchester and Floyd (1977) (Fig. 5.4a & b). The latter interpretation is supported by the nearly flat REE pattern (Fig. 5.10b) and a weakly sloping spider diagram pattern (Fig. 5.10a), indicating that the meta-gabbro-norite samples collectively reflect the composition of a mafic composition protolith. These trends are, collectively, in good agreement with the occurrence of plagioclase as well as such mafic minerals as ortho- and clinopyroxene and that are confirming that the nature of the magma generating this rock is of a basaltic composition. However, enrichment of Rb, Ba and Pb, as shown on the multi-element spider plot (Fig. 5.10a), is indicating that there is an influence of a crustal component either due to crustal contamination or due to the overall composition of the source area of the meta-gabbro-norite. A well-pronounced negative Eu anomaly, as clearly shown on the REE plot (Fig. 5.10b), suggests that there was retention of plagioclase component in the source area. The meta-gabbro-norite compositions range between calc-alkaline and tholeiitic magma composition (Fig. 5.5), and hold the chemical characteristics of a rift and continental arc type tectonic magmas as defined by Verma et al. (2008, 2013). The results shown on Fig. 5.6a and b, further indicate that the meta-gabbro-norite holds the chemical characteristics of a depleted mantle source, source of Mid Oceanic ridge Basalt (MORB)-melt, and that, it has no affinity to an enriched mantle-source, source of Ocean Island Basalt (IOB)-like melt. The present study based on the

latter interpretations concludes that this meta-gabbro-norite should be regarded as forming part of the Oorkraal Suite following the suggestion of Hamman et al. (1996); and that is not directly related to Koperberg Suite as suggested by Andreoli (1987, 1991a).

Similarly the meta-syenite samples are also of magmatic origin, as shown on the classification diagram of Winchester and Max (1982) (Fig. 5.3), but are different as they are of felsic composition (Fig. 5.4a & b). This corresponds to the relatively negatively sloping patterns in both REE plots and spider diagrams (Fig. 5.10c and d) of this lithology, reflecting the presence of a crustal component or derivation from a crustal source. A felsic composition is also indicated by the abundance of K-feldspar in the mineralogical composition of this rock, which conforms to the high K, calc-alkaline composition of this rock (Fig. 5.5b). The presence of a Nb-Ta “trough” in the spider diagram pattern of this rock (Fig. 5.10c) is suggestive of the involvement of a crustal component and reflects a subduction related tectonic environment (Rollinson, 1993). The relative depletion of P and Ti, as shown on the spider diagram (Fig. 5.10c), also suggests the presence and retention of apatite as well as magnetite/ilmenite in the source area from which the magma forming this meta-syenite was generated. Suggestions were also made with regards to the classification of this meta-syenite, given the fact that it has orthopyroxene and therefore should be termed a charnockite or having affinity to a group of charnockitic intrusion. However, two interpretations may be possible in this case, as it may either be part of the post-tectonic charnockite of the Little Namaqualand Suite (hence the name charnockite) or be part of the pre- to syn-tectonic bi-modal felsic magma which was emplaced at the same time as the Oorkraal Suite magma (hence the name meta-syenite).

The original sedimentary signature has only been retained for the pink gneiss samples amongst all the gneisses (biotite gneiss, feldspathic biotite garnet gneiss, and pink gneiss) represented on the classification diagram of Winchester and Max (1982) (Fig. 5.3). The biotite gneiss and feldspathic biotite garnet gneiss straddle the boundary between the magmatic and sedimentary fields (showing a dispersed distribution that is suggestive of a mixed origin characteristics) (Fig. 5.3). The effects of partial melting in these gneisses, as pointed out in chapter 4, may be responsible for influencing their chemical composition in the latter diagram (Fig. 5.3). They have the chemical compositions which seemingly reflect a mixed origin, such as that of a “volcaniclastic”, or a compositional equivalent of the volcaniclastic nature. Certain element ratios, such as Th/Sc, Cr/Zr and Al_2O_3/TiO_2 , collectively suggest that the protoliths to these gneisses were derived from a provenance of felsic to intermediate composition (Fig. 5.12a).

Some element-based factors (such as the CIA and CIW), furthermore suggests that the detritus forming these gneisses also underwent little to low degrees of weathering in their provenance (or source area). They are all collectively displaying the signature of subduction-related processes, as shown by the presence of Nb-Ta “troughs” in their multi-element spider diagram patterns (Fig. 5.13), and also clearly, consistently reflect a continental island arc tectonic setting (Fig. 5.14). Additional trends, for example, using MgO-K₂O-Na₂O (Fig. 5.12c) as well as Ni vs. TiO₂ (Fig. 5.12a), as the protolith indicators indicate that the protoliths to these gneisses have the overall composition of predominantly arkoses, and, to a lesser extent, psammitic sediments. This, in combination with the studies of Moore (1983, 1989) and Albat (1984), suggests that these gneisses should be regarded as meta-arkoses generated from the metamorphism of continental arc sediments.

Features of partial melting, for example the presence of coarse grained quartz and alkali feldspar assemblages, migmatitic segregations and pegmatitic textures in the rocks, as reported by Waters and Whales (1984) along the southern section of the Namaqualand, have also been detected in this study through the mineralogical and textural characteristics of enderbite and garnetiferous quartzofeldspathic rock. It is therefore suggested here that both the enderbite and garnetiferous quartzofeldspathic rock have likely been generated through partial melting during prograde dehydration metamorphism. It also is suggested here that the garnetiferous quartzofeldspathic rock corresponds with the Ibiqas Granite (S-type granite), as proposed by Macey et al. (2011), due to the fact that the mineralogical composition of this rock (dominated by almandine garnet and alkali feldspar) reflects a generation of melt derived either from a metasedimentary rock or an equivalent of peraluminous igneous rock.

The suggestion that enderbite is a melt product of the meta-gabbro is based on the observation of the close association both chemically and mineralogically as well as spatial proximity in the boreholes of these two rock types (Fig. 4.2). A partial melt origin is also suggested by the presence of sulphide mineralisation in the enderbite, suggesting remobilisation and redistribution of the sulphides contained within the host meta-gabbro at a local scale during high grade metamorphism, partial melting and deformation. Table 6.1 gives a summary of the proposed protoliths based on interpretation of this study.

Table 6-1: Proposed protoliths

Litho-type	Mineralogical Evidence	Textures	Proposed Protolith	Alternative Protolith
-------------------	-------------------------------	-----------------	---------------------------	------------------------------

Meta-gabbronorite	Two pyroxenes + plagioclase	Granoblastic and gneissic foliation	Gabbronorite/or two pyroxene granulite	Gabbro or norite
Garnetiferous quartzofeldspathic rock	Garnet + quartz + alkali feldspar	Poikiloblastic	partial melt segregation	Peraluminous igneous rock
Biotite gneiss	Quartz, alkali feldspar and biotite	Gneissic foliation	Psammitic arkoses/sandstone	Semi-pelitic or granitic/rhyolitic rock
Feldspathic biotite garnet gneiss	Quartz and k feldspar + garnet	Gneissic foliation	Psammitic arkoses/sandstone	Semi-pelitic or granitic/rhyolitic rock
Pink gneiss	Quartz and feldspar + biotite	Gneissic foliation	Psammitic sediments	Semi-pelitic or granitic/rhyolitic rock
Meta-syenite	Alkali feldspar (≥ 65 -70 wt. %)	Relict interlocking textures	Syenite	Monzonite/granite
Enderbite	Plagioclase+ feldspar + orthopyroxene	Pegmatitic	A partial melt segregation from a gabbronorite	A partial melt segregation from norite or gabbro

6.1.3 Metamorphism and deformation

The work of Albat (1984) and Waters (1986b) on the metamorphic evolution of southern Namaqualand made it unnecessary for us to undertake geobarometry and geothermometry analyses, and that the findings of these earlier workers could simply be confirmed from mineral parageneses. The consistency in these authors' works as well as supporting evidence from a number of regional metamorphic studies in the Namaqua Sector, and the Okiep Copper District, (e.g. Robb et al., 1999; Clifford et al., 2004; Clifford and Barton, 2012), suggest temperature and pressure conditions in the upper amphibolite to upper granulite facies grade (temperatures $\geq 750^{\circ}\text{C}$ and pressure = 5-6 kbar). Waters (1988) suggested thermal conditions reaching up to dehydration partial melting conditions based on the supracrustal sequences of the Kamiesberg Group he studied along the southern portion of the Kliprand area. He made use of multiple mineral reaction processes, such as $\text{biotite} + \text{sillimanite} + \text{quartz} = \text{garnet} + \text{K-feldspar} + \text{liquid}$ to infer a low pressure-granulite facies metamorphism and anti-clockwise P-T regime for the whole south-western and western portion of the Namaqua Sector encompassing both the Okiep Copper District as well as the Garies and Kliprand areas. Albat (1984) used two models for the purpose of discussing the thermal evolution path and the nature of high temperature-low-pressure granulite facies metamorphism in the supracrustal sequences around the Kliprand area. The pros and cons of the models as proposed by these earlier worker will be discussed and follow on with interpretation from the present study.

6.1.3.1 Models of Albat (1984)

The graphical illustrations of the two models proposed by Albat (1984) are shown on Figure 6.1a and b, respectively. The first model (Fig. 6.1) proposed that the western Namaqua Sector was affected by a series of cumulative metamorphic events occurring contemporaneously with a specific deformation event (e.g. D_1+M_1 ; D_2+M_2 and D_3+M_3). The model therefore evoked the concept of thermal peaks and thermal troughs to separate different periods of thermal fluctuation in the metamorphic history of the Namaqua Sector (Fig. 6.1).

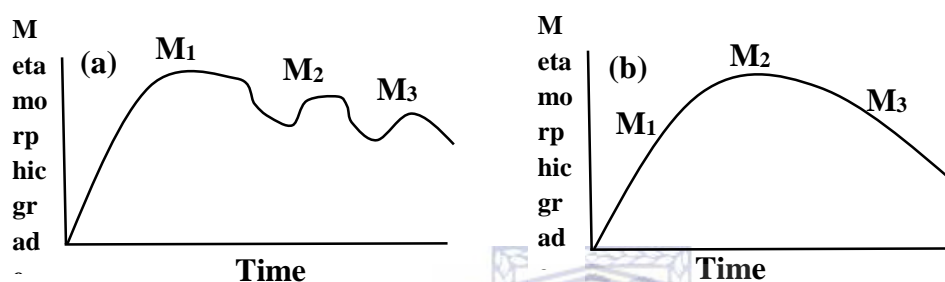


Figure 6-1: Two schematic models for the metamorphic regime of the western Namaqua Sector. (a): Successive metamorphic events labelled as M_1 , M_2 and M_3 , showing the changes in the thermal regime through time. (b) A single metamorphic event attaining the maximum thermal climax (M_2) after which the temperature cools off gradually.

The first model suggests that the western Namaqua Sector rocks were heated in a cycle of three successive metamorphic events accompanied by three phases of deformation, from D_1+M_1 through D_2+M_2 , to D_3+M_3 . The M_2 metamorphic event represents an amphibolite facies metamorphic event and is recorded as the second highest thermal event in the cycle. M_3 is a granulite facies condition and post-dates the M_2 event. The model thus suggests that the metamorphism in the western Namaqua Sector followed a characteristic anti-clockwise pressure temperature time (P-T-t) path due to the fact that the thermal peak increased progressively to a granulite facies condition, M_3 , and subsequently cooled off approximately isobarically. Robb et al. (1999) recommended this model for the whole western Namaqua Sector after examining the regional metamorphism of the Okiep Copper District and surrounds. Waters (1990), for example, argued that such peak metamorphic conditions in the western Namaqua Sector could only have been attained or facilitated by magmatic accretion that might have been achieved by emplacement of a thick basaltic body which was underplated at least 10

km below the present level of erosion, accompanied by voluminous felsic intrusions into the mid-crust.

The second model, by contrast, suggests that the western Namaqua Sector rocks were heated gradually to a maximum granulite facies condition (M_2) and subsequently cooled off gradually thereafter (Fig. 6.1). This model therefore challenges the existence of several periods of thermal fluctuations in the metamorphic history of the western Namaqua Sector and rather promotes a single continuous thermal path reaching a thermal climax (M_2) after which the peak metamorphic conditions gradually subsided. M_2 , according to this model, is documented as the prograde (thermal high) event of granulite facies conditions. M_3 represents amphibolite facies conditions which were superimposed onto the M_2 event as its retrograde phase. This model, to some extent, is similar to the first model, but in reverse, in that the granulite facies metamorphism, M_2 , which is the highest thermal event, pre-dated the later amphibolite facies event, M_3 . This model thus, in summary, suggests a clockwise pressure temperature time (P-T-t) path for the western Namaqua Sector metamorphism.

6.1.3.2 Present study interpretation

Textural evidence recorded from the present study correlates well with the second model rather than first model. The former model offers features which explain much of the thermal path and P-T regime under which the Hondekloof prospect could possibly have been metamorphosed. No textural evidence suggesting the occurrence of multiple metamorphic events, such as coronas, were observed in the investigated rocks, thus failing to corroborate the first model. Corona textures provide tangible evidence of thermal highs and lows and support several periods of thermal fluctuations in the metamorphic history (Waters and Whales, 1984; Waters, 1986b). Temperature-sensitive minerals, such as garnet and biotite, would have recorded such a metamorphic history by preserving several temperature-dependent features, for example, textural zonation patterns within minerals (Waters, 1986b). Each zone or pattern would have been unique and characteristic for each specific thermal period in the metamorphic record (Waters and Whales, 1984; Waters, 1986b). Ideally, several metamorphic reaction features, such as coronas and double coronas, would be expected to have been preserved in the rock record if model 1 was applicable in the study area. No such features were observed during the present study.

The second model is supported, in this current study, by the occurrence of mineral reaction textures such as pyroxene being replaced by amphibole (hornblende) in the meta-gabbro. Furthermore, chlorite and epidote (green assemblages) replace such minerals as biotite and plagioclase in such lithologies as the biotite gneiss, suggesting that the latest metamorphic event, which is M₃, probably cooled off to a near greenschist facies conditions. This interpretation corroborates well with the textural evidence described in numerous sections in chapter 4. This suggests that the magma that formed the meta-gabbro and Hondekloof deposit possibly intruded prior to the D₂ deformation event and was affected by the M₂ granulite facies metamorphism. The present interpretation does not, however, by any means, rule out the possibility of having another higher thermal event prior to M₂ in the area. Nevertheless, no textural evidence was observed to lead to such a conclusion during the present study. But, if a pre-M₂ peak metamorphic assemblage exists, then any evidence of its existence must have been destroyed and is not preserved in the rock record. Alternatively, a previous high grade metamorphic event, if it exists, may have occurred prior to intrusion of the precursor to the meta-gabbro.

6.1.4 Tectonic evolution

Very little is known about the nature, age and tectonic evolution of the Garies terrane outcrops. Reliance is, however, placed on the work of Albat (1984) and Macey et al. (2011) for interpretations of the tectonic evolution of the Kliprand area and surroundings. Based on the limited data available and consideration on previous work available, two simplified tectonic scenarios are envisaged and discussed.

6.1.4.1 Extensional analogue (local scale)

The local geology, most particularly the structural configuration as well as the petrographic and geochemical characteristics of the lithological units that occur within the Kliprand area provide numerous evidences of multiple phases of local deformations in study area. It is with that knowledge that models of local and regional scales were developed, and discussed concurrently in order to accommodate interpretations of multiple phases of deformation in the study. Figure 6.2a summarizes the various stages involved during the extensional regime which acted locally within a back arc basin (under the assumption that the Kliprand area is a portion of a back-arc basin within the regional collisional system of the Namaqua Sector). It is here suggested that the Garies-Kliprand area may be regarded as a portion of an old thickened

lithospheric-continental crustal block or a localized back arc basin and an extensive mobile belt in the anatomy of a collisional system of the Namaqua Sector with the Kaapvaal Craton (Albat, 1984). The block underwent a localized rifting/crustal extension (in the local scale) (Fig. 6.2a-stage 1) leading to opening up of a back arc basin due to continuous lithospheric thinning (Fig. 6.2a-stage 2). Subsequently further extension occurred, causing erosional debris (the sediments which would be lithified into the pink gneiss, biotite gneiss, etc.) to become available and deposited in the basin (Fig. 6.2a-stage 3). Continued extension led to continuous accommodation which, in turn, led to basin sagging. Crustal extension led to mantle upwelling and partial melting (Fig. 6.2a-stage 4), with intrusions of the mantle-derived magma subsequently occurring. Throughout this time, however, deposition of detritus into the basin was continuous (Fig. 6.2a-stage 5). Burial subsequently and progressively occurred (Fig. 6.2a-stage 6) and the whole area underwent a regional granulite facies metamorphism (caused by the overall compressive regime and crustal thickening and/or pressure of the overlying stratigraphic successions, or simply as the lower sediments got buried to deeper and deeper levels) (Fig. 6.2a-stage 7). Exhumation occurred subsequently, with the overall regional compressional stress, coupled with multiple intense erosional periods being the driving forces which mechanically unroofed the stratigraphic units of the upper successions and ultimately exposed the granulite facies rocks at the surface (Fig. 6.2a-stage 8).

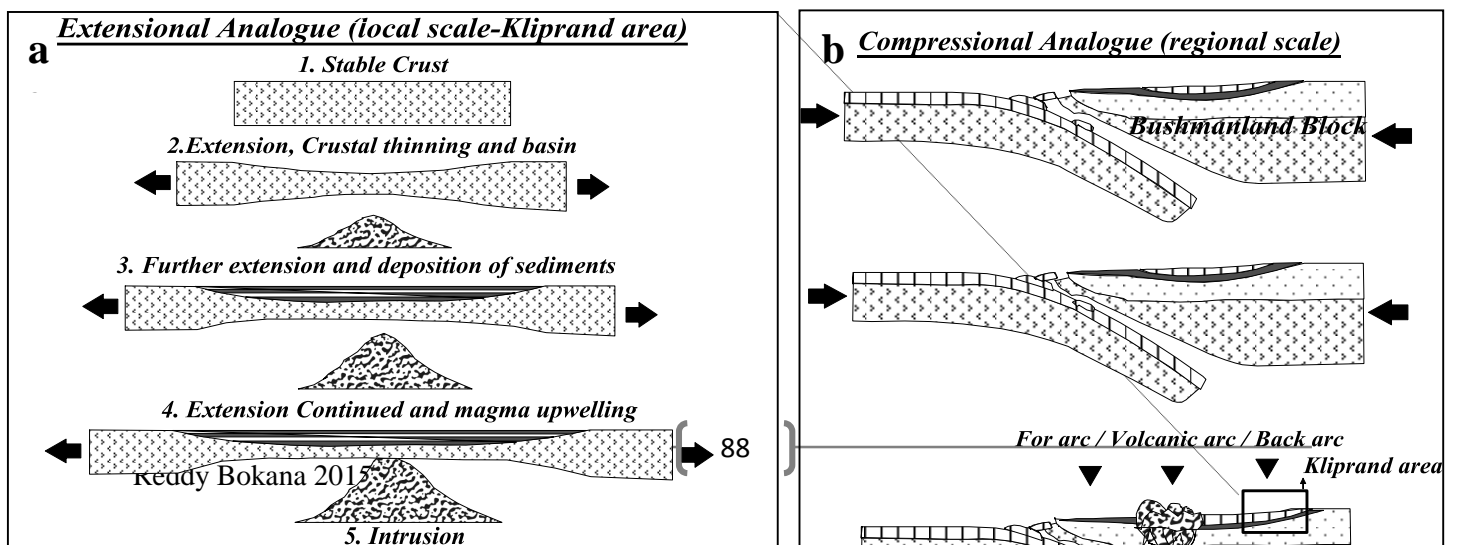
6.1.4.2 Compressional analogue (Regional scale)

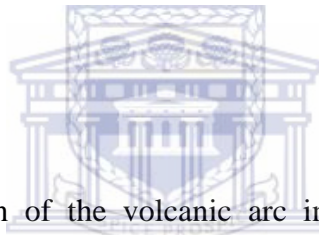
This model, in contrast to the previous one, attempts to explain the compressional forces acting regionally in the framework of a convergence subduction-related scenario (Fig. 6.2b). This model proposes that the Garies Terrane, as a whole, should be considered as forming part of a large subduction-related collisional system in the Namaqua Sector (Fig. 6.2b-stage 1), wherein the Kliprand and surrounding areas would represent the arc-related basins which have opened up and developed either in front of, or behind a volcanic arc (see suggestions of Albat, 1984).

Meta-sedimentary rocks, such as the biotite gneiss and pink gneiss, derived from arc settings as shown both by arc-signature (Fig. 5.14), and by subduction-related signature in them (Fig. 5.13). Those of magmatic origin, by contrast, were derived either from a local rifting (e.g. the meta-gabbro-norite) (Fig. 5.7) or by the recycled crustal materials which underwent melting (e.g. the meta-syenite). A plausible scenario for developing an arc related basin locally within the Kliprand area, in a major compressional regime, such as that of the Namaqua Sector

configuration, is here explained by a north-south subduction process of the Kaapvaal Craton-Rehoboth cratonic block beneath the Bushmanland Subprovince.

There are a wide range of pre- to syn-tectonic metamorphosed sedimentary rocks as well as a large volume of bimodal igneous rocks which are locally exposed in the Kliprand area (Macey et al., 2011). The occurrence of these mixed- litho-types and their multiple characteristics and origins provide evidence that the Garies Terrane, if not regionally, but at least locally, has been subjected to a multiple phases of tectonic events. Sedimentation in active convergent and subduction related settings commonly occurs in basins which have opened up either in front of (i.e. the fore-arc basin) or behind (i.e. the back arc basin) a volcanic arc zone (Keller et al., 2002). Continuous opening either in back-arc or in fore-arc basins commonly ends with a series of magmatic intrusions occurring concurrently with sedimentation in the basin (Faccenna et al., 2001; Keller et al., 2002). Evidence of sedimentation, based on the presence of a variety of meta-arkoses, as well as bimodal magmatism, as shown by the existence of the meta-gabbro and meta-syenite, provide clear indications of a rift-type continental back arc environment. The geochemistry of the meta-gabbro (spider diagram Fig.5.10a), and their tectonic setting classification on multiple tectonic discrimination diagrams of Verma et al. (2008) (Fig. 5.7), in particular, support the involvement of a rift arc setting signature. Prominent Nb and Ta “troughs” in the multi-element trace element diagrams (spider diagrams) (Fig 5.13a, c, and e) of all the meta-arkoses clearly attest to the fact that these rocks regionally have a subduction related signature and hence collisional tectonic setting. These features confirm that the protoliths (sediments) which formed these meta-arkoses were derived from provenances which were generated from a subduction-related type of setting. The meta-gabbro, by contrast, does not show a Nb and Ta subduction “trough” or anomaly in its spider diagram (as clearly shown for the meta-syenite samples) (Fig. 5.10a & c). This suggests that the meta-gabbro, likely, could have been generated by magmatism within the back arc basin, and that its parental magma was produced further away from the actual metasomatized mantle wedge (and hence no subduction signature was retained).





The actual location and position of the volcanic arc in the overall regional subduction collisional model (Fig. 6.2b), to date, is still puzzling and has yet to be well understood. The volcanic arc terrane of the Richtersveld Subprovince, located farther to the north of the study area, has been suggested as a possible candidate for the volcanic arc representation (Albat, 1984). The possibility of having a possible, enigmatic and, as yet, unidentified crustal block flanking the south-western margin of the Garies Terrane can also not be completely ruled out as a possible scenario and theory. Such a crustal block would then have probably detached from the whole Namaqua Sector during the break up of Gondwana or before or during the break up of Rodinia. However, if this is true, the whereabouts of such a block, and, as to where it went and its present location, may result in a protracted debate and -un-resolvable matter. The subduction signature, as shown in the various samples of the biotite gneiss, pink gneiss and others (Fig. 5.13) clearly suggests that the protoliths to these rocks were generated in a collisional arc-related type of setting. This information, in combination with the position of these samples in the tectonic discrimination diagram of Bhatia and Crook (1986) (Fig. 5.14), support the involvement of a collisional arc basin as a host tectonic setting.

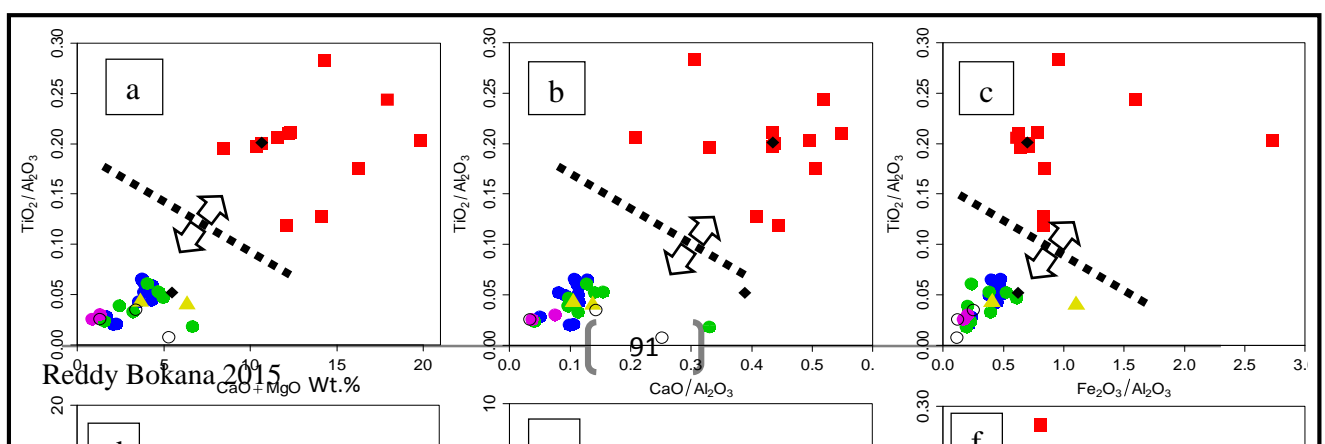
The metamorphism of these rocks to granulite facies grade furthermore suggests a burial history to at least 20 km below the surface; assuming a general geothermal gradient at the time estimated to have been around 35°C/km (see Albat, 1984). The fact that these rocks occur at, or near the surface at the present day simply suggest that they must have been uplifted, exhumed and intensely eroded after such a deep burial occurred. Following on from this, the granulite facies metamorphism, M₂, which largely coincided with D₂ deformation, has been estimated to have occurred during the early Namaquan Orogeny at 1187 ± 22 Ma following the suggestion of Clifford et al. (1981) and Clifford and Barton (2012). Evidence of pre-Namaqua events (apart from intrafolial folds) have, however, not been preserved in the rock record, making it extremely difficult to substantiate the early stages of the model with firm evidence. Crustal shortening associated with D₃ deformation, has, however, been well preserved as symmetrical folding foliation fabrics within the biotite gneisses (Plate 4.5a & b). Based on field observations, this shortening event is estimated to have had the orientation of a north-south orientation relative to the current position and present-day orientation of the study area. This orientation is also confirmed by the structural studies of Albat (1984) and Macey et al. (2011) which, together, support the findings of this study. Field evidence of north-south compressional folding, as well as biotite-hornblende-rich xenoliths with a sinistral sense of shear have also been preserved in the meta-pelitic gneisses forming part of the Kamiesberg Group of the Namaqualand stratigraphy (see Plate 8.4 in appendix). This interpretation is consistent with the result obtained by G. Abrahams (pers. comm., October 2014), whose work has provided a large amount of field evidence quantifying the magnitude and orientation of the various stress fields which likely operated in the study area. Confirmation of this north-south orientation (of the principal stress during D₃) is also in excellent agreement with the structural work of Albat (1984), as well as that of Joubert (1986).

6.1.5 Vectoring and controls on the mineralization (Ni, Cu, Co and Zn)

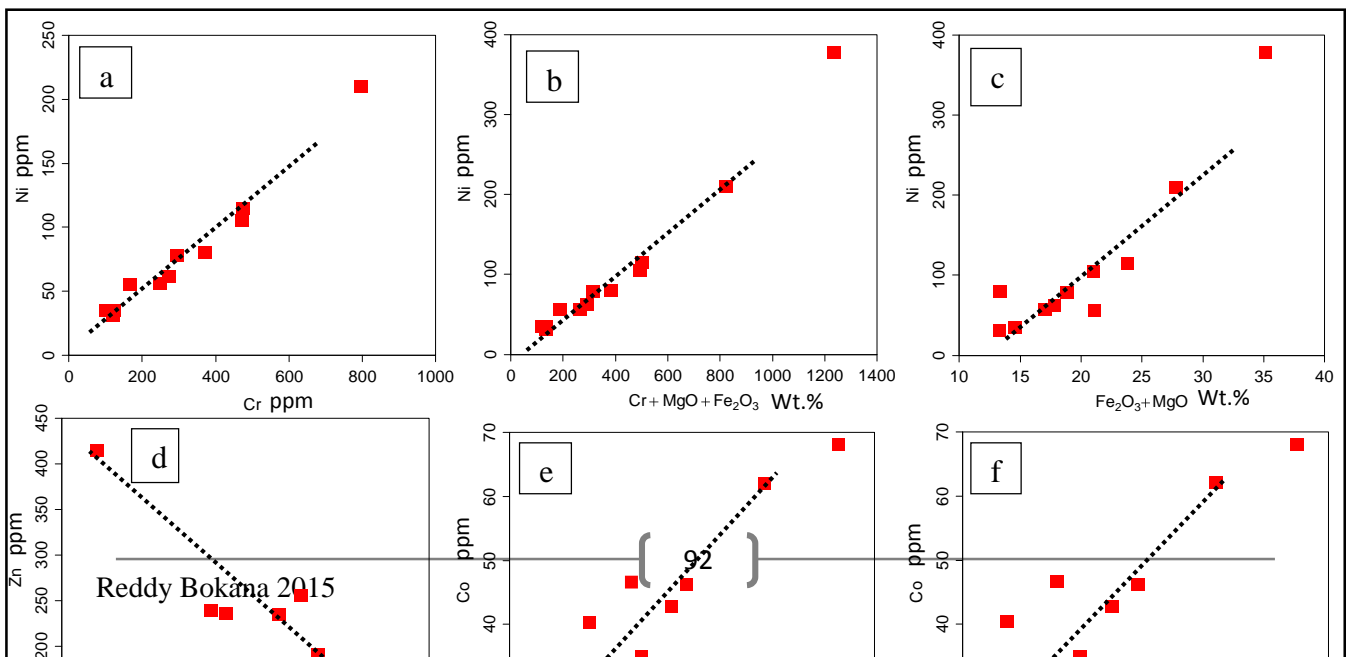
Two conceptual models based on multivariate statistical analyses (on the basis of element relationships) were built in order to understand the distribution of the mineralization. Only specific elements, such as Ni, Cu, Co and Zn, are given particular attention for vectoring (as they represent the mineralization). Important relationships between the mineralization and the different host rocks and identifying the nature of those relationships were established as the main focus of this geostatistical analysis. Sulphide mineralization in several samples of the meta-gabbro-norite both in core specimen (Plate 4.1c) as well as in thin sections (Plate 4.2c) indicate that the meta-gabbro-norite occurs as the actual ore-host lithology (amongst the many

host lithologies which are reported). Multiple geochemical vectors (or indices) have thus been created and are robust in isolating the meta-gabbro norite' samples from within the large group of hosts (Fig. 6.3). These vectors, most particularly $\text{CaO} + \text{MgO}$ vs. $\text{TiO}_2/\text{Al}_2\text{O}_3$, $\text{CaO}/\text{Al}_2\text{O}_3$ vs. $\text{TiO}_2/\text{Al}_2\text{O}_3$ and others have shown consistency in isolating the meta-gabbro norite samples from within the large group of hosts by plotting them on different binary diagrams (Fig. 6.3). The robustness of these indices suggest that they can be used as chemographic indices for showing the position and/or highlighting areas where the meta-gabbro norite spatially occurs. The use of geochemistry as an exploration tool in highly deformed and granulite facies area such as the Kliprand area is necessary and thus the importance of the vectors proposed in this study. The main criteria in developing these vectors has been that the other litho-types, in general, have shown to have more Al-contents relative to the overall Al-contents of the meta-gabbro norite. The latter has been attributed to the large amount of felsic minerals (for example feldspars) that those litho-types have in comparison to the overall amounts of felsic minerals that the meta-gabbro norite has (and hence high and low Al-contents, respectively).

The observation that certain elements are strongly correlated with Ni, Co and Zn was reported on Table 5.4 and the nature of their relationships were also explained on Table 5.5. Stepwise regression analysis, which evaluates the percentage to which one element can be predicted using the concentration of other elements, has indicated that there are several possibilities of determining several path-finder elements for each commodity elements studied (see Table 5.5). Several indices developed and applied have, indeed, shown that elements such as Cr, MgO and Fe_2O_3 are potentially useful for prediction of the distribution of Ni in the host lithologies (most particularly in the meta-gabbro norite). Other indices, such as $\text{MgO} + \text{P}_2\text{O}_5$, as well as Na_2O , are also useful and have shown potential for being used for prediction of Co and Zn concentration (see Table 5.5). Figure 6.3 show multiple vectors for which the actual ore-host (the meta-gabbro norite) is set aside from within the large group of hosts using geochemistry as an exploration tool. A derivation of the enderbite from the meta-gabbro norite through a partial melting is geochemically supported by the closer association of the enderbite sample with the meta-gabbro norite sample in several diagrams shown on Fig. 6.3.



Copper, despite being one of the commodity elements, could not be predicted using any of the potential vectors which have been developed. Due to it not showing any valuable correlation matrix, as well as lack of showing any coefficient of determination, the distribution of Cu is considered less predictable or unpredictable in comparison to the other commodity elements. Metamorphism and deformation of the ore deposit are considered as the driving factor which, due to the mobility of Cu, in the metamorphic fluid, may have been responsible for affecting its distribution (as Cu can be easily remobilized during metamorphism or metasomatism). But other elements, by contrast, such as Ni, Zn and Co as shown on Figure 6.4, display closer relationships with numerous indices which are developed as their vectors. It is therefore suggested that some of these vectors may be used as an exploration tool for determining the position of many of these commodity elements in different host rocks, either, for the Hondekloof deposit or for similar deposits.



It was also envisaged that there is a good relationship between plagioclase content, Al₂O₃ content and Ni content in several samples of the meta-gabbro. Those samples which have lots of plagioclase and high Al₂O₃ and Na₂O contents, have low Ni contents. This observation is suggesting that the barren-meta-gabbro and mineralized meta-gabbro can be separated on the basis of the mineralogical composition of plagioclase and its Al₂O₃ content (Table 6.2). Those samples of meta-gabbro having a high Al₂O₃-content and lots of plagioclase are considered either as barren or less mineralized compared to those which have less plagioclase and with a low Al₂O₃ content. This observation is shown petrographically in Plate 4.2a and c, wherein a higher plagioclase content equates with lesser amounts of mineralization and vice versa, and which is also in good agreement with respect to geochemical compositions in terms of the variation of Al and Ni contents (Table 6.2). A major conclusion drawn was that the barren or less mineralized meta-gabbro samples, as well as the mineralized meta-gabbro samples, are separated based on Al and plagioclase contents (see Table 6.2).

Table 6-2: Determination of a mineralized and a less mineralized meta-gabbro sample

Sample ID	Al contents (%)	Ni-content (ppm)	Interpretation
H493-1d	16.54	55.57	less mineralised or barren
H 582-6	8.36	6896.82	Mineralized

This discrimination is based on Aluminium content and the amounts of plagioclase in the samples. It is also known that only two sample shown on table 6.2 is statistically not a very conclusive result.

6.1.6 Classification of the Hondekloof prospect

There are specific criteria for which the nature of a magmatic nickel sulphide mineralization is compared and classified (Table 6.3). These are: (1) the amount of sulphide, or the amount of base-metal, such as Cu, contained within the sulphide, (2) the fractionation state, in terms of MgO content of the parental magma, and (3) the environment of deposition (e.g. Naldrett, 1999, 2004; Hronsky, 2007; Song et al., 2008, 2011). With regards to these criteria, therefore, the Hondekloof deposit could tentatively be classified as being a disseminated, low MgO, and conduit-type of magmatic nickel sulphide mineralization.

Since it is possible to classify a magmatic Ni sulphide deposit based on tectonic setting characteristics (Hronsky, 2007; Song et al., 2008, 2011), an attempt was also made to identify the tectonic setting in which the Hondekloof deposit was deposited. The assumption made here, however, is that there are only four tectonic environments that are suitable as potential hosts to a magmatic Ni sulphide deposit, namely: (1) a layered mafic intrusion, (2) a komatiite-hosted deposit, (3) a large igneous province, and (4) a conduit system (Song et al., 2008, 2011). Selection of the conduit system as principal host type was made based on the fact that the Oorkraal Suite, which acts as the main ore-bearer for the Hondekloof mineralization, has no features seemingly reflecting the characteristics of either a layered mafic intrusion (e.g. the presence of layering or tabular stratigraphic layers), or a komatiite hosted deposit (due to the lack of ultra-mafic rocks such as komatiite in the succession), or a large igneous province (such as the presence of flood basalts in the area). However, this interpretation can also become intriguing given the fact that the presence of a related eruptive magmatic component (such as a volcanic or plutonic intrusion) has not been proven conclusively in the case of the Hondekloof deposit; which is a pivotal requirement for developing a conduit-type model. In addition, the highly metamorphosed and deformed nature of the area makes this interpretation tentative. Nevertheless, it is here assumed that the meta-gabbro, being part of the Oorkraal Suite, possibly acted as the conduit pipe to the previously existing country rocks and meta-sedimentary formations (namely biotite gneiss, feldspathic biotite garnet gneiss and pink gneiss).

Song et al. (2011) argued that intrusions which host conduit types of mineralization generally do not exceed dimensions of more than 10 km in size (i.e. due to the fact that the size of such intrusions are controlled by the size and shape of a regional fault which the nickeliferous magma

used as a conduit). A conduit style is tentatively supported here by the notion that the Oorkraal Suite only extends to about 3.5 km in dimension (Macey et al. 2011). This observation, in combination with a lack of features, that would, otherwise, suggest other tectonic environments, suggests that the Hondekloof deposit is a conduit type of magmatic Ni sulphide deposit. It should be noted, however, again that the highly deformed nature of the rocks makes this interpretation suggestive and tentative at best. A more comprehensive study of the actual sulphide mineralisation of the Hondekloof deposit is required before a firm, conclusive classification for the deposit can be given.

Table 6-3: criteria for classifying a magmatic Ni sulphide deposit (after Naldrett, 1999, 2004; Hronsky, 2007, Song et al., 2008, 2011)

Based on:	Class I	Class ii	Class iii	Class iv	The Hondekloof classification
1. Sulphide content based classification	Massive type: Characteristics: ≥ 40 modal % Examples: Kambalda style (Australia)	Disseminated type: Characteristics: ≤ 10 modal % Examples: Noril'sk style (Russia); Nkomati (South Africa)			Disseminated type Reason: disseminated ore textures and lack of massive ores (Chapter 4).
2. Parental magma (MgO content) based classification	High MgO Characteristics: 18-30% MgO content, Ore grade range: 0.5-0.7% Ni Examples: Kambalda style (Australia)	Low MgO Characteristics: 8-12% MgO content, Ore grade range: 0.2-0.4% Ni, 0.2-0.4% Cu Examples: Noril'sk style (Russia); Voisey's Bay style (Canada)			Low MgO-type Reason: The overall MgO content of the meta-gabbro-norite (the main host to the sulphide ores) ranges between 3.32 and 9.78 wt.% (Fig. 5.1)
3. Tectonic setting based classification	Layered mafic intrusion Examples: Stillwater (America), Great Dyke (Zimbabwe);	Komatiite Based Examples: Kambalda (Australia), Thompson (Canada)	Conduit system Examples: Noril'sk (Russia); Voisey's Bay (Canada);	Large Igneous Province	Conduit type Reason: size of the Oorkraal Suite intrusion (3.5 km)

Bushveld (South
Africa)Nkomati (South
Africa)

6.2 Conclusion

The overall litho-geochemical characterization of the country rocks to the Hondekloof deposit dealing with the host rock classification, tectonic evolution and origin of the protoliths and an attempt at general mineralization characterization were among the subjects dealt with in this study. Using both petrography (petrology) and geochemistry as combined geological tools for undertaking host rock classification including, but not limited to, origin and protoliths and geochemical characterization, has demonstrated that there are as much as seven lithological units (namely meta-gabbro-norite and biotite gneiss, feldspathic biotite garnet gneiss and pink gneiss, meta-syenite as well as enderbite and garnetiferous quartzofeldspathic rock) that occur in the Hondekloof deposit. Petrologically and geochemically, these lithological units are broadly subdivided into two main groups both in terms of origin affinity (igneous and sedimentary) (Fig. 5.3) as well as compositional affinity (mafic and felsic) (Fig. 5.4a and b). Based on these classification schemes, the meta-gabbro-norite, which acts as the ore-bearer at the Hondekloof deposit, herein referred to as the actual host rock, is determined to have affinities to (1) igneous origin (Fig. 5.3), (2) mafic composition (Fig. 5.4a and b) and also (3) having the chemical characteristics and nature of a depleted mantle source (like MORB) (Fig. 5.6a and b). Similar to the meta-gabbro-norite, the meta-syenite also has an affinity to igneous origin, but felsic in composition, whereas, on the other hand, the biotite gneiss, feldspathic biotite garnet gneiss and pink gneiss have affinity to sedimentary origin, with various natures of sedimentary protoliths varying in composition between felsic and intermediate (Fig. 5.4a and b), somewhat with or without mixed-origin characteristics like “volcaniclastic”, and differ from the enderbite and the garnetiferous quartzofeldspathic rock, which have been classified as the products of partial melting during metamorphism. Based on a relatively broad understanding of the overall regional tectonic evolution of Namaqualand (e.g. Joubert, 1977; Albat, 1984; Macey et al., 2011), coupled with our current understanding of the development of the local tectonism of the Garies terrane to date, a simplified step by step tectonic model (Fig. 6.2) falling within the framework of a subduction-related collisional setting and particularly within a local back arc basin-system has been tailored and proposed for the Kliprand area.

Evaluation of the pressure-temperature conditions for estimation of the degree of metamorphism using mineral paragenesis principles (Fig. 4.2) revealed that the multiple lithological units investigated were metamorphosed to temperature (T) and pressure (P) conditions of granulite facies (T: 750-875 °C, and P: 4-6 kbar, respectively). This P-T condition, coupled with the knowledge of regional geothermal gradient of southern Namaqualand, 35 °C/km (Albat, 1984), together have indicated that these lithological units, including the Hondekloof deposit, must have been buried to a depth of at least 20 to 25 km for such thermal and pressure conditions to become available in the crust presuming the requirement of the modern plate tectonic principles. It is therefore assumed that the principles of modern plate tectonics as being applied in the modern era must have also been applicable in the very same way as in the Precambrian and Proterozoic times for such P-T conditions to be applicable in the study area.

A particular attention on geochemical vectoring focusing on multivariate statistical approach, with a lesser emphasis on some geological controls (such as ore minerals and (liberation) textures, mineral chemistry, magmatic and metamorphic ore-forming processes) developed for the sake of pathfinder identification to Ni mineralization, purely based on a statistical approach, have demonstrated applicability in this study in two ways. Firstly, in isolating the actual host lithology from within the large group of country rocks (Fig. 5.15; Fig. 6.3 and table 5.4), and, secondly, for targeting some commodity elements (e.g. Ni, Cu, Zn, Co) based on the knowledge of their pathfinder elements (Fig. 5.16; Fig. 6.4 and Table 5.6). This technique, although not well-developed, can have a profound significance for exploration of Ni mineralization if coupled with a good understanding of a few other geological controls.

A relatively broad nickel mineralization classification scheme, some features of which are not entirely well developed (due to some analytical and geological constraints), have led to some relevant findings suggesting, tentatively, that the Hondekloof deposit could be classified as a low MgO, conduit-type, and disseminated magmatic nickel sulphide deposit.

6.3 Recommendation and future work

There are several outstanding questions surrounding the actual age of the Hondekloof prospect. Lack of having such information made it difficult for this study to substantiate the tectonic model proposed with conclusive evidence. Consequently it is thus suggested that some of the

host lithologies examined require dating in order to fully understand and determine their origin, genesis, time of origin and emplacement and that of the orebody at large. In addition, isotopic information will also be needed as it may help to constrain the source of the sulphide ores and that of the meta-gabbro.

7. REFERENCES

- ❖ Albat, H.M. (1983). Garnet-cordierite thermometry/barometry and the temperature-pressure conditions of formation of granulite-facies metapelites in the Kliprand area. Annual Report, Precambrian Research Unit, University of Cape Town, 18–20, pp. 105–115.
- ❖ Albat, H.M. (1984). The Proterozoic granulite facies terrane around Kliprand, Namaqualand Metamorphic complex. Bulletin, Precambrian Research Unit, University of Cape Town, 33, 386 pp.
- ❖ Abu El-Enen, M.M. (2011). Geochemistry, provenance, and metamorphic evolution of Gabal Samra Neoproterozoic metapelites, Sinai, Egypt, *Journal of African Earth Sciences* 59, 269–282.
- ❖ Andreoli, M.A.G., Andersen, N.J.B., Levin, M., Niemand, N. (1987). Geology of the Vaalputs radioactive waste disposal site in the Republic of South Africa. Explanatory notes for the geological map of the site on the scale 1:250 000, Department of Geotechnology Atomic Energy Corporation of South Africa, Limited, 39 pp.
- ❖ Andreoli, M.A.G., Moore, J.M., Hambleton-Jones, B.B. (1991a). Geology and mineralogy of the Hondekloof nickel prospect, Kliprand, Cape Province. Internal Report, Schonland Research Centre, University of Witwatersrand, 31 pp.
- ❖ Andreoli, M.A.G., Hart, R.J., Ashwal L.D., Brynard, H.J. (1991b). A petrological and geochemical investigation of certain potential pathfinders to mineralised Koperberg Suite

- intrusions. Internal Report, Schonland Research Centre, University of the Witwatersrand, 32 pp.
- ❖ Andreoli M.A.G., Hart R.J., Ashwal L.D., Coetzee H. (2006). Correlations between U, Th content and metamorphic grade in the western Namaqualand belt, South Africa, with implications for radioactive heating of the crust. *Journal of Petrology*, 47, 1095-1118.
 - ❖ Baars, F.J. (1990). Geologic and petrologic evidence for granulite-facies partial melting in the Garies–Platbakkies supra-crustal gneiss belt, Namaqualand Metamorphic Complex, South Africa. M.Sc. thesis, University of Cape Town. 128 pp.
 - ❖ Bailie, R., Gutzmer, J. (2011). Age and primary architecture of the Copperton Zn-Cu VMS deposit, Northern Cape Province, South Africa. *Ore Geology Reviews* 39, 164–179.
 - ❖ Bailie, R., Armstrong, R., Reid, D. (2007a). The Bushmanland Group supracrustal succession, Aggeneys, Bushmanland, South Africa: Provenance, age of deposition and metamorphism. *South African Journal of Geology*, 110, 59-86.
 - ❖ Bailie, R., Armstrong, R., Reid, D. (2007b). Composition and single zircon U-Pb emplacement and metamorphic ages of the Aggeneys Granite Suite, Bushmanland, South Africa: *South African Journal of Geology*, 110, 87–110.
 - ❖ Bailie, R., Gutzmer, J., Strauss, H., Stüeken, E., McClung, C. (2010). Sulfur isotope characteristics of metamorphosed Zn–Cu volcanogenic massive sulfides in the Areachap Group, Northern Cape Province, South Africa. *Mineralium Deposita*, 45, 481–496.
 - ❖ Bailie, R., Gutzmer, J., Rajesh, H.M., Armstrong, R. (2011). Age of ferroan A-type post-tectonic granitoids of the southern part of the Keimoes Suite, Northern Cape Province, South Africa. *Journal of African Earth Sciences*, 60, 153–174.
 - ❖ Bailie, R., Rajesh, H.M., Gutzmer, J. (2012). Bimodal volcanism at the western margin of the Kaapvaal Craton in the aftermath of collisional events during the Namaqua-Natal Orogeny: The Koras Group, South Africa. *Precambrian Research* 200–203, 163–183.
 - ❖ Becker, T., Schreiber, U.M., Kampunzu, A.B., Armstrong, R.A. (2006). Mesoproterozoic rocks of Namibia and their plate tectonic setting. *Journal of African Earth Sciences* 46, 112-140.
 - ❖ Bekker, P.G. (1980). The detailed geology and geochemistry of the Hondekloof prospect (Nuwefontein ptn. 3 block 3018AD, Kliprand). Internal Report, Okiep Copper Company Limited, 10 pp.

- ❖ Bhatia, M.R., Crook, K.A.W. (1986). Trace element characteristics of graywackes and tectonic setting discrimination of sedimentary basins. *Contributions to Mineralogy and Petrology* 92, 181-193.
- ❖ Buchanan, D.L., Nolan, J. (1979). Solubility of sulfur and sulfide immiscibility in synthetic tholeiitic melts and their relevance to Bushveld-Complex rocks. *The Canadian Mineralogist* 17(2), 483-494.
- ❖ Bucher, K., Grapes, R. (2011). *Petrogenesis of Metamorphic Rocks* (8th ed.). Springer. pp. 348-351.
- ❖ Burnham, C.W. (1967). Hydrothermal fluids in the magmatic stage. In H.L. Barnes (ed.), *Geochemistry of Hydrothermal Ore Deposits*. Holt, Rinehart and Winston, pp. 34–76.
- ❖ Burnham, C.W. (1979) Magmas and hydrothermal fluids. In H.L. Barnes (ed.), *Geochemistry of Hydrothermal Ore Deposits*, 2nd edn. John Wiley & Sons, pp. 71–136.
- ❖ Candela, P.A. (1991) Physics of aqueous phase evolution in plutonic environments. *American Mineralogist*, 76, 1081–1091.
- ❖ Candela, P.A. and Holland, H.D. (1984). The partitioning of copper and molybdenum between silicate melts and aqueous fluids. *Geochimica et Cosmochimica Acta*, 48, 373–380.
- ❖ Cardona, A., Valencia, V., Bustamante, C., García-Casco, A., Ojeda, G., Ruiz, J., Saldarriagad, M. (2010). Tectonomagmatic setting and provenance of the Santa Marta Schists, northern Colombia: Insights on the growth and approach of Cretaceous Caribbean oceanic terranes to the South American continent. *Journal of South American Earth Sciences* 29, 784–804.
- ❖ Cawthorn R.G., Meyer, F.M. (1993). Petrochemistry of the Okiep Copper District basic intrusive bodies, northwestern Cape Province, South Africa. *Economic Geology* 88, 590–605.
- ❖ Clifford, T.N., Barton, E.S. (2012). The Okiep Copper District, Namaqualand, South Africa: a review of the geology with emphasis on the petrogenesis of the cupriferous Koperberg Suite. *Mineral Deposita*, 47, 837–857.
- ❖ Clifford, T.N., Stumpfl, E.F., Burger, A.J., McCarthy, T.S., Rex, D.C. (1981). Mineral-chemical and isotopic studies of Namaqualand granulites — South Africa: a Grenville analogue. *Contributions to Mineralogy and Petrology*, 77, 225-250.
- ❖ Clifford, T.N., Barton, E.S., Retief, E.A., Rex, D.C., Fanning, C.M. (1995). A crustal progenitor for the intrusive anorthosite-charnockite kindred of the cupriferous Koperberg

- Suite, Okiep district, Namaqualand, South Africa; new isotope data for the country rocks and the intrusives. *Journal of Petrology*, 16, 154–188.
- ❖ Clifford, T.N., Barton, E.S., Stern, R.A., Duchesne, J-C. (2004). U-Pb calendar for Namaquan (Grenville) crustal events in the granulite-facies terrane of the Okiep Copper District of South Africa. *Journal of Petrology*, 45, 669–691.
 - ❖ Colliston, W.P., Schoch, A.E. (2006). The distribution and diagnostic features of deformed plutonic rocks in two terranes of the Namaqua mobile belt along the Orange (Gariiep) River, South Africa. *South African Journal of Geology* 109, 369–392.
 - ❖ Cornell, D.H., Pettersson, Å. (2007). Ion probe zircon dating of metasediments from the Areachap and Kakamas Terranes, Namaqua-Natal Province and the stratigraphic integrity of the Areachap Group. *South African Journal of Geology* 110, 575–584.
 - ❖ Cornell, D.H., Hawkesworth, C.J., Van Calsteren, P., Scott, W.D. (1986). Sm–Nd study of Precambrian crustal development in the Prieska-Copperton region, Cape Province. *Transactions of the Geological Society of South Africa*, 89, 17–28.
 - ❖ Cornell, D.H., Kröner, A., Humphreys, H.C., Griffin, G. (1990a). Age of origin of the polymetamorphosed Copperton Formation, Namaqua-Natal Province, by single grain zircon Pb–Pb dating: *South African Journal of Geology*, 93, 709–714.
 - ❖ Cornell, D.H., Theart, H.F.J., Humphreys, H.C. (1990b). Dating a collision-related metamorphic cycle at Prieska copper mines, South Africa. In: Spry, P.G., Bryndzia, T. (Eds.), *Regional Metamorphism of Ore Deposits and Genetic Implications*, vol. 11. VSP, Utrecht, pp. 97–116.
 - ❖ Cornell, D.H., Humphreys, H.C., Theart, H.F.J., Scheepers, D.J. (1992). A collision-related pressure-temperature-time path for Prieska copper mine, Namaqua-Natal tectonic Province: South Africa. *Precambrian Research*, 59, 43–71.
 - ❖ Cornell, D.H., Thomas, R.J., Moen, H.F.G., Reid, D.L., Moore, J.M., Gibson, R.L. (2006). The Namaqua-Natal Province. In: Johnson, M.R., Anhaeusser, C.R., Thomas, R.J. (Eds.), *The Geology of South Africa*. Geological Society of South Africa, Johannesburg/Council for Geoscience, Pretoria, 325–379.
 - ❖ Cox, R., Lowe, D.R., Cullers, R.L. (1995). The influence of sediment recycling and basement composition on evolution of mudrock chemistry in the southwestern United States. *Geochimica et Cosmochimica Acta* 59, 2919–2940.
 - ❖ Dalziel, I.W.D., Mosher, S., Gahagan, L. (2000). Laurentia–Kalahari collision and the assembly of Rodinia. *Journal of Geology* 108, 499–513.

- ❖ De Beer, J.H., Meyer, R. (1984). Geophysical characteristics of the Namaqua–Natal belt and its boundaries, South Africa. *Journal of Geodynamics* 1, 473–494.
- ❖ De Beer, C. H., Macey, P.H., Pether, J., Nel, Z.E. (2010). The geology of the Garies area- Geological Map sheet: 3017 Garies. Council for Geoscience.
- ❖ Duchesne, J.C., Vander Auwera, J., Liégeois, J.P., Barton, E.S., Clifford, T.N. (2007). Geochemical constraints on the petrogenesis of the Okiep Koperberg Suite and granitic plutons in Namaqualand, South Africa: a crustal source in Namaquan (Grenville) times. *Precambrian Research*, 153, 116–142.
- ❖ Eglinton, B.M. (2006). Evolution of the Namaqua-Natal belt, southern Africa — a geochronological and isotope geochemical review: *Journal of African Earth Sciences*, 46, 93–111.
- ❖ Eglinton, B.M., Armstrong, R.A. (2003). Geochronological and isotopic constraints on the Mesoproterozoic Namaqua–Natal Belt: evidence from deep borehole intersections in South Africa. *Precambrian Research*, 125, 179–189.
- ❖ Faccenna, C., Becker, T.W., Lucente, F.P., Jolivet, L., Rossetti, F. (2001). History of subduction and back-arc extension in the Central Mediterranean. *Geophysical Journal International*, 145, 809–820.
- ❖ Fedo, C.M., Nesbitt, H.W., Young, G.M. (1995). Unravelling the effects of potassium metasomatism in sedimentary rocks and paleosols, with implications for paleoweathering conditions and provenance. *Geology* 23, 921–924.
- ❖ Frimmel, H.E. (2004). Formation of a late Mesoproterozoic supercontinent: the South Africa–East Antarctica connection. In: Eriksson, P.G., Altermann, W., Nelson, D.R., Mueller, W.U., Catuneanu, O. (Eds.), *The Precambrian Earth: Tempos and Events*. Elsevier Science BV, Amsterdam, pp. 240–255.
- ❖ Ghavami-Riabi, R., Theart, H.F.J., De Jager, C. (2008). Detection of concealed Cu–Zn massive sulfide mineralization below eolian sand and a calcrete cover in the eastern part of the Namaqua Metamorphic Province, South Africa. *Journal of Geochemical Exploration*, 97, 83–101.
- ❖ Girty, G.H., Ridge, D.L., Knaack, C., Johnson, D., Al-Riyami, R.K. (1996). Provenance and depositional setting of Paleozoic chert and argillite, Sierra Nevada, California. *Journal of Sedimentary Research* 66, 107–118.
- ❖ Gose, W.A., Johnston, S.T., Thomas, R.J. (2004). Age of magnetization of Mesoproterozoic rocks from the Natal sector of the Namaqua-Natal belt, South Africa. *Journal of African Earth Sciences*, 40, 137–145.

- ❖ Grandstaff, D.F., Edlman, M.J., Foster, R.W., Zbinden, E., Kimberly, M.M. (1986). Chemistry and mineralogy of Precambrian paleosols at the base of the Dominion and Pongola Groups, (Transvaal, South Africa). *Precambrian Research* 32, 97–132.
- ❖ Grantham, G.H. (2000a). Interim report on the geology of sheet 3018 AA (Bovlei). Internal report, Council for Geoscience (compilation of the 1:250 000 sheet 3018 Loeriesfontein). (Unpublished).
- ❖ Grantham, G.H. (2000b). Report on the geology of sheet 3018 AC (Leliefontein). Internal report, Council for Geoscience (compilation of the 1:250 000 sheet 3018 Loeriesfontein). (Unpublished).
- ❖ Grantham, G.H., Eglington, B.M., Thomas, R.J., Mendonidis, P. (2001). The nature of the Grenville-age charnockitic A-type magmatism from the Natal, Namaqua and Maud Belts of southern Africa and western Dronning Maud Land, Antarctica. Special Issue on the Evolution of the Namaqua, Natal and Maud Belts, Japan–South Africa Joint Research Memoirs of the National Institute of Polar Research 55, pp. 59–86.
- ❖ Grantham, G.H., Maboko, M.A.H., Eglington, B.M. (2003). A review of the evolution of the Mozambique Belt and implications for the amalgamation and dispersal of Rodinia and Gondwana. In: Yoshida, M., Windley, B.F., Dasgupta, S. (Eds.), *Proterozoic East Gondwana: Supercontinent Assembly and Breakup*, vol. 206. Geological Society, pp. 401–425.
- ❖ Grisolia, M.F.P., Oliveira, E.P. (2012). Sediment provenance in the Palaeoproterozoic Rio Itapicuru greenstone belt, Brazil, indicates deposition on arc settings with a hidden 2.17–2.25 Ga substrate, *Journal of South American Earth Sciences* 38, 89–109.
- ❖ Groenewald, P.B., Grantham, G.H., Watkeys, M.K. (1991). Geological evidence for a Proterozoic to Mesozoic link between southeastern Africa and Dronning Maud Land, Antarctica. *Journal of the Geological Society of London* 148, 1115–1123.
- ❖ Hamman, J.N., Rozendaal, A., Jordaan, W. (1996). Gabbro-norite hosted Ni-Cu-(Co) sulphide mineralization in southern Namaqualand and its relationship to the cupriferous Koperberg Suite of the Okiep Copper District, South Africa. *South African Journal of Geology*, 99, 153–167.
- ❖ Hanson, R.E., Brueckner, H.K., Onstott, T.C., Wardlaw, M.S., Johns, C.C., Hardcastle, K.C. (1988). Reconnaissance geochronology, tectonothermal evolution, and regional significance of the Middle Proterozoic Choma-Kalomo block, southern Zambia. *Precambrian Research* 42, 39–61.

- ❖ Harnois, L. (1988). The CIW index: a new chemical index of weathering. *Sedimentary Geology* 55, 319–322.
- ❖ Hartnady, C. J. H., Joubert, P., Stowe, C. W. (1985). Proterozoic crustal evolution in southwestern Africa. *Episodes*, 8, 236– 244.
- ❖ Haughton, D.R., Roeder, P.L., Skinner, B.J. (1974). Solubility of sulfur in mafic magmas. *Economic Geology* 69 (4), 451-467.
- ❖ Hoffman, P.F. (1991). Did the breakout of Laurentia turn Gondwanaland inside-out? *Science* 252, 1409–1412.
- ❖ Hollings, P., Wyman, D. (2005). The geochemistry of trace elements in igneous systems: principles and examples from basaltic systems. In: En Linnen, R.L., Samson, I.M. (Eds.), *Rare-Element Geochemistry and Mineral Deposits*, GAC Short Course Notes, vol. 17. Geological Association of Canada, pp. 1–16.
- ❖ Holwell, D. A., McDonald, I. (2010). A review of the behaviour of platinum group elements within natural magmatic sulfide ore systems. The importance of semi-metals in governing partitioning behaviour. *Platinum Metals Review*, 54, 26-36.
- ❖ Hronsky, J. (2007, Jun). Introduction to nickel sulphide exploration. Presented data of the Western Mining Services, Australia.
- ❖ Hutchinson, D., McDonald, I. (2008). Laser ablation ICP-MS study of platinum-group elements in sulphides from the Platreef at Turfspruit, northern limb of the Bushveld Complex, South Africa. *Mineralium Deposita*, 43, 695-711.
- ❖ Jackson, C.J. (1998). The geology of the area east of Garies, Northern Cape. Sheet 3018CA Buffelsfontein. Internal report, Council for Geoscience, 1998-0315. (Unpublished).
- ❖ Irvine, T.N., Barager, W.R.A. (1971). A guide to the chemical classification of the common volcanic rocks. Canada. *Journal of Earth Sciences*, 8, 523–548.
- ❖ Jacobs, J., Thomas, R.J., Weber, K. (1993). Accretion and indentation tectonics at the southern edge of the Kaapvaal craton during the Kibaran (Grenville) orogeny. *Geology*, 21, 203-206.
- ❖ Jacobs, J., Thomas, R.J., Weber, K. (1995). K–Ar, $^{40}\text{Ar}/^{39}\text{Ar}$ and apatite fission-track evidence for Neo-Proterozoic and Mesozoic basement rejuvenation events in the Heimefrontfjella and Mannefallknausane (East Antarctica). *Precambrian Research* 75, 251–262.

- ❖ Jacobs, J., Falter, M., Thomas, R.J., Kunz, J., Jeßberger, E.K. (1997). $^{40}\text{Ar}/^{39}\text{Ar}$ thermochronological constraints on the structural evolution of the Mesoproterozoic Natal Metamorphic Province, South Africa. *Precambrian Research* 86, 71–92.
- ❖ Jacobs, J., Thomas, R.J. (2001). A titanite fission track profile across the southeastern Archaean Kaapvaal Craton and the Mesoproterozoic Natal Metamorphic Province, South Africa: evidence for differential cryptic Meso- to Neoproterozoic tectonism. *Journal of African Earth Sciences*, 33, 323-333.
- ❖ Jenner, G.A. (1996). Trace element geochemistry of igneous rocks: geochemical nomenclature and analytical geochemistry. In: Wyman, D.A. (Ed.), *Trace Element Geochemistry of Volcanic Rocks: Applications for Massive Sulphide Exploration*. Short Course Notes, vol. 12. Geological Association of Canada, pp. 51–77.
- ❖ Joubert, P. (1971). The regional tectonism of the gneisses of part of the Namaqualand Metamorphic Complex. *Bulletin of the Precambrian Research Unit, University of Cape Town*, 10, 220 pp.
- ❖ Joubert, P. (1986). Namaqualand – a model of Proterozoic accretion? *Transactions of the Geological Society of South Africa* 89, 79–96.
- ❖ Joubert, P., Waters, D.J. (1980). The occurrence of kyanite at Zoutpan and metamorphism in western Namaqualand. *Annual Report, Precambrian Research Unit, University of Cape Town*, 17, pp. 74–87.
- ❖ Keller, A.R., Fisk, M.R., Smellie, J.L., Strelin, J.A., Lawver, L.A., White, W.M. (2002). Geochemistry of back arc basin volcanism in Bransfield Strait, Antarctica: Subducted contributions and along-axis variations, *Journal of Geophysical Research*, 107, 1029-2001.
- ❖ Lehumo Resource Company (2008). Technical report Hondekloof nickel project.
- ❖ Li, C., Naldrett, A. J. (1993). Sulfide capacity of magma; a quantitative model and its application to the formation of sulphide ores at Sudbury, Ontario. *Economic Geology* 88, (5), 1253-1260.
- ❖ Lombaard, A.F., the exploration staff of the Okiep Copper Company Limited. (1986). The copper deposits of the Okiep District, Namaqualand. In: Anhaeusser, C.R., Maske, S. (Eds.), *Mineral Deposits of Southern Africa*, vol. II. Geological Society of South Africa, pp. 1421–1445.
- ❖ Macey, P.H; Siedfried H.P; Minaar, H; Almond, J., Botha, P.M.W. (2011). The geology of the Loriesfontein area- Loriesfontein Geological Map, 3018DA. Council for Geoscience.

- ❖ Maier, W.D., Andreoli, M.A.G., Groves, D.I., Barnes, S.-J. (2013). Petrogenesis of Cu-Ni sulphide ores from Okiep and Kliprand, Namaqualand, South Africa: constraints from chalcophile metal contents. *South African Journal of geology*, 115, 499-514.
- ❖ Matthews, P.E. (1981). Eastern or Natal sector of the Namaqua–Natal Mobile Belt in southern Africa. In: Hunter, D.R. (Ed.), *Precambrian of the Southern Hemisphere*. Elsevier, Amsterdam, pp. 705–725.
- ❖ Mavrogenes, J.A., O’Neill, H.S.C. (1999). The relative effects of pressure, temperature and oxygen fugacity on the solubility of sulfide in mafic magmas. *Geochimica et Cosmochimica Acta* 63 (7-8), 1173-1180.
- ❖ McDonough W. F. and Sun, S. (1995). The composition of the Earth. *Chemical Geology*, 120, 223-253.
- ❖ McLennan, S.M., Hemming, S. (1992). Samarium/Neodymium elemental and isotopic systematics in sedimentary rocks. *Geochimica et Cosmochimica Acta* 56, 887–898.
- ❖ McLennan, S.M., Taylor, S.R., McCulloch, M.T., Maynard, J.B. (1990). Geochemical and Nd-Sr isotopic composition of deep-sea turbidites: crustal evolution and plate tectonic associations. *Geochimica et Cosmochimica Acta* 54, 2015-2050.
- ❖ McLennan, S.M., Hemming, S., McDaniel, D.K., Hanson, G.N. (1993). Geochemical approaches to sedimentation, provenance and tectonics. In: M.J. Johnsson and A. Basu (Eds.), *Processes controlling the composition of clastic sediments*. Geological Society of America Special Paper, 284, 21-40.
- ❖ McClung, C.R. (2006). Basin analysis of the Bushmanland Basin, Namaqualand Metamorphic Complex, Northern Cape Province, South Africa. Unpublished PhD thesis, University of Johannesburg, South Africa, 320pp.
- ❖ McCourt, S., Armstrong, R.A., Grantham, G.H., Thomas, R.J. (2006). Geology and evolution of the Natal belt, South Africa. *Journal of African Earth Sciences*, 46, 71–92.
- ❖ McDonough W. F. and Sun, S. (1995). The composition of the Earth. *Chemical Geology* 120, 223-253.
- ❖ McIver, J.R., McCarthy, T.S., Packham, B.V. (1983). The copper-bearing basic rocks of Namaqualand, South Africa. *Mineralium Deposita* 18, 135–160.
- ❖ Middlemost, E.A.K. (1975). The basalt clan. *Earth Science Reviews*, 11, 337-364.
- ❖ Mielke, P., Winkler, H. G. F. (1979). Eine bessere Berechnung der Mesonorm für granitische Gesteine. *Neues Jahrbuch für Mineralogie, Monatshefte*, 471–480.
- ❖ Moen, H.F.G. (1999). The Kheis Tectonic Subprovince, South Africa: A lithostratigraphic perspective. *South African Journal of Geology*, 120, 27-42.

- ❖ Moen, H.F.G., Toogood, D.J., 2007. The Geology of the Onseepkans area. Explanation: Map Sheet 2818, 1:250 000 scale, Council for Geoscience, Pretoria.
- ❖ Moore, A.E., Verwoerd, W.J. (1985). The olivine melilitite-“kimberlite”-carbonatite Suite of Namaqualand and Bushmanland, South Africa. *Transactions of the Geological Society of South Africa*, 88, 281–294.
- ❖ Moore, J.M. (1983). Geochemical and genetic aspects of cordierite gneisses from south-central Namaqualand. Report, Precambrian Research Unit, University of Cape Town, 18–20, 116–131.
- ❖ Moore, J. M. (1989). A comparative study of metamorphosed supracrustal rocks from the western Namaqualand metamorphic complex. *Precambrian Research Unit Bulletin* 37, 370 pp.
- ❖ Moore, J.M., Watkeys, M.K., Reid, D.L. (1990). The regional setting of the Aggeneys/Gamsberg base metal deposits, Namaqualand, South Africa. In: Spry, P.G., Bryndzia, L.T. (Eds.), *Regional Metamorphism of Ore Deposits and Genetic Implications: Proceedings of the 28th International Geological Congress*. Washington, USA, VSP, Utrecht, Netherlands 85, 77–95.
- ❖ Nakamura, N. (1974). Determination of REE, Ba, Fe, Mg, Na and K in carbonaceous and ordinary chondrites. *Geochemica et Cosmochimica Acta* 38, 757-775.
- ❖ Naldrett, A.J. (1999). World-class Ni-Cu-PGE deposits: key factors in their genesis. *Mineralium Deposita* 34, 227-240.
- ❖ Nesbitt, H.W. (2003). Petrogenesis of siliciclastic sediments and sedimentary rocks. In: Lentz, D.R. (Ed.), *Geochemistry of Sediments and Sedimentary Rocks: Evolutionary Considerations to Mineral Deposit-Forming Environments*. Geological Association of Canada, *GeoText* 4, pp. 39-51.
- ❖ Naldrett, A.J. (2004). *Magmatic sulfide deposits: geology, geochemistry and exploration*. Springer, Berlin, 727 pp.
- ❖ Nicolaysen, L.O., Burger, A.J. (1965). Note on an extensive zone of 1000 million-year old metamorphic and igneous rocks in Southern Africa. *Science de la Terre* 10, 487–516.
- ❖ Nicollet C., & Andriambololona, D. R. (1980). Distribution of transition metals in crustal metabasic igneous rocks. *Chemical Geology* 28, 78–90.
- ❖ Norwicky, T.E., Frimmel, H.E.F., Waters, D.J. (1995). The occurrence of osumilite in pelitic granulites of the Namaqua Metamorphic Complex. *South African Journal of Geology* 98, 191–201.

- ❖ Pearce, J.A. (1982). Trace element characteristics of lavas from destructive plate boundaries. In: Thorpe, R.S. (Ed.), *Andesites*. John Wiley & Sons, pp. 525–548.
- ❖ Pearce, J.A., Norry, M.J. (1979). Petrogenetic implications of Ti, Zr, Y, and Nb variations in volcanic rocks. *Contributions to Mineralogy and Petrology* 69, 33–47.
- ❖ Pearce, J.A. (1996). A user's guide to basalt discrimination diagrams. In: Wyman, D.A. (Ed.), *Trace Element Geochemistry of Volcanic Rocks: Applications for Massive Sulphide Exploration*. Short Course Notes, Geological Association of Canada 12, 79–113.
- ❖ Pettersson, Å., Cornell, D.H., Moen, H.F.G., Reddy, S., Evans, D. (2007). Ion-probe dating of 1.2 Ga collision and crustal architecture in the Namaqua-Natal Province of southern Africa. *Precambrian Research*, 158, 79–92.
- ❖ Pettersson, Å., Cornell, D. H., Mosher, S. (2008). Metamorphic zircon data from two Mesoproterozoic components of Rodinia: the Llano Uplift (Texas, North America) and the Namaqua-Natal Province (South Africa). Nordic Geological winter meeting, Aalborg 2008, Abstract volume, p 80.
- ❖ Pettersson, Å., Cornell, D.H., Yuhara, M., Hirahara, Y. (2009). Sm-Nd data for granitoids across the Namaqua Sector of the Namaqua-Natal Province, South Africa: Geological Society of London Special Publications, 323, 219-230.
- ❖ Raith, J.G., Cornell, D.H., Frimmel, H.E., De Beer, C.H. (2003). New insights into the geology of the Namaqua tectonic province, South Africa, from ion probe dating of detrital and metamorphic zircon. *Journal of Geology* 111:347–366.
- ❖ Raith, M.M., Raase, P., Reinhardt. (2012). *Guide to Thin Section Microscopy*, 2nd Edition, ISBN 978-3-00-37671-9.
- ❖ Reid, D.L. (1979). Total rock Rb–Sr and U–Th–Pb isotopic study of Precambrian metavolcanic rocks in the lower Orange River region, Southern Africa. *Earth and Planetary Science Letters*, 42, 368-378.
- ❖ Reid, D.L. (1997). Sm–Nd age and REE geochemistry of Proterozoic arc-related igneous rocks in the Richtersveld Subprovince, Namaqua Mobile Belt, southern Africa. *Journal of African Earth Sciences*, 24, 621–633.
- ❖ Reid, D.L., Welke, H.J., Erlank, A.J., Moyes, A.B. (1987). The Orange River Group: a major Proterozoic calc-alkaline volcanic belt in the western Namaqua Province, southern Africa. In: Pharoah, T.C., Beckinsale, R.D., Richard, D. (Eds.), *Geochemistry and mineralization of Proterozoic volcanic suites*, Geological Society of South Africa. Special Publication, 327–346.

- ❖ Ripley, E.M., Lightfoot, P.C., Li, C., Elswick, E.R. (2003). Sulfur isotopic studies of continental flood basalts in the Noril'sk region: implications for the association between lavas and ore-bearing intrusions. *Geochimica et Cosmochimica Acta*, 67, 2805-2817.
- ❖ Robb, L.J., Armstrong, R.A. and Waters, D.J. (1999). Nature and duration of mid-crustal granulite facies metamorphism and crustal growth: Evidence from single zircon U-Pb geochronology in Namaqualand, South Africa: *Journal of Petrology* 40, 1747–1770.
- ❖ Robertson, S. (1999). BGS Rock Classification Scheme, volume 2: Classification of metamorphic rocks. British Geological Survey Research Report, RR 99–02. 26 pp.
- ❖ Rollinson, H.R. (1993). Using Geochemical Data: Evaluation, Presentation, and Interpretation. Longman Scientific & Technical Ltd., Harlow, 352 pp.
- ❖ Ryan, P.J., Lawrence, A.L., Lipson, R.D., Moore, J.M., Paterson, A., Stedman, D.P., Van Zyl, D. (1986). The Aggeneys base metal sulphide deposits, Namaqualand district. In: C.R. Anhaeusser and S. Maske (Eds.), *Mineral Deposits of Southern Africa*, vol. II, Special Publication of the Geological Society of South Africa, 1447-1474.
- ❖ SACS (South African Committee for Stratigraphy) (1980). Stratigraphy of South Africa. Part 1 (Comp. L.E. Kent), Lithostratigraphy of the Republics of South Africa, South West Africa/Namibia and the Republics of Bophuthatswana, Transkei and Venda. Handbook Geological Survey of South Africa 8, 690 pp.
- ❖ Saunders, A.D., Storey, M., Kent, R.W., Norry, M.J. (1992). Consequences of plume–lithosphere interactions. In: Storey, B.C., Alabaster, T., Pankhurst, R.J. (Eds.), *Magmatism and the Causes of Continental Break-up*. Geological Society of London, Special Publication. Geological Society of London, London, pp. 41–60.
- ❖ Schmitz, M.D., Bowring, S.A. (2004). Lower crustal granulite formation during Mesoproterozoic Namaqua-Natal collisional orogenesis, southern Africa. *South African Journal of Geology*, 107, 261-284.
- ❖ Schoch, A.E., Conradie, J. (1990). Petrochemical and mineralogical relationships in the Koperberg Suite, Namaqualand. *American Mineralogist* 75, 27–36.
- ❖ Singletary, S.J., Hanson, R.E., Martin, M.W., Crowley, J.L., Bowring, S.A., Key, R.M., Ramokate, L.V., Direng, B.B., Krol, M.A. (2003). Geochronology of basement rocks in the Kalahari Desert, Botswana, and implications for regional Proterozoic tectonics. *Precambrian Research* 121, 41–71.
- ❖ Song, X.Y., Zhou, M.F., T, Y., Xiao, J.F. (2008). Controls on the metal compositions of magmatic sulfide deposits in the Emeishan large igneous province, SW China, *Chemical Geology* 253, 38–49.

- ❖ Song, X., Wang, Y., Chen, L. (2011). Magmatic Ni-Cu-(PGE) deposits in magma plumbing systems: Features, formation and exploration, *Geoscience Frontiers* 2, 375-384.
- ❖ Spear, T. (1989). *Metamorphic Phase Equilibria and Pressure-Temperature-Time Paths*. Mineral Society of American Monograph 1.
- ❖ Stacey, J.S., Kramers, J.D. (1975). Approximation of terrestrial lead isotope evolution by a two-stage model. *Earth and Planetary Science Letters* 26, 207–221.
- ❖ Stern, R.J., Dickinson, W.R. (2010). The Gulf of Mexico is a Jurassic back-arc basin. *Geological Society of America* 6, 739–754.
- ❖ Steven, G., Clemens, J.D., Droop, G.T.R. (1997). Melt production during granulite-facies anatexis: experimental data from “primitive” metasedimentary protoliths. *Contributions to Mineralogy and Petrology*, 128, 352-370.
- ❖ Stowe, C.W. (1983). The Upington Geotraverse and its implications for craton margin tectonics. In: Botha, B.J.V. (Ed.), *The Namaqualand Metamorphic Complex*, Special Publication of the Geological Society of South Africa 10, pp. 147–171.
- ❖ Stowe, C.W. (1986). Synthesis and interpretation of structures along the northeastern boundary of the Namaqua Tectonic province, South Africa. *Transactions of the Geological Society of South Africa* 89, 185–198.
- ❖ Taylor, E. (1990). The geology and Ni-metallogenesis in the Namaqualand Mobile Belt, Kliprand, North-West Cape, South Africa. Unpublished BSc. (Honours) Project, University of the Witwatersrand, South Africa, 69pp.
- ❖ Taylor, S.R., McLennan, S.H. (1985). *The Continental Crust: Its Composition and Evolution*. Blackwell, Oxford. 312 pp.
- ❖ Thomas, R.J. (1989). A tale of two tectonic terranes. *South African Journal of Geology* 92, 306-321.
- ❖ Thomas, R.J., Agenbacht, A.L.D., Cornell, D.H., Moore, J.M. (1994). The Kibaran of southern Africa: Tectonic evolution and metallogeny. *Ore Geology Reviews* 9, 131-160.
- ❖ Thomas, R.J., Jacobs, J., Eglington, B.M. (2000). Geochemistry and isotopic evolution of the Mesoproterozoic Cape Meredith Complex, West Falkland. *Geological Magazine* 137, 537–553.
- ❖ Van Aswegen, G. (1974). The geology of the Namaqualand Metamorphic Complex and younger formations northwest of Loeriesfontein, Cape Province. M.Sc. thesis, University of the Orange Free State. (Unpublished).

- ❖ Van Bever Donker, J.M. (1980). Structural and metamorphic evolution of an area around Kakamas and Keimoes, Cape Province, South Africa. *Bulletin of the Precambrian Research Unit* 28, 165 pp.
- ❖ Van de Kamp, P.C., Leake, B.E. (1985). Petrography and geochemistry of feldspathic and mafic sediments of the northeastern Pacific margin. *Transactions of the Royal Society of Edinburgh: Earth Sciences* 76, 411–449.
- ❖ Van Niekerk, H.S. (2006). The origin of the Kheis Terrane and its relationship with the Archean Kaapvaal Craton and the Grenvillian Namaqua Province in southern Africa. PhD Thesis, University of Johannesburg. 260 pp.
- ❖ Van Zwieten, A.J.M., McCarthy, T.S., Cawthorn, R.G. (1996). A petrogenetic model for the Koperberg Suite: evidence from the Jubilee Mine, Namaqualand, South Africa. *South African Journal of Geology*, 99, 121–134.
- ❖ Verma S.P., Guevara M., Agrawal S. (2008). Discriminating four tectonic settings: Five new geochemical diagrams for basic and ultrabasic volcanic rocks based on log-ratio transformation of major-element data. *Journal of Earth System Science* 115, 485–528.
- ❖ Verma, S. P., Pandarinath, K., Verma, S. K. and Agrawal, S. (2013). Fifteen new discriminant-function-based multi-dimensional robust diagrams for acid rocks and their application to Precambrian rocks. *Lithos*, 168-169, 113-123.
- ❖ Waters, D.J. (1986a). Metamorphic history of sapphirine-bearing and related magnesian gneisses from Namaqualand, South Africa. *Journal of Petrology* 27, 541–565.
- ❖ Waters, D.J. (1986b). Metamorphic zonation and thermal history of pelitic gneisses from western Namaqualand, South Africa. *Transactions of the Geological Society of South Africa* 89, 97–102.
- ❖ Waters, D.J. (1988). Partial melting and the formation of granulite facies assemblages in Namaqualand, South Africa. *Journal of metamorphic Geology* 6, 387-404.
- ❖ Waters, D.J. (1989). Metamorphic evidence for the heating and cooling path of Namaqualand granulites. In: J.S. Daly, R.A. Cliff and B.W.D. Yardley, (Eds.), *Evolution of Metamorphic Belts*. Special Publication of the Geological Society 43, 357–363.
- ❖ Waters, D. J. (1991). Hercynite-quartz granulites: phase relations, and implications for crustal processes. *European Journal of Mineralogy* 3, 367–386.
- ❖ Waters, D.J., Whales, C.J. (1984). Dehydration melting and the granulite transition in metapelites from southern Namaqualand, South Africa. *Contributions to Mineralogy and Petrology* 88, 269–275.

- ❖ Watson, E. B., Harrison, M. (1983). Zircon saturation revisited: temperature and composition effects in a variety of crustal magma types. *Earth and Planetary Science Letters* 64, 295-304.
- ❖ Weaver, C.E. (1989). *Clays, Muds, and Shales*. Elsevier, Amsterdam. 819 pp.
- ❖ Wendlandt, R.F. (1982). Sulfide saturation of basalt and andesite melts at high-pressures and temperatures. *American Mineralogist* 67 (9-10), 877-885.
- ❖ Winchester, J.A., Floyd, P.A. (1977). Geochemical discrimination of different magma series and their differentiation products using immobile elements. *Chemical Geology* 20, 325–343.
- ❖ Winchester, J.A., Max, M.D. (1982). The geochemistry and origin of the Precambrian rocks of the Rosslare Complex, SE Ireland. *Journal of the Geological Society, London* 139, 309–319.
- ❖ Winchester, J.A., Max, M.D., Long, C.B. (1987). Trace element correlation in the reworked Proterozoic Dalradian metavolcanic suites of the western Ox Mountains and NW Mayo inliers, Ireland. In: Pharaoh, T., Beckinsale, R.D., Rickard, D. (Eds.), *Geochemistry and mineralization of Proterozoic Volcanic suites*. Geological Society of London, Special Publication 33, 489–502.
- ❖ Yigitbas, E., Winchester, J.A., Ottley, C.J. (2008). The geochemistry and setting of the Demirci Paragneisses of the Sünnice Massif, NW Turkey. *Turkish Journal of Earth Sciences* 17, 421–431.
- ❖ Zelt, G.A.D. (1980). Granulite facies metamorphism in Namaqualand, South Africa. *Precambrian Research*, 13, 253–274.



8. APPENDICES

**Appendix 1. Extended abstract published and presented on the 27th edition
of international applied geochemistry symposium in Tucson, Arizona,
United States of America, 2015.**



THE LITHOGEOCHEMICAL CHARACTERIZATION OF THE HONDEKLOOF NICKEL MINERALIZATION, KLIPRAND AREA, GARIES TERRANE, NAMAQUALAND, SOUTH AFRICA

Reddy N. Bokana¹, Russell Bailie², Jan van Bever Donker³

Department of Earth Sciences, Applied geology Section, University of the Western Cape,
Private Bag X17, Bellville 7535, Cape Town, South Africa

¹3008694@myuwc.ac.za / personal: rbokana@yahoo.fr Tel +27 78 72 62 358 / +242 06 472
29 05

²rbailie@uwc.ac.za Tel +27 78 72 62 358; Fax +27 21 959 3118

³jvanbeverdonker@uwc.ac.za

Abstract

A series of magmatic Ni-Cu (Co-Zn) sulphide mineralization, namely the Hondekloof deposit, is present in the Kliprand area at the border between the Northern Cape and Western Cape Provinces of South Africa. The deposit occurs in the central parts of the metamorphic high grade Garies Terrane, Namaqua Sector, along the south-western margin of the Mesoproterozoic Namaqua-Natal Metamorphic Province (Figure 8-1).

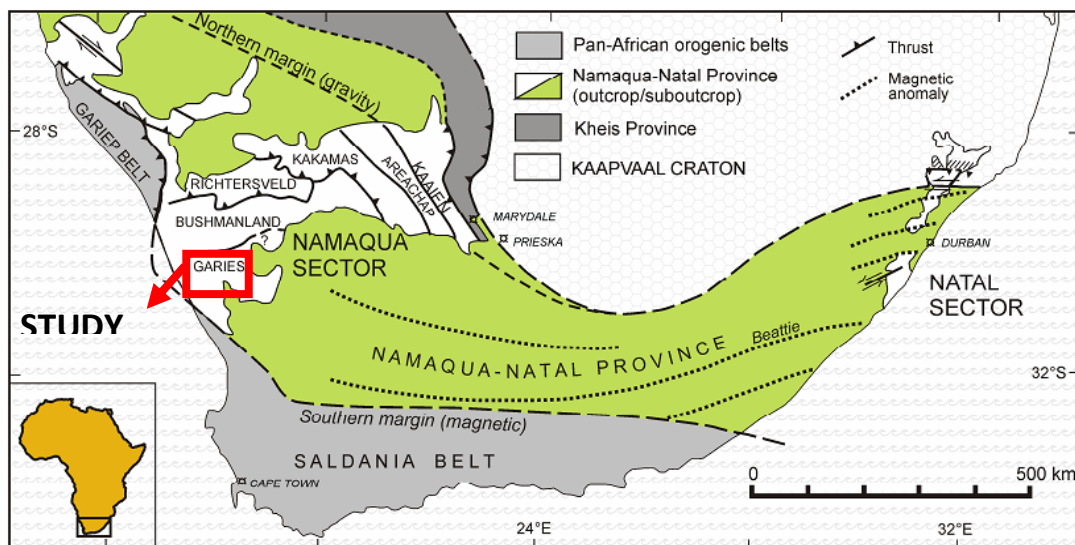


Figure 8-1. Simplified geological map of southern Africa, from Cornell et al. (2006)

Given the sub-economic value yielded from the evaluation of three of its known massive sulphide lenses the Hondekloof deposit has received relatively little attention in terms of ongoing scientific research. Therefore many aspects related to the genesis, classification and tectonic evolution of the deposit, to date, remain relatively unclear. The present contribution has therefore been geared to addressing some of these issues in view of new data obtained.

Six exploration boreholes were logged, examined and sampled at the deposit site in Kliprand. A total of seven host rocks, namely meta-gabbro, biotite gneiss, feldspathic-biotite-garnet gneiss, pink gneiss, meta-syenite as well as enderbite along with a garnetiferous quartzofeldspathic rock, distributed unevenly in the different boreholes, are present. A comprehensive geological investigation involving core, petrographic and geochemical analysis, undertaken in view of producing a new set of data and interpretation has added significantly to our current understanding of this deposit. The Hondekloof deposit and its host rocks locally formed within a rift continental back-arc basin and carry a signature of a regional collisional subduction system.

The meta-gabbro, which forms part of the pre-to-syn-tectonic Ookraal Suite, metamorphosed to granulite facies grade, occurs as the actual host rock hosting the disseminated base metal sulphides in association with ortho- and clinopyroxene, and lesser plagioclase. Both the enderbite and garnetiferous quartzofeldspathic rocks occur as melt products seen as veins formed during prograde metamorphism. Certain geochemical indices, of which the combination of element-ratios such as $\text{TiO}_2/\text{Al}_2\text{O}_3$ vs. $\text{CaO} + \text{Al}_2\text{O}_3$, and $\text{TiO}_2/\text{Al}_2\text{O}_3$ vs. $\text{CaO}/\text{Al}_2\text{O}_3$ and $\text{MgO}/\text{Al}_2\text{O}_3$ vs. TiO_2 as well as Cr vs. Ni and $\text{Cr} + \text{MgO} + \text{Fe}_2\text{O}_3$ vs. Ni , along with others, which were created as vectors to the mineralisation, have significantly shown potential for pointing towards the direction of the mineralization (Fig. 2).

The disseminated nature of the sulphide mineralization, as well as the fact that the ores were subjected to both metamorphism and deformation suggest that the mineralization occurred syn-genetically to its host rock and that the deposit was buried to a depth of at least 20 km within the crust to experience granulite facies metamorphism (assuming the geothermal gradient of the Garies Terrane at the time was $35^\circ\text{C}/\text{km}$). Thereafter the area was uplifted, eroded and exhumed to shallow level. In particular, the presence of partial melt products, such as the enderbite within the meta-gabbro, which itself carries mineralization locally, suggests that some of the sulphide ores may have been locally remobilized during prograde metamorphism.

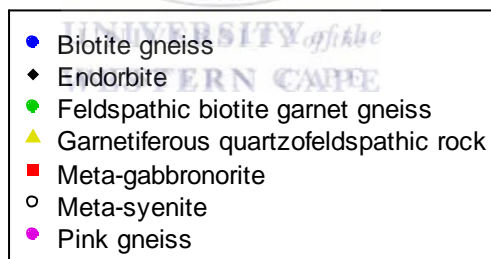
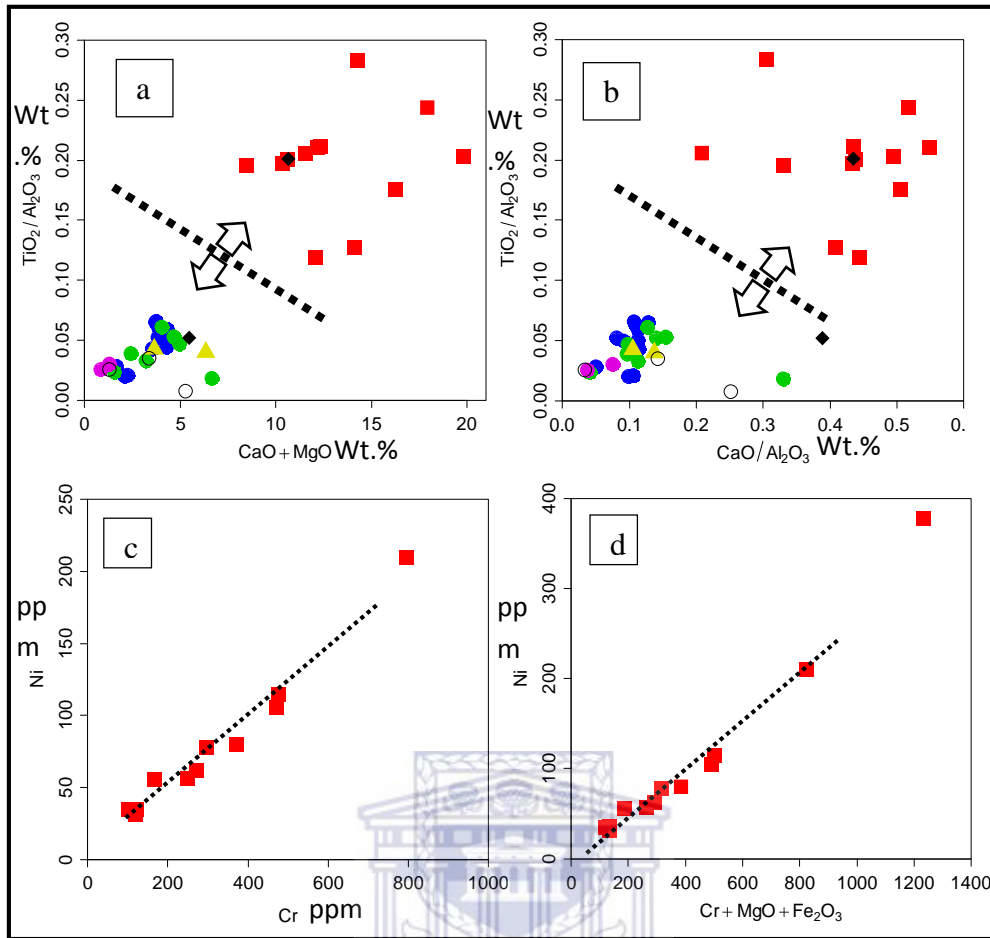


Figure 8-2. Geochemical indices as vectors for pointing towards the direction of the mineralization. a) $\text{TiO}_2/\text{Al}_2\text{O}_3$ vs. $\text{CaO} + \text{MgO}$; b) $\text{CaO}/\text{Al}_2\text{O}_3$ vs. $\text{TiO}_2/\text{Al}_2\text{O}_3$; c) for discrimination of the actual host, the meta-gabbronorite from the large group of host. b) Cr. vs Ni and $\text{Cr} + \text{MgO} + \text{Fe}_2\text{O}_3$ vs. Ni as pathfinders of Ni within the meta-gabbronorite. The dotted line and opposite headed arrows indicate the separation.

The results obtained, with regards to the criteria applicable for classifying magmatic Ni sulphide deposits suggests that the Hondekloof deposit could be classified as being: 1) a low-MgO type, 2) a conduit type and, 3) a disseminated type of magmatic Ni sulphide mineralization.

References

CORNELL, D.H., THOMAS, R.J., MOEN, H.F.G., REID, D.L., MOORE, J.M., GIBSON, R.L. (2006). The Namaqua-Natal Province In: Johnson, M.R., Anhaeusser, C.R., Thomas, R.J. (Eds.), *The Geology of South Africa*. Geological Society of South Africa, Johannesburg/Council for Geoscience, Pretoria, 325–379.





Appendix 2 Field description of the examined boreholes

UNIVERSITY of the
WESTERN CAPE

Field Geology of the examined boreholes

Figure 4.1 has provided a summary description of the distribution of the lithologies both within and around the Hondekloof gossan outcrops. The augen gneiss of the Little Namaqua Suite (Plate 8.1), by far, occurs as the most extensive outcrop on most drilling of the boreholes (Fig. 4.1). This gneiss is characterized by a series of conjugate joint sets and several micro-features, developed as syn-kinematic set of joints (Plate 8.1).



Plate 8-1: Field evidence of “east-west and north-south-south Syn-kinematic joints on the augen gneiss of the Little namaland Siute within the western lense of the Hondekloof deposit.

There is a clear contact between the meta-gabbro-norite and the meta-pelitic gneiss of the Kamiesberg Group in the central extension of the orebody (Plate 8.2a). Several veins, composed of plagioclase, alkali feldspar and quartz (identified as enderbite in the boreholes), cut through the meta-gabbro-norite in several locations on the central extension orebody (Plate 8.2b).

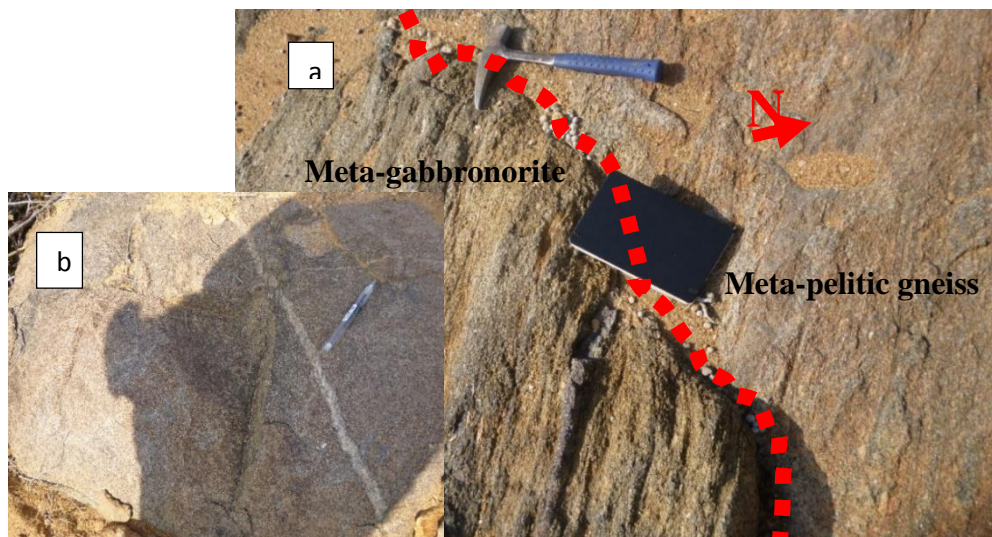


Plate 8-2: a: Sharp intrusion of the meta-gabbro-norite into the meta-pelitic gneiss of the Kamiesberg Group. b: A feldspathic vein crosscutting the weathered meta-gabbro-norite.

Several veins composing of garnet, quartz and alkali feldspathic (termed garnetiferous quartzofeldspathic rock) cut through the meta-gabbronorite, the pink gneiss (Plate 8.3) and the meta-pelitic gneiss in several section within the orebody extensions (Fig. 4.1).



Plate 8-3: Evidence of the garnetiferous quartzofeldspathic veins cutting through the pink gneiss. Photo taken in the eastern extension of the orebody

There are also several structural information preserving evidences of deformation, metamorphism and partial melting on the meta-pelitic gneiss of the Kamiesberg Group (plate 8.4). This gneiss has, however, not been identified in the collection of the boreholes studied, but preserves abundant features such as those shown on Plate 8.4. The features include compressional folding (Plate 8.4a), biotite-hornblende-rich xenoliths (Plate 8.4b), partial melt veins (Plate 8.4c), with abundant parasitic folds (m-, s- and z-folds) developed along the limbs of the major Kliprand dome feature.

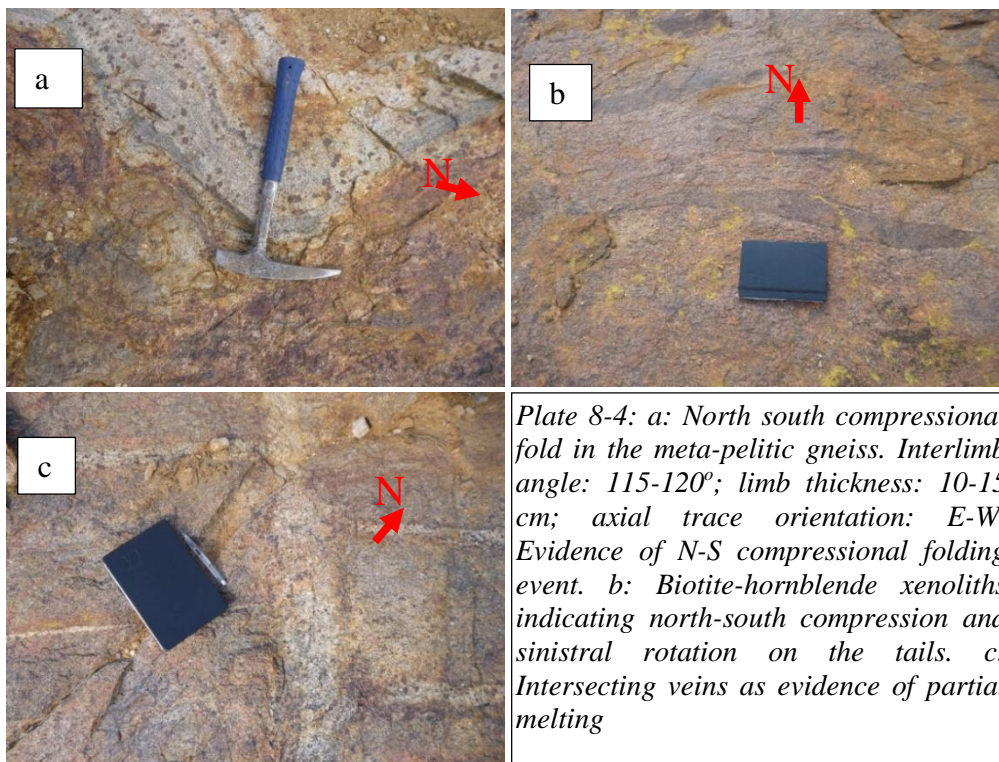


Plate 8-4: a: North south compressional fold in the meta-pelitic gneiss. Interlimb angle: 115-120°; limb thickness: 10-15 cm; axial trace orientation: E-W. Evidence of N-S compressional folding event. b: Biotite-hornblende xenoliths indicating north-south compression and sinistral rotation on the tails. c: Intersecting veins as evidence of partial melting